IDENTIFICATION AND CONTROL OF AN AUTOMATED OFF HIGHWAY AGRICULTURAL VEHICLE

BY

NANJUN LIU

THESIS

Submitted in partial fulfillment of the requirements
for the degree of Master of Science in Mechanical Engineering
in the Graduate College of the
University of Illinois at Urbana-Champaign, 2011

Urbana, Illinois

Advisor:

Professor Andrew Alleyne

Abstract

The main objective of this study was to develop an automated agricultural vehicle guidance system that can be easily transplanted from vehicle to vehicle. The proposed solution to this problem is to first perform a tractor model identification, and then use a pole placement technique to place the closed loop dominant poles in their desired locations. One of the most difficult aspects of designing a controller for vehicle guidance is arriving at a good model of vehicle lateral dynamics.

This study presents a new approach for identifying the lateral dynamics of an automated off-highway vehicle. A second order model is proposed to represent the vehicle lateral dynamics. An Iterative Learning Identification (ILI) method is used to identify the model parameters. Simulation and experimental results show the convergence of parameters with arbitrarily chosen initial estimations. The estimation results are compared to other traditional identification methods: least squares estimation and gradient based adaptive estimation. The results highlight the practical benefits of the ILI approach – i.e. that it can be performed in a relatively small section of field and therefore done prior to actual usage or engagement with crops

To my family

Acknowledgements

First and foremost, I would like to thank my advisor, Dr. Alleyne, for all his guidance and inspirations. I started to understand ‘control’ in a more practical sense than solving exam problems. You helped me grow as a researcher, to find out a problem, and to search for a way of solving. Above all this, you help me find and understand the weakness of myself, and your caring and encouragement showed me a way of improvement.

Next in line, I want to thank my peers in Alleyne’s research group, who are all among the most intelligent, hardworking, and fantastic people I’ve ever met. First of all, I would like to thank Yangmin for being such a nice lab mate and a good friend, for offering technical support and for sharing good time together. Thanks also goes to Kira for helping me revising my presentation in the late evening, discussing with me the questions I have on research and helping me setting the timelines for my thesis writing; to Sandipan for helping me understanding difficult paper and theorem; to Dave for your insight in technical issues; to Neera for your help in both research related and beyond; to Vikas, Bin, and Tim, for your willingness to discuss and share opinions; to Erick, for your help in classes we shared; to Megan and Justin, it has been so nice to know you over the last few months, and I’m excited for the coming years of having you in the lab.

I must also thank Matthew D Potter, Jeff Wetstphal, Greer Ashley, Tyler Schleicher, Swaroop Mannepalli, Richard J Erwin, Timothy A Wilcox, Joshua T Lawson, and Ryan C Burnley from John Deere for their technique insight, tractor equipment setup and software tools supporting. I’m also grateful to Larry Meyer for his assistance during the field experiments.

I would also like to thank two people outside of the technical group. Jing, thanks for being such a wonderful roommate and friend, and thanks for driving a tractor and recording data with me although you are majored in ‘Asian study’. Lei, thanks for your encouragement, support, and willingness to work on the farm with me on chilly winters and late evenings. Helping me find the broken pins in the CAN card, which has taken me weeks to find.

Last but not least, I must thank my parents for giving me their selfless love and support. Dad, thanks for being such a good example of researcher, who is able to explain what robust control is to me when I was in high school. Mom, your love is something that is not ever replaceable, and is the most important in my life. I’m so lucky to have you two to be my parents, with whom I can always share everything.

Finally, I would like to acknowledge John Deere Corporation for funding my research.

Table of Contents

List of Tables

List of Figures

Nomenclature

a_y	inertial acceleration of the vehicle at the c.g. in the direction of y axis
$C_{\alpha f}$	cornering stiffness of the front tires
$C_{\alpha r}$	cornering stiffness of the rear tires
d_s	distance from vehicle mass center to the output measurement sensor
δ	front wheel steering angle
ε	yaw angle of vehicle body
ε_d	desired yaw angle set by the road
F_{yf}	lateral tire force of the front tires
F_{yr}	lateral tire force of the rear tires
I_z	yaw moment of inertia of the vehicle
l_f	distance from vehicle c.g. to the front axle
l_r	distance form vehicle c.g. to the rear axle
m	mass of the vehicle
R	road radius
ψ	yaw angle
$\dot{\psi}$	yaw rate
y_r	lateral distance between the vehicle c.g. and the center line of road

Chapter 1
Introduction

This thesis presents a new approach for identifying the lateral dynamics of an automated off-highway agricultural vehicle. This method will allow the vehicle to be identified in a relatively small section of field and therefore done prior to the actual usage or engagement with crops. A feedback controller can then be designed based on the identified model. This will allow for easier tuning of feedback controllers for different vehicles. A second order model is proposed to represent the vehicle lateral dynamics. An Iterative Learning Identification (ILI) method is used to identify the model parameters. Simulation and experimental results show the identified model to be very representative of the actual tractor dynamics. The feedback controller designed based on the identified model is capable of achieving the design specifications for closed loop performance. The estimation results are compared to other traditional identification methods: least squares estimation and gradient based adaptive estimation. Relative benefits and drawbacks of the alternate approaches are also discussed.

The organization of this introductory chapter is as follows. First, a motivation for off-highway agricultural vehicle research is given, with specific emphasis on automatic steering. Second, a short literature review of the area of automatic agricultural vehicle research is given. Third, the specific goals of this thesis are described, including the motivation for using the particular type of identification method chosen. An introduction for Iterative Learning Identification is also presented. Finally, a summary of the remaining chapters in the thesis is provided.

1.1 Motivation for agricultural vehicle research

Agriculture has always been central to the development of human civilization. The world population is slated to grow from 7 billion currently to over 9 billion by the year 2050. At the same time, a growing world population demands space to live thereby reducing the arable land available for generating crops. If one adds in the growing burden on current water resources by the growing population it becomes readily apparent that future agriculture will have to 'do more with less.' In short, the yields of future agricultural systems will have to greatly outperform those of the present if we are to meet the predicted need. There are several ways in which to make gains in agriculture. Improved crop genetics is a clear one, along with improved fertilizers. However, a large factor in the gains of modern agriculture is the increased mechanization and automation of the entire agricultural process. A key facet of the overall mechanization is the improved functionality of modern machines that work to plant, monitor, harvest, and condition the fields of operation.

The concept of precision farming, or precision agriculture, first emerged in the United States in the early 1980s. As defined, precision agriculture is a farming practice of using remote sensing, soil sampling and information management tools to optimize agriculture production. The goal of precision agriculture is to optimize field-level management with regard to crop science, environmental protection and economics. Precision agriculture uses information technologies, like Global Positioning Systems (GPS), Geographical Information Systems (GIS), and remote sensing to target inputs and management practices to variable field conditions. In this study, we will be focusing on agricultural GPS guidance, which is an important step in the whole precision farming process.

Automatic guidance can effortlessly perform monotonous field operations, which involve parallel swathing, and repetitive passages over similar rows. It can also improve an operator's ability to control complex farm machinery, which frequently includes monitoring many machine sub-systems. Overlapping or skipping field areas in simple operations like tillage or chemical applications can be reduced by using a GPS based guidance system. Work in low visibility situations can also be made possible with the help of GPS based automatic guidance systems.

The economic paybacks in using a GPS based automatic guidance system was analyzed summarized by Samuel Gan-Mor and Rex L. Clark from the University of Georgia in 2001 [1]. Table1.1 demonstrates that the market value for, or the profit in, using these GPS technologies ranges from a few cents up to a few dollars per acre.

Table 1.1 The additional cost farmers are paying for conventional operation performed with a GPS controlled system vs. Manual control [1]

The field operation	The automatic technology vs. the manual control	Cost difference $/acre
Variable rate application of fertilizers or lime	GPS controller driven	+1.08
Variable rate application of chemicals	GPS controller driven	+0.09
Variable rate seedings	GPS controller driven	+2.56

Matt Watson and Jess Lowenberg- Deboer from Purdue University have also demonstrated the benefit of using a GPS based guidance system [2]. They examined at a 1800 acre farm on a 50/50 corn-soybean rotation, which was considered a typical size crop operation in west central Indiana. It was indicated in the study that with the use of GPS guidance system, the average field operating speed can be increased by 20%. This will result in a saving of around 85 hours per season, not counting harvest, which would allow for work on additional farm land. Clearly, it has been previously demonstrated that use of automation in agriculture can both increase efficiency of resource use and reduce the time needed to perform necessary tasks.

1.2 Literature review on agricultural automatic guidance design

The historical development of an automatic tractor can be dated back to the early 20th century. In 1924, Willrodt [3] developed a steering attachment for tractors. This device can be adapted to be coupled to the forward axle of a tractor to follow a furrow that is previously formed, thus provide guidance for the tractor. The schematic of this type of steering attachment, and its relative position to a tractor is shown in Fig. 1.1. In 1941, Andrew [4]

developed a complete system of spiral farming based on piano wire winding upon a large diameter spool positioned centrally in a field. These early attempts of automatic steering are mostly mechanical, and did not receive much attention at the years they were proposed.

With the change in the agricultural industry over the past several decades, automatic guidance steering using electronic systems is well recognized not only by researchers, but also by manufacturers and agricultural producers. The advancement in sensors and technologies enabled the automatic steering system to be easily accessible and affordable. Many research works have been aimed at the development of guidance systems using location sensors that are based on image analysis, GPS, leader cable, laser beams, or other technologies. The research works that were conducted in the early 21st century are reviewed by Reid et al [5], Keicher and Seufert [6], and Torii respectively [7]. A more recent review is conducted by Li et al [8]. The framework for automation is shown in Fig. 1.2, and the closed loop architecture for an automatic guidance system is presented in Fig. 1.3.

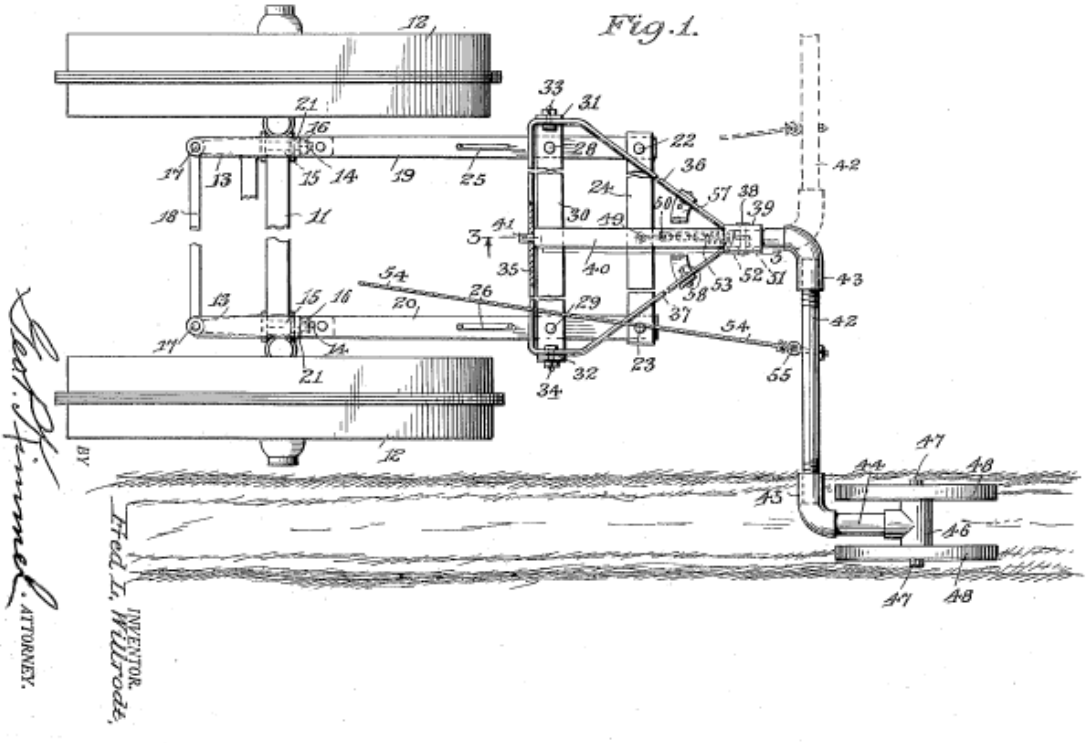

Figure 1.1 steering schematic of tractor guidance (scanned from U.S. Patent 1506706)

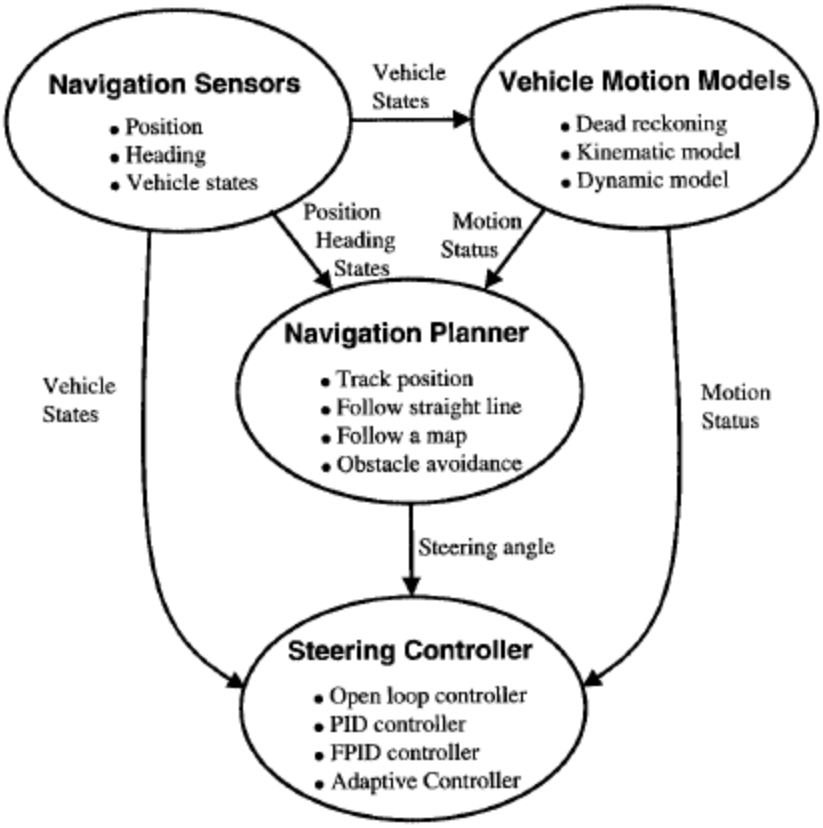

Figure 1.2 Basic elements of agriculture vehicle automation systems [5]

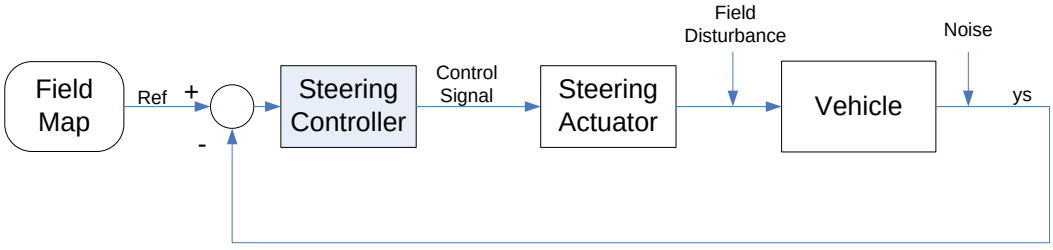

Figure 1.3 Closed loop architecture for automatic guidance system

Navigation sensors are used to provide information on vehicle position and vehicle heading. There are different types of navigation sensors used in the guidance study. The key heading and position sensors have included machine vision, GPS, with some work taking place with geomagnetic direction sensors (GDS) and inertial sensors. Mechanical feelers are capable of sensing the relative position of the tractor to the desired trajectory using a linkage.

These systems are quite effective at speed up to 10 km/h in maize, where the course is limited to straight rows. At slower speed, the systems can be used on curved rows [9]. Machine vision, incorporating a sensor mounted on the vehicle, is also a sensing modality that is capable of providing both relative position and heading of the vehicle. Previous research [10] has illustrated some performance equivalence of different sensing systems. For example, [10] illustrated that a machine vision based system was capable of guiding a small grain combine at the same accuracy level as the GPS recording system available.

In this research, a Global Positioning System (GPS) based guidance system was developed for a tractor. GPS based guidance system research has been extensive throughout the world due to their low cost, high accuracy and absence of drift and bias. In 1995, researchers in Stanford University successfully developed a Carrier-Phase GPS system for guiding a John Deere 7800 tractor [11]. A kinematic model was used in the research, and the discrete model was identified using recursive transfer function system identification techniques base on a Least Mean Squares algorithm. Least Mean Squares algorithm is a recursive type approach. Feed-forward U-turn trajectories were designed to require sufficient excitation of the vehicle dynamics, providing rich data for identification of an appropriate vehicle model in post-processing. A 1^{st} order model is used to describe the 'control to steering angle' transfer function, and a 2^{nd} order model is used to describe the 'control to heading angle' transfer function. The technique used for vehicle automatic control was a discrete Linear Quadratic Regulator/ Estimator. The control gains were chosen to minimize a quadratic cost function based on control inputs and state deviations from nominal. The experimental result shows zero mean with standard deviation of 5 centimeters. In 2000, this work of CDGPS based automatic tractor guidance has been generalized to non-linear trajectories, real-time model identification, and control along sloped terrain [12].

Researchers at the University of Illinois have also developed a GPS based automatic guidance system for agriculture vehicles operating at high field speed [13]. In the study [13], a second order model is developed for agriculture vehicles based on open loop frequency response test. The dynamics of steering equipment is also found to be important for controller design. A second order differentiator was implemented as the steering controller,

and the model-based guidance controller can provide adequate guidance system performance at forward velocities up to 6.8m/s.

1.3 Goals of current research

The studies we have listed above have focused on the design of a steering controller for a particular tractor. However, the level of performance degrades for so-called retrofit systems that effectively bolt-on to existing vehicles. If those types of method need to be transplanted to other vehicles, the whole design process needs to be repeated, a key aspect of this re-design involves accurately identification of vehicle parameters. The main difficulties lie in the different structure/ dynamics of each vehicle and the different tasks each vehicle needs to perform. Those variations in plant parameters or operating conditions will in turn change the controller performance. If the same level of closed loop performance needs to be maintained for different operating conditions, the controller needs to be designed for each application.

One of the possible solutions to this problem can be represented using a flowchart shown in Fig. 1.4. The idea of this type of steering controller design approaches involves the identification of the tractor model, and controller design based on the identified tractor model. The first two steps in the flowchart correspond to the tractor model identification, where the third step in the flowchart gives the specification for controller design. The fourth step is the controller design based on the identified plant model, with the last step being the evaluation of the closed loop performance. This design process can be iterated if the designed controller does not meet the initial design requirement.

One of the most difficult aspects of designing a controller for vehicle guidance is arriving at an appropriate model of vehicle dynamics and disturbances. Ground vehicle dynamics range from very simple to overwhelmingly complex, and there is no single model that is widely accepted in the literature [11]. Especially for the purpose of controller design, a very complex model is not always the most appropriate to use. Tractor dynamics model identification can be based on vehicle parameter estimation, which includes vehicle mass, moment of inertia, and cornering stiffness [14]. With those parameter measurements, an

accurate dynamics model can be obtained. However, these parameters are sometimes hard to measure and not always accessible.

Open loop tests [13] for tractors using sinusoidal (frequency domain) or pseudo-random binary sequence (time domain) control inputs posed a problem in our experimental conditions. Only a limited amount of data could be taken before the vehicle traveled to the end of the particular test field of operation. For this reason, a closed loop identification scheme is required. Since the identification experiment usually requires some level of excitation, an open-field with no crop is thus optimal for the identification purpose. Since field area is a very valuable resource in agriculture, the identification needs to be conducted in as small an area of field as is feasible. In addition, with the current agriculture steering products, the choices of reference signals are limited. Those reasons differentiate the identification of a tractor model from other general system identification problems, and these constraints need to be taken into consideration in choosing an appropriate identification algorithm.

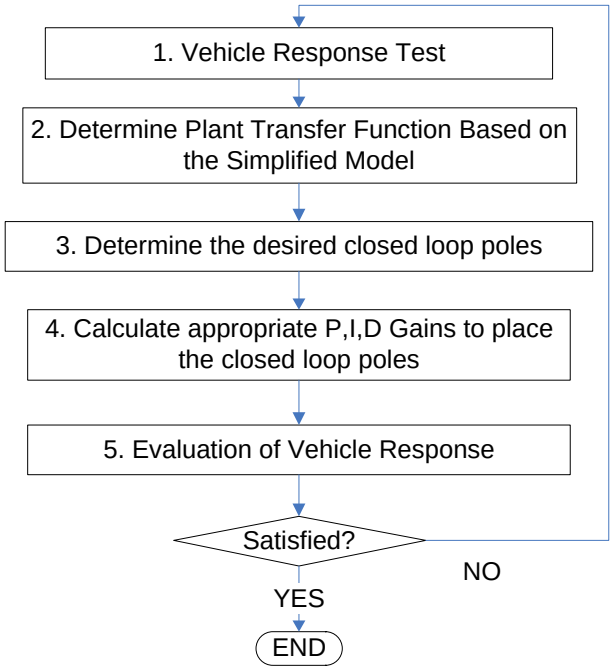

Figure 1.4 Automatic steering controller development flowchart

The goal of this research is to develop a practical tractor dynamics identification protocol for the purpose of controller design with constraints in identification field area and limitation in the selection of reference trajectories. Since the tractors are capable of repeating its trajectories, iterative learning identification is one of the possible solutions.

1.4 Introduction of Iterative Learning Identification (ILI)

Iterative Learning Identification (ILI) is a novel approach for closed loop identification [15] [16] [17]. This method achieves identification by applying Iterative Learning Control (ILC) [18]concepts in the presence of measurement noise without any knowledge of the feedback controllers in the loop.

A comparison between ILI and ILC can be found in Fig. 1.5. The purpose of ILI is to find an optimal set of parameters in the estimated plant model to minimize the model error $e_{\text{model}}{}^{j}$ measured in Fig. 1.5 (a). It stores the estimated parameters in j-th trial, and multiplies it by a learning gain L_{γ}. It then measures the model error from the current trial and multiply it by a learning gain of L_{e}. The estimated parameters at a future j+1-th trial is thus updated based on the summation of the previous terms. In ILC, the purpose is to find an optimal set of feedforward signal to minimize the output error. The architecture is shown in Fig. 1.5 (b), where the current feedforward signal is updated based on the feedforward signal generated from the previous trial, and the output error measured from the current trial.

ILI considers systems that repeat the same reference trajectory with a view to sequentially improving parameter estimation accuracy. The algorithm generates the estimation of parameters from the new trial by adding a ‘correction’ term to the estimated parameters from the previous trial. ILC is based on the notion that the performance of a system that executes the same task multiple times can be improved by learning from previous executions (trials, iterations, passes).

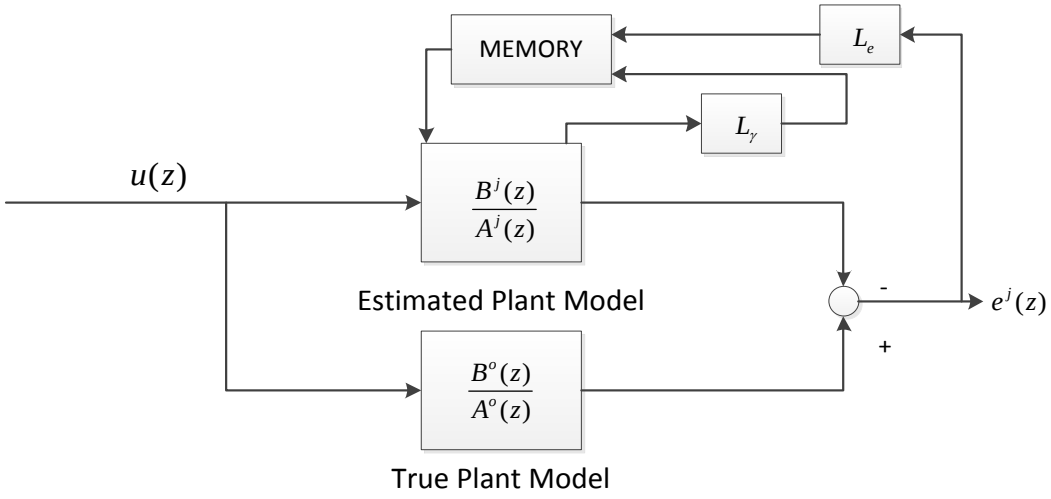

(a)

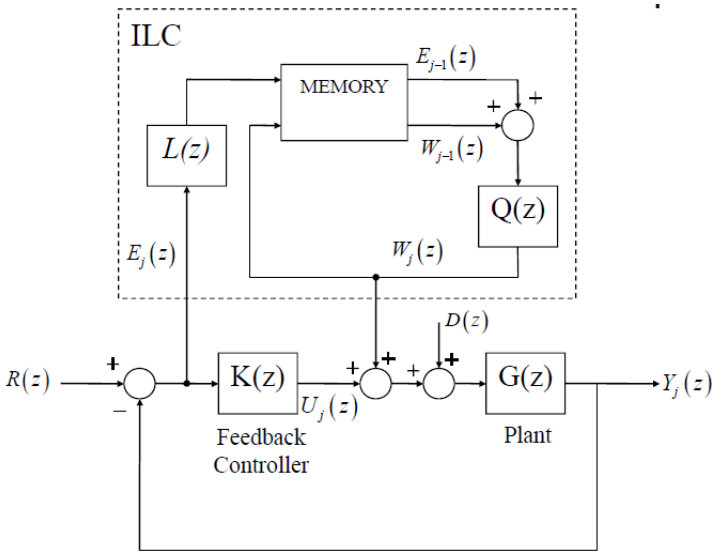

(b)

Figure 1.5 (a) ILI architecture (b) ILC architecture [18]

The effectiveness of ILI has been previously demonstrated through numerical examples. One of the most important reasons for using ILI is that this type of algorithms can be repeated in a relatively small area, which enables us to identify the tractor dynamics model in a relatively small amount of field.

1.5 Overview of remaining chapters

The remaining chapters are organized as follows. In chapter2, a second order agricultural vehicle model is developed based on a well-known bicycle model. Chapter 3 discusses the parameter identification methods, including Iterative Learning Identification (ILI), and two classical identification approaches – Least Square Estimation and Gradient Adaptive Estimation. In chapter 4, the simulation results for both the ILI method and the classical approaches are presented with a highlight in the benefits for ILI. Chapter 5 compares the experimental identification results between ILI and the classical identification methods. In chapter 6, a controller is developed based on the identified model from ILI, and the setup and results for the hardware-in the loop test are also presented. Conclusions and future works are discussed in Chapter 7.

Chapter 2
Lateral Vehicle Dynamics

The purpose of the study is to develop a lane-keeping system, which is capable of automatically controlling the steering to keep the vehicle in its lane. Therefore, controlling the lateral vehicle dynamics are the main interest of this study. In this chapter, low order vehicle lateral dynamics model is developed.

A vehicle lateral dynamics model can range from simple to very complex. However, those complex models are not proper to use, especially since controller and estimator design require a simple, typically linearized model of plant dynamics. For most vehicle control applications, it has been demonstrated that a relatively low order 'bicycle model' dynamics are usually sufficient for a linearized version of the plant.

This chapter is organized as follows. Section 2.1. describes two widely recognized lateral vehicle models: kinematic model and bicycle model. Section 2.2 gives the simplified result of a bicycle model. The structure of this simplified bicycle model will be adopted in the following chapters for the tractor machine. The nomenclature of this chapter is included in the end of the chapter.

2.1 Lateral Vehicle Model

2.1.1 Kinematic Model [19]

A kinematic model describes the vehicle motion without consideration of the forces that cause the motion. It is obtained purely based on the geometric relationships governing the system with a 'bicycle model' assumption.

The basic assumptions in 'bicycle' model are that both the left and right front wheels were represented by one front wheel, and both the left and right rear wheels were represented by one rear wheel for an all-wheel steering vehicle (Figure 2.1). From the Ackerman turning geometry, this assumption is not exactly true because the wheels on the inside and outside of a turn need to trace out circles of different radii. However, when the turning radius is sufficiently big comparing to the vehicle geometry, the left and right steering angles are approximately equal, and the difference is ignored.

The geometric relationships of a 'bicycle' model with two degrees of freedom are shown in Figure 2.1. The two degrees of freedom are represented by vehicle lateral position y, and vehicle yaw angle ψ, which describes the orientation of the vehicle. The influence of road bank angle is not taken into account in developing the model. Assuming all-wheel steering vehicle, the steering angles for the front and rear wheels are represented by δ_f and δ_r, respectively. For a front-steered vehicle, the rear steered wheel angle δ_r equals to 0 for all the time. The center of gravity (c.g.) is at point C. The distances from the vehicle c.g. to the front and rear wheels axles are l_f and l_r, respectively. The vehicle slip angle β is the angle between the vehicle velocity at c.g. and the vehicle longitudinal axis.

From geometric analysis, the following equations of motion can be obtained [19].

$$\begin{aligned} \dot{x} &= V\cos(\psi+\beta) \\ \dot{y} &= V\sin(\psi+\beta) \\ \dot{\psi} &= \frac{V\cos\beta}{l_f+l_r}(\tan\delta_f-\tan\delta_r) \end{aligned} \qquad (2.1)$$

In this model, V denotes the longitudinal velocity of the vehicle, and can be time varying. One major assumption of a kinematic model is that the velocity vectors at point A and B are in the direction of the orientation of the front and rear wheels respectively. This equals to assuming that there are no 'slip angles' on both wheels. This is a reasonable assumption for low speed motion of the vehicle.

This model has been adopted for low speed agricultural vehicle guidance design. Researchers in Stanford University have successfully developed a Carrier- Phase GPS system

for guiding a John Deere 7800 tractor based on a kinematic tractor model [20]. The experimental result shows zero mean with standard deviation of 5 centimeters.

However, since this study is hoping to generalize the design of an autonomous controller to high speed operations as well, the kinematic model is not adopted. Instead, a more generalized 'bicycle' model which released the assumption of no 'slip angles' is being used in this work.

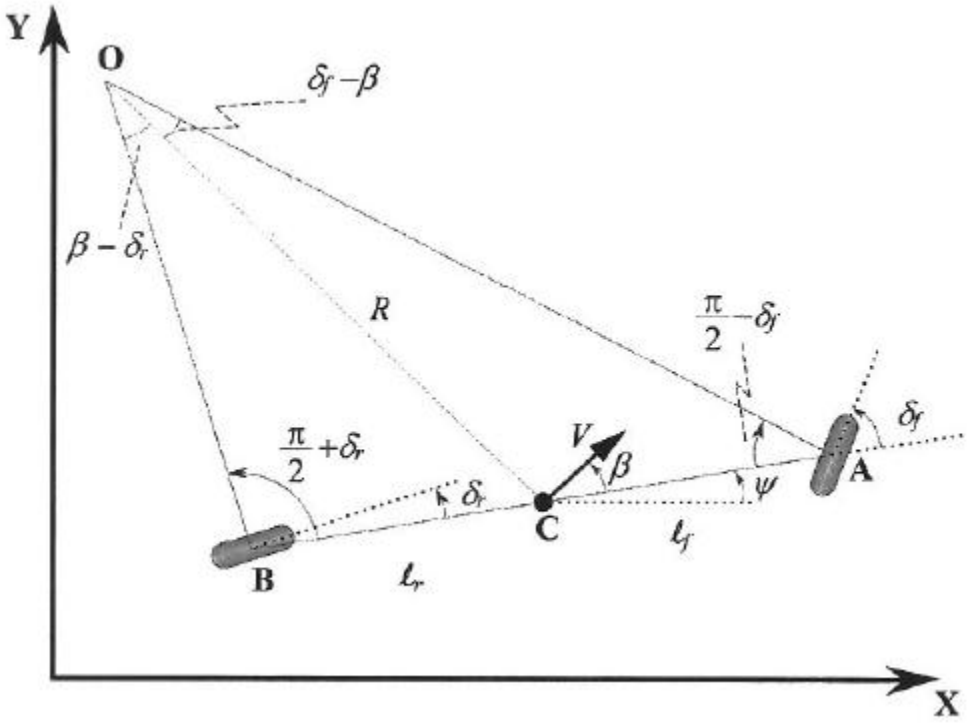

Figure 2.1 Kinematics of lateral vehicle motion (scanned from [19])

2.1.2 Bicycle Model [19]

At higher vehicle speeds, instead of using a kinematic model, a dynamic model needs to be developed. This dynamics model takes into account the fact that the velocity at each wheel is not in the direction of the wheel. In other words, 'slip angles' are not zero.

As shown in Fig. 2.2, there are two degrees of freedom considered in the vehicle model. The two degrees of freedom are represented by vehicle lateral position y and vehicle yaw angle ψ. The vehicle lateral position is measured along the lateral axis of the vehicle to a point O which is the center of rotation of the vehicle. The vehicle yaw angle ψ is measured with respect to the global X axis. The longitudinal velocity of the vehicle at the center of gravity (c.g.) is denoted by V_x.

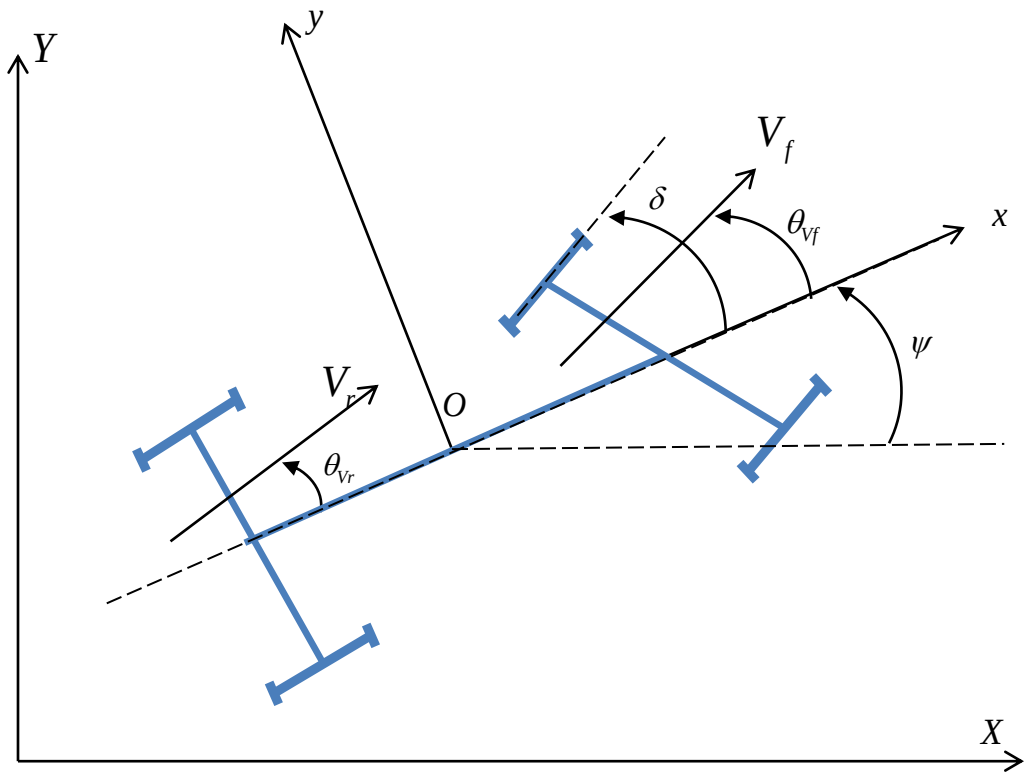

Figure 2.2 Lateral Vehicle Dynamics

By applying Newton's second law for motion along the y axis,

$$ma_y = F_{yf} + F_{yr} \qquad (2.2)$$

where $a_y = \frac{d^2y}{dt^2}$ is the inertial acceleration of the vehicle at c.g. in the direction of the *y* axis and F_{yf} and F_{yr} are the lateral tire forces of the front and rear wheels respectively. Two

terms contribute to a_y: the acceleration which is due to motion along the y axis and the centripetal acceleration $V_x\dot{\psi}$. Hence

$$a_y = \ddot{y} + V_x\dot{\psi} \qquad (2.3)$$

Substituting from Eq. 2.3 into Eq. 2.2, the equation for the lateral translation motion of the vehicle is obtained as

$$m(\ddot{y} + V_x\dot{\psi}) = F_{yf} + F_{yr} \qquad (2.4)$$

Moment balance about the z axis yields the equation ofr the yaw dynamics as

$$I_z\ddot{\psi} = l_f F_{yf} - l_r F_{yr} \qquad (2.5)$$

where l_f and l_r are the distances of the front tire and the rear tire respectively from the c.g. of the vehicle.

Experimental results show that the lateral tire force of a tire is proportional to the "slip-angle" for small slip-angle. The slip angle of a tire is defined as the angle between the orientation of the tire and the orientation of the velocity vector of the wheel. Fig. 2.2, the slip angle of the front wheel is

$$\alpha_f = \delta - \theta_{V_f} \qquad (2.6)$$

where θ_{V_f} is the angle between the velocity vector of the front wheel makes with the longitudinal axis of the vehicle and δ is the front wheel steering angle. The rear slip angle is similarly given by

$$\alpha_r = -\theta_{V_r} \qquad (2.7)$$

By taking the assumption that the lateral tire force of a tire is proportional to the 'slip angle', the lateral force for the front wheels of the vehicle can therefore be written as

$$F_{yf} = C_{\alpha f}(\delta - \theta_{V_f}) \qquad (2.8)$$

where the proportionality constant $C_{\alpha f}$ is called the cornering stiffness of both front tires, δ is the front wheel steering angle.

Similarly, the lateral tire for the rear wheels can be written as

$$F_{yr} = C_{\alpha r}(\delta - \theta_{V_r}) \qquad (2.9)$$

where $C_{\alpha r}$ is called the cornering stiffness of the rear tires, θ_{V_r} is the angle between the velocity vector of the rear wheel makes with the longitudinal axis of the vehicle.

To calculate θ_{V_f}

$$\tan(\theta_{V_f}) = \frac{V_y + l_f\dot{\psi}}{V_x} \qquad (2.10)$$

Using small angle approximation and use the notation $V_y = \dot{y}$,

$$\theta_{V_f} = \frac{\dot{y} + l_f\dot{\psi}}{V_x} \qquad (2.11)$$

Similarly, θ_{V_r} can be calculated as,

$$\tan(\theta_{V_r}) = \frac{V_y - l_r\dot{\psi}}{V_x} \qquad (2.12)$$

$$\theta_{V_r} = \frac{\dot{y} - l_r\dot{\psi}}{V_x} \qquad (2.13)$$

Substituting from Eqs, 2.6, 2.7, 2.11, and 2.13 into Eqs. 2.4 and 2.5, the state space model can be written in (2.14).

$$\frac{d}{dt}\begin{bmatrix} y \\ \dot{y} \\ \psi \\ \dot{\psi} \end{bmatrix} = \begin{bmatrix} 0 & 1 & 0 & 0 \\ 0 & \frac{C_{\alpha f}+C_{\alpha r}}{mV} & -\frac{C_{\alpha f}+C_{\alpha r}}{m} & \frac{l_f C_{\alpha f} - l_r C_{\alpha r}}{mV} \\ 0 & 0 & 0 & 1 \\ 0 & \frac{l_f C_{\alpha f} - l_r C_{\alpha r}}{I_z V} & -\frac{l_f C_{\alpha f} - l_r C_{\alpha r}}{I_z} & \frac{l_f^2 C_{\alpha f} + l_r^2 C_{\alpha r}}{I_z V} \end{bmatrix} \begin{bmatrix} y \\ \dot{y} \\ \psi \\ \dot{\psi} \end{bmatrix} + \begin{bmatrix} 0 \\ -\frac{C_{\alpha f}}{m} \\ 0 \\ -\frac{l_f C_{\alpha f}}{I_z} \end{bmatrix} \delta \qquad (2.14)$$

where y is the vehicle lateral position, ψ denotes the yaw angle, $C_{\alpha f}$ and $C_{\alpha r}$ are called the cornering stiffness of the front tires and rear tires respectively, m is the vehicle mass, V is the longitudinal velocity, I_z is the vehicle inertia, and δ is the front wheel steering angle.

Equation (2.14) defines vehicle lateral dynamics in vehicle coordinate. When the objective is to develop a steering control system for automatic guidance, it is useful to utilize a dynamic model in which the state variables are in terms of position and orientation error with respect to the road.

Hence the lateral model developed in Eq. (2.14) will be re-defined in terms of the following error variables [21]:

y_r, the distance of the c.g. of the vehicle from the center line of the road as shown in Figure 2.3

$\psi - \psi_d$, the orientation error of the vehicle with respect to the road as shown in Figure 2.3, where desired road yaw angle is ψ_d, the yaw angle of the vehicle body respect to the vehicle longitudinal axis is ψ.

Now, assume that the road radius R is large so that the small angle assumptions as in the 'bicycle model' can be made. Define the rate of change of the desired orientation of the vehicle as

$$\psi_d = \frac{V_x}{R} \qquad (2.15)$$

$$y_r = y + V_x(\dot{\psi} - \dot{\psi}_{des}) \qquad (2.16)$$

Substitute Eqs. (2.15) and (2.16) into Eq. (2.14), a state space model with the state variables defined as the position and orientation error with respect to the road can be written as

$$\frac{d}{dt}\begin{bmatrix} y_r \\ \dot{y}_r \\ \psi-\psi_d \\ \dot{\psi}-\dot{\psi}_d \end{bmatrix} = \begin{bmatrix} 0 & 1 & 0 & 0 \\ 0 & \frac{C_{\alpha f}+C_{\alpha r}}{mV} & -\frac{C_{\alpha f}+C_{\alpha r}}{m} & \frac{l_f C_{\alpha f}-l_r C_{\alpha r}}{mV} \\ 0 & 0 & 0 & 1 \\ 0 & \frac{l_f C_{\alpha f}-l_r C_{\alpha r}}{I_z V} & -\frac{l_f C_{\alpha f}-l_r C_{\alpha r}}{I_z} & \frac{l_f^2 C_{\alpha f}+l_r^2 C_{\alpha r}}{I_z V} \end{bmatrix} \begin{bmatrix} y_r \\ \dot{y}_r \\ \psi-\psi_d \\ \dot{\psi}-\dot{\psi}_d \end{bmatrix} + \begin{bmatrix} 0 \\ -\frac{C_{\alpha f}}{m} \\ 0 \\ -\frac{l_f C_{\alpha f}}{I_z} \end{bmatrix} \delta + \begin{bmatrix} 0 \\ \frac{l_f C_{\alpha f}-l_r C_{\alpha r}}{m} - V^2 \\ 0 \\ \frac{l_f^2 C_{\alpha f}+l_r^2 C_{\alpha r}}{I_z} \end{bmatrix} \frac{1}{R} \qquad (2.17)$$

Making the small angle assumption, the output taken as the measurement of lateral deviation from a sensor located a distance d_s ahead of the vehicle c.g., can be expressed as:

$$y_s = y_r + d_s(\varepsilon - \varepsilon_d) = [1, 0, d_s, 0]\begin{bmatrix} y_r \\ \dot{y}_r \\ \varepsilon-\varepsilon_d \\ \dot{\varepsilon}-\dot{\varepsilon}_d \end{bmatrix} \qquad (2.18)$$

The state space model in (2.17) and (2.18) can be expressed using transfer functions from the front wheel steering angle, $\delta(s)$, to the lateral measurement from the sensor, $y_s(s)$. The road curvature $\frac{1}{R}$ can be looked as a disturbance term in in (2.17).

This model has been widely recognized for automatic vehicle designs [20] [22] [23] [24].

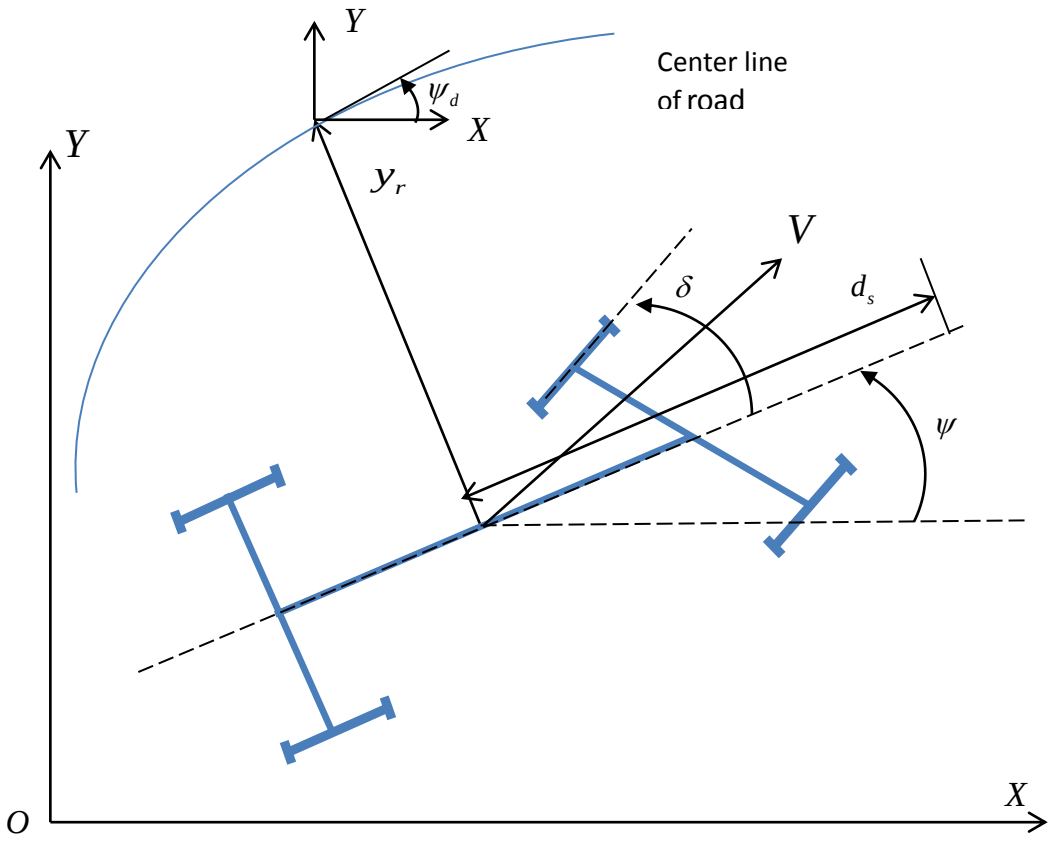

Figure 2.3 Vehicle lateral dynamics with respect to desired road

2.2 Simplified Bicycle Model

2.2.1 Simplification of the bicycle model

Substitute a typical set of agricultural tractor parameters [25] from Table 2.1 into Eqs (2.17) and (2.18), then assume that the vehicle longitudinal velocity is fixed at 5mph and the sensor is placed 0.5 meter ahead of vehicle c.g. If the road curvature is zero, the state space model can be expressed as in Eq. (2.19).

Table 2.1 A typical set of tractor parameters

Parameter	symbol	value
Longitudinal Velocity	V	5 mph
Moment of Inertia	I_z	35709Kg-m^2
Vehicle Mass	m	9391Kg
CG to front wheel	l_f	1.7m
CG to rear wheel	l_r	1.2m
Rear cornering Stiffness	$C_{\alpha r}$	486N/rad
Front cornering Stiffness	$C_{\alpha f}$	220N/rad
CG to magnetic sensor	d_s	3m

$$\frac{d}{dt}\begin{bmatrix} y_r \\ \dot{y}_r \\ \varepsilon-\varepsilon_d \\ \dot{\varepsilon}-\dot{\varepsilon}_d \end{bmatrix} = \begin{bmatrix} 0 & 1 & 0 & 0 \\ 0 & -5.058 & 12.44 & -3.906 \\ 0 & 0 & 0 & 1 \\ 0 & -1.379 & 3.391 & -12.09 \end{bmatrix}\begin{bmatrix} y_r \\ \dot{y}_r \\ \varepsilon-\varepsilon_d \\ \dot{\varepsilon}-\dot{\varepsilon}_d \end{bmatrix} + \begin{bmatrix} 0 \\ 6.897 \\ 0 \\ 7.304 \end{bmatrix}\delta$$

$$y_s = \begin{bmatrix} 0 & 6.897 & 0 & 7.304 \end{bmatrix}\begin{bmatrix} y_r \\ \dot{y}_r \\ \varepsilon-\varepsilon_d \\ \dot{\varepsilon}-\dot{\varepsilon}_d \end{bmatrix} \qquad (2.19)$$

The transfer function from $\delta(s)$ to $y_s(s)$ is expressed as:

$$G(s) = 62.3202\frac{(s+8.3455)(s+1.7497)}{s^2(s+39.2902)(s+10.8859)} \qquad (2.20)$$

Agriculture vehicles usually operate in a relatively low frequency range as compared to on-highway vehicles due to their relatively low sampling frequency. Examining Eq. (2.20) shows that the fourth order vehicle model has two poles (-39.2902, -10.8859) and one zero (-8.3455) which characterize dynamics at least 4 times faster than the other poles (0,0) and zero (-1.7497). The root locus plot of the 4th order model Eq. (2.20) is shown in Figure 2.4 .

Therefore, the 4th order model in Eq. (2.20) can be further simplified by truncating the high frequency poles and zeros into a simple second order formulation in the form of

$$G(s) = k\frac{s+a}{s^2} = \frac{b_1 s + b_0}{s^2} \qquad (2.21)$$

where b_1 and b_0 are positive constants which depend on the vehicle parameters and operating conditions.

Using the parameters from Table 2.1, the simplified second order model is expressed as:

$$G(s) = 2.1276\frac{s+1.7497}{s^2} \qquad (2.22)$$

and its root locus plot is shown in Figure 2.4 .

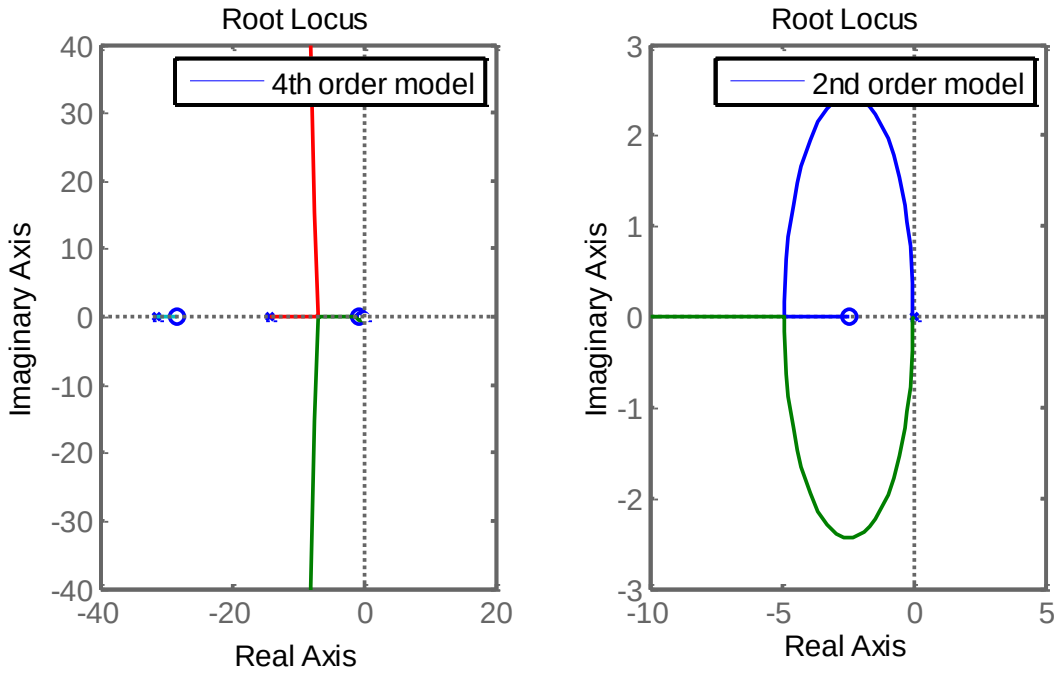

Figure 2.4 Root locus plot of the 4th order and 2nd order system

2.2.2 Frequency and time domain verification of the simplified model

The Bode plot comparison of the 4th order model from and the 2nd order model from is shown in Figure 2.5. From the plots, we see that the 2nd order model (2.22) is representative of the 4th order model (2.20) for low frequency operations.

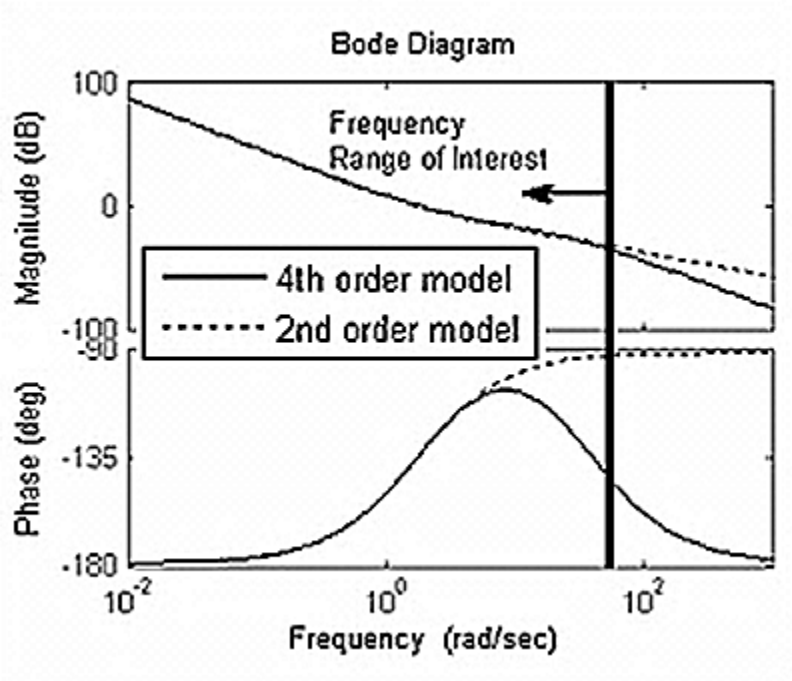

Figure 2.5 Bode plot for a 4th order and 2nd order model

Open loop simulations are also performed to confirm that the responses of the 2nd order model (2.22) are representative of a 4th order model (2.20) under typical low frequencies.

Three types of input signals are used in the simulation: sinusoidal, ramp and trapezoidal [26]. For the steering commands shown in Figure 2.6, the simulated responses by the 4th order model and the second order model are shown in Figure 2.7. According to Figure 2.7, a 2nd order model is representative of a 4th order one in the open loop simulation.

Previous investigation [27] has also demonstrated the suitability of a 2nd order model for agricultural vehicle application. In their study, the 2nd order model is obtained from experiment by taking the sinusoidal sweep of an agricultural vehicle. This model structure is verified in Chapter 4 with experimental results.

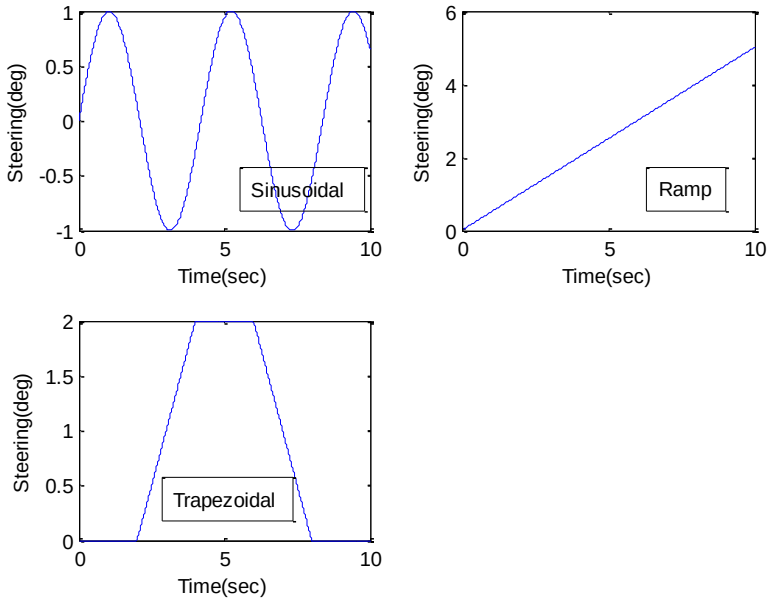

Figure 2.6 Steering commands in open loop simulation

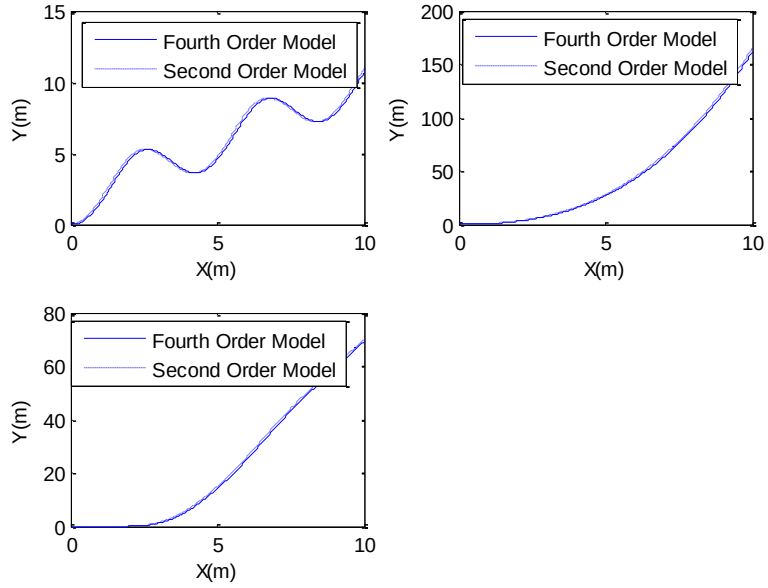

Figure 2.7 response of vehicle in open loop simulation

Chapter 3

Parameter Estimation Methods

In the previous chapter, a low order vehicle dynamics model structure is developed. The controller design will be made possible if the parameters in the vehicle dynamics model are determined. This chapter will introduce three different parameter estimation approaches – Least Square Estimation, Adaptive Estimation, and Iterative Learning Identification – which will be adopted in the study to estimate the parameters in the tractor dynamics model.

3.1 General Description and Input Signal Selection

3.1.1 General Description of Parameter Estimation

There are two ways to obtain the parameters in the vehicle dynamics model. One is to estimate the vehicle dynamics model based on vehicle parameters estimation, which includes vehicle mass, moment of inertia, and cornering stiffness. However, these parameters are hard to measure and not always accessible.

Another way to obtain the vehicle parameters is by using system identification methods. System identification is the field of modeling dynamic systems from experimental data. A dynamic system – in our example, tractor dynamics system – can be characterized by their structures and parameters. The structure of a dynamic system can be determined either by analytic approach or by experimental approach. The structure of the tractor dynamics model is obtained analytically from vehicle dynamics analysis, and is discussed in Chapter 2. When the structure of the system is known, parameter estimation is used to determine the system parameters. When input signals are applied to a system, response signals are

generated by the system. Parameter estimation uses a collection of available system signals, based on certain system structure information and optimality criteria, to produce estimates of the system parameters.

In general terms, an identification experiment is performed by exciting the system and observing its input and output over a time interval [28]. These signals are recorded. We then try to fit a parametric model of the process to the recorded input and output sequences. The first step is to determine an appropriate form of the model (in our case, the tractor model structure is determined in chapter 2). As a second step, some parameter identification method is used to estimate the unknown parameters of the model. Three different parameter estimation methods are introduced in this chapter to estimate the unknown parameters. The model obtained is then tested to see whether it is an appropriate representation of the system. Both simulation and experimental validations are shown respectively for the case of tractor dynamics model identification in Chapter 4 and 5. The procedures for system identification in general are illustrated in Fig. 3.1.

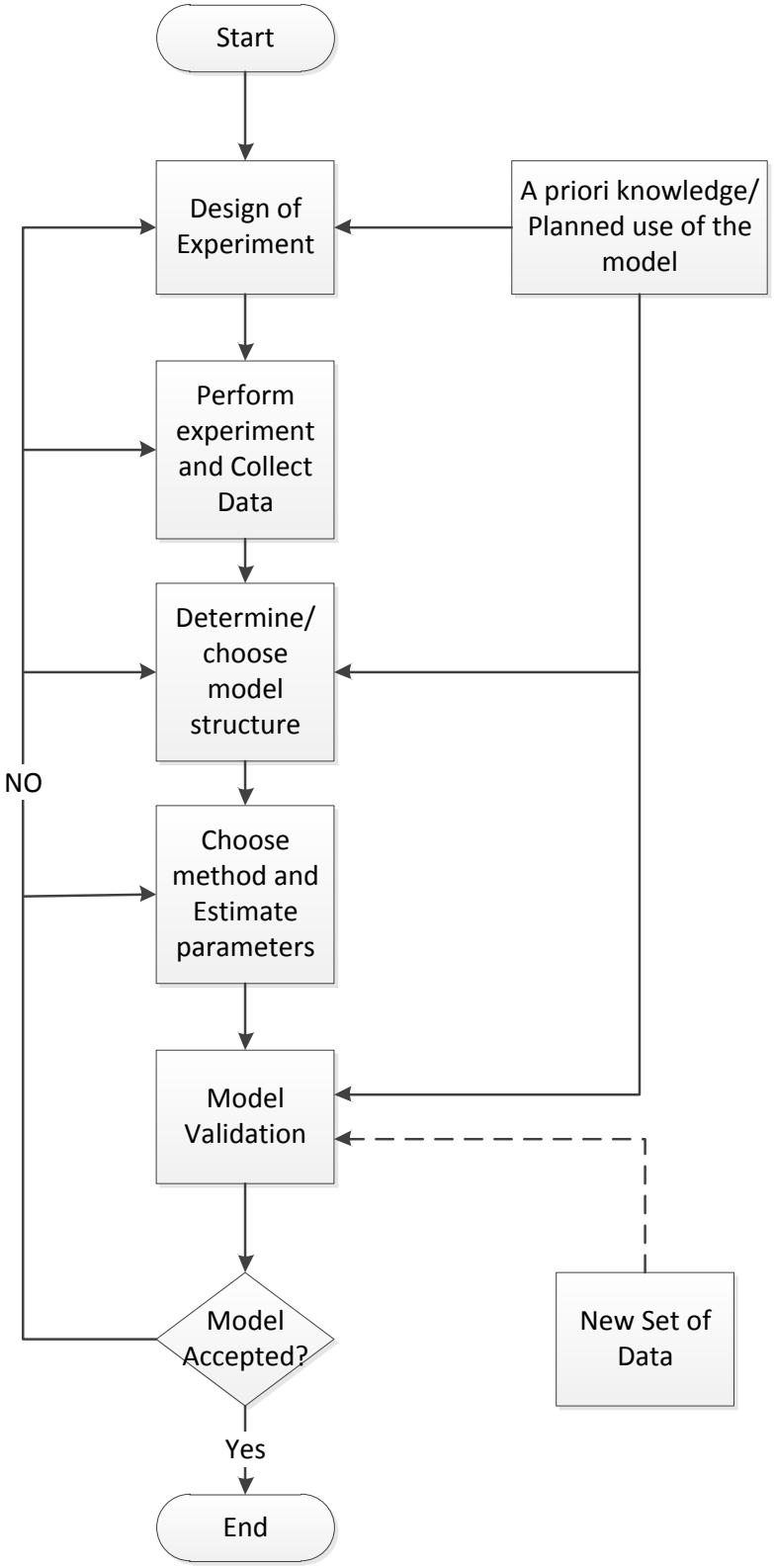

Figure 3.1 Schematic flowchart of system identification [28]

3.1.2 Identification in Closed Loop

A set of sinusoidal tests within a range of frequencies are analyzed to determine the system's frequency response. This open loop sinusoidal sweep approach is challenging in agricultural settings due to the limited area available to perform the necessary tests. The two integrators present in the vehicle dynamics suggest a spatial drift during open loop tests. Since land, and the resident crops, in an agricultural setting are very valuable, the open loop sine sweep approach is limited.

There are many systems work under feedback control. This is typical, for example, in the process industry for the production of paper, cement, glass, etc. For some systems, the open loop system may be unstable or so poorly damped that no identification experiment can be performed in open loop. This is true for the case of a tractor dynamics model. If open loop experiment is used for the identification, tractor would soon reach the boundary of the field. Closed loop identification is considered more appropriate for farm vehicle identification.

3.2 Classic Approaches

3.2.1 Least Squares Estimation (LSE)

3.2.1.1 System Description

Least squares estimation is one of the most common system identification approaches. This section presents a discussion and analysis of linear regression and its application to the tractor model structure. The linear regression is the simplest type of parametric model. The corresponding model structure in discrete domain can be written as

$$y(t) = \varphi^T(t)\theta \qquad (3.1)$$

Where $y(t)$ -- system output – is called regressed variable, and is a measurable quantity. $\varphi(t)$ is called regression variables or regressors, and is also a known quantity. θ is called the parameter vector, and is a vector of unknown parameters.

The problem is to find an estimate $\hat{\theta}$ of the parameter vector θ from measurements $y(1), \varphi(1), \ldots, y(N), \varphi(N)$, where N denotes the number of data points.

The system linear equations are:

$$\begin{aligned} y(1) &= \varphi^T(1)\theta \\ y(2) &= \varphi^T(2)\theta \\ &\vdots \\ y(N) &= \varphi^T(N)\theta \end{aligned} \qquad (3.2)$$

This can be written in matrix notation as

$$Y = \Phi\theta \qquad (3.3)$$

Where

$$Y = \begin{bmatrix} y(1) \\ \vdots \\ y(N) \end{bmatrix} \qquad (3.4)$$

$$\Phi = \begin{bmatrix} \varphi^T(1) \\ \vdots \\ \varphi^T(N) \end{bmatrix} \qquad (3.5)$$

3.2.1.2 LSE Algorithm

Assume we have already obtained an estimate of the parameter vector $\hat{\theta}$. Now, introduce the equation of error, which is also known as the residuals.

$$\varepsilon(t) = y(t) - \varphi^T(t)\hat{\theta} \qquad (3.6)$$

The error is defined as

$$\varepsilon = \begin{bmatrix} \varepsilon(1) \\ \vdots \\ \varepsilon(N) \end{bmatrix} \qquad (3.7)$$

Therefore,

$$\varepsilon = Y - \Phi\hat{\theta} \tag{3.8}$$

Define a loss function

$$V(\theta) = \frac{1}{2}\varepsilon^T\varepsilon = \frac{1}{2}\|\varepsilon\|^2 \tag{3.9}$$

Substitute (3.6) into (3.9), we have

$$\begin{aligned} V(\theta) &= \frac{1}{2}\varepsilon^T\varepsilon \\ &= \frac{1}{2}(Y - \Phi\hat{\theta})^T(Y - \Phi\hat{\theta}) \\ &= \frac{1}{2}(\theta^T\Phi^T\Phi\theta - \theta^T\Phi^TY - Y^T\Phi\theta + Y^TY) \\ &= \frac{1}{2}[\theta - (\Phi^T\Phi)^{-1}\Phi^TY]^T(\Phi^T\Phi)[\theta - (\Phi^T\Phi)^{-1}\Phi^TY] \\ &\quad + \frac{1}{2}[Y^TY - Y^T\Phi(\Phi^T\Phi)^{-1}\Phi^TY] \end{aligned} \tag{3.10}$$

The second term, $[Y^TY - Y^T\Phi(\Phi^T\Phi)^{-1}\Phi^TY]$ does not depend on θ. Since $(\Phi^T\Phi)$ is positive definite, the first term $[\theta - (\Phi^T\Phi)^{-1}\Phi^TY]^T(\Phi^T\Phi)[\theta - (\Phi^T\Phi)^{-1}\Phi^TY]$ is always greater than or equal to zero. Thus can be minimized by setting the first term to zero. This gives

$$\hat{\theta} = (\Phi^T\Phi)^{-1}\Phi^TY \tag{3.11}$$

Therefore, least squares estimate gives an estimate of parameter vector θ by minimizing the cost function defined in (3.9).

Example

Let us apply the theorem to the case of tractor dynamics model structure. From Chapter 2, the tractor lateral model can be written in the form of Eq. (3.12).

$$G(s) = k\frac{s+a}{s^2} = \frac{b_1s + b_0}{s^2} \tag{3.12}$$

Rewrite Eq. (3.12) in z-domain gives,

$$G(z) = \frac{Y(z)}{U(z)} = \frac{b_1 T z + b_0 T^2 - b_1}{z^2 - 2z + 1} \quad (3.13)$$

Using Euler approximation, Eq. (3.13) can be reformulated as Eq. (3.14) where T denotes the sampling time.

$$y(k+2) - 2 * y(k+1) + y(k) = b_1 * T * u(k+1) + (b_0 T^2 - b_1 T) * u(k) \quad (3.14)$$

Define

$$\theta = \begin{bmatrix} b_1 T \\ b_0 T^2 - b_1 T \end{bmatrix} \quad (3.15)$$

A comparison with Eq. (3.3) gives

$$Y = \begin{pmatrix} y(3) - 2y(2) + y(1) \\ y(4) - 2y(3) + y(2) \\ : \\ : \\ y(N) - 2y(N-1) + y(N-2) \end{pmatrix} \Phi = \begin{pmatrix} u(2) & u(1) \\ u(3) & u(2) \\ : & : \\ : & : \\ u(N-1) & u(N-2) \end{pmatrix} \quad (3.16)$$

The estimate of θ is obtained through (3.11).

3.2.2 Gradient based Adaptive Estimation

3.2.2.1 System Model

Consider a linear time-invariant system described by the differential equation [29]

$$A(s)[y](t) = B(s)[u](t) \quad (3.17)$$

Where, *y(t)* and *u(t)* are the measured system input and output;

$$A(s) = s^n + a_{n-1} s^{n-1} + \cdots + a_1 s + a_0 \quad (3.18)$$

$$B(s) = b_m s^m + b_{m-1} s^{m-1} + \cdots + b_1 s + b_0 \quad (3.19)$$

are polynomials in s with s being the time differentiation operator, $s[x](t) = \dot{x}(t)$; and a_i, b_i are the unknown but constant system parameters to be estimated.

We can define

$$\theta = \begin{bmatrix} b_m & \dots & b_0 & a_{n-1} & \cdots & a_0 \end{bmatrix} \quad (3.20)$$

$$Y = \begin{bmatrix} u^{(m-1)}(t) & \dots & u(t) & -y^{(n-1)}(t) & \cdots & -y(t) \end{bmatrix} \quad (3.21)$$

And solve Eq. (3.17) for the highest derivative to get

$$y^{(n)} = \theta^T Y \quad (3.22)$$

3.2.2.2 Gradient Algorithm

A normalized gradient algorithm for updating the parameter estimate $\theta(t)$ is to choose the derivative of $\theta(t)$, in a steepest descent direction, to successively generate $\theta(t)$ to minimize a normalized quadratic cost function.

Choose a stable polynomial $\Lambda(s) = s^n + \lambda_{n-1}s^{n-1} + \cdots + \lambda_1 s + \lambda_0$. Operating both sides of by the stable filter $\frac{1}{\Lambda(s)}$, we have

$$z := \frac{1}{\Lambda(s)} y^{(n)} = \frac{s^n}{\Lambda(s)} y \quad (3.23)$$

Define a regressor vector

$$\phi := \frac{1}{\Lambda(s)} Y = \begin{bmatrix} \frac{s^{m-1}}{\Lambda(s)}u(t) & \dots & \frac{1}{\Lambda(s)}u(t) & -\frac{s^{n-1}}{\Lambda(s)}y(t) & \cdots & -\frac{1}{\Lambda(s)}y(t) \end{bmatrix} \quad (3.24)$$

Substitute Eq. (3.24) and Eq. (3.23) into Eq. (3.22), we can get the normalized output, z:

$$z = \theta^T \phi \quad (3.25)$$

According to Eq. (3.25), the prediction of z can be defined as:

$$\hat{z} = \hat{\theta}^T \phi \quad (3.26)$$

Since the output signal *y* is measurable, the normalized output *z* is also measurable. Define normalized estimation error to be the error between the normalized measured output and the normalized estimated output as in Eq.(3.27) .

$$e_n := \frac{\hat{z} - z}{m^2} \qquad (3.27)$$

where

$$m^2 = 1 + n_s^2 \qquad (3.28)$$

and n_s is a normalizing signal such that $\frac{\phi}{m} \in L_\infty$.

Define the cost function

$$J(\hat{\theta}) := \frac{(e_n m)^2}{2} = \frac{((\hat{\theta} - \theta)^T \phi)^2}{2m^2} \qquad (3.29)$$

also note that J is convex in n_s.

$$\nabla J(\hat{\theta}) = e_n \phi \qquad (3.30)$$

The steepest descent direction of $J(\hat{\theta})$ is $-\frac{\partial J(\hat{\theta})}{\partial \hat{\theta}}$. For the above chosen $J(\hat{\theta})$, this suggests the adaptive update law for $\hat{\theta}(t)$:

$$\dot{\hat{\theta}} = -\Gamma e_n \phi \qquad (3.31)$$

Example

Rewrite Eq. (3.12) in the general form for adaptive estimation as in Eq. (3.17)

$$y^{(n)} = \theta^T Y \qquad (3.32)$$

Where

$$\theta = \begin{bmatrix} b_1 & b_0 \end{bmatrix}^T \qquad (3.33)$$

$$Y = \begin{bmatrix} \dot{u}(t) & u(t) \end{bmatrix}^T \qquad (3.34)$$

Let us choose *m = 1*, $\Lambda(s) = s^2 + s + 1$ and $\Gamma = 0.1\begin{bmatrix} 1 & 0 \\ 0 & 1 \end{bmatrix}$, the regressor vector can be expressed as:

$$\phi := \frac{1}{\Lambda(s)} Y = \begin{bmatrix} \frac{su(t)}{s^2+s+1} & \frac{u(t)}{s^2+s+1} \end{bmatrix} \quad (3.35)$$

The parameter update law can be obtained using Eq. (3.31)

3.3 Iterative Learning Identification

Iterative learning identification (ILI) is a novel approach for closed loop identification [30] [31] [32]. This method achieves identification by applying Iterative Learning Control (ILC) [33] concepts in the presence of measurement noise without any knowledge of the feedback controller in the loop. Iterative Learning Identification (ILI) considers a system that repeats the same reference trajectory with a view to sequentially improving parameter estimation accuracy. The algorithm generates the estimation of parameters from the new trial by adding a 'correction' term to the estimated parameters from a previous trial.

3.3.1 System Description

Consider a continuous time SISO system described by transfer function

$$\begin{aligned} y(s) &= \frac{B^o(s)}{A^o(s)} u(s) \\ &= \frac{b_0{}^o + b_1{}^o s + \cdots + b_{m-1}{}^o s^{m-1}}{a_0{}^o + a_1{}^o s + \cdots + a_{n-1} s^{n-1} + s^n} u(s) \end{aligned} \quad (3.36)$$

This transfer function describes the relationship between the input signal $u(s)$, and output signal $y(s)$, where $a_i{}^o \in R(i = 1, 2, ..., n)$ and $b_i{}^o \in R(i = 1, 2, ..., m)$ are coefficient parameters. Define p as a differential operator, and reformulate Eq. (3.36) to express the relationship between the input $u(t)$ and output signal $y(t)$ in the time domain. This results in:

$$\begin{aligned} y(t) &= \frac{B^o(p)}{A^o(p)} u(t) \\ &= \frac{b_0{}^o + b_1{}^o p + \cdots + b_{m-1}{}^o p^{m-1}}{a_0{}^o + a_1{}^o p + \cdots + a_{n-1} p^{n-1} + p^n} u(t) \end{aligned} \quad (3.37)$$

Basic assumptions for ILI are similar to those of its counterpart, ILC. We assume the following.

- Plant is stable or stabilized with a feedback controller *K(p)*
- Though the true plant parameters $a_i^o \in R(i=1,2,...,n)$ and $b_i^o \in R(i=1,2,...,m)$ are unknown, $A^o(p)$ and $B^o(p)$ are coprime and their orders *n* and *m* are known.
- Assume the trial itself is repeatable during time interval [0,T] with the same initial condition
- Assume white noise

The goal is to find the true estimates of $A^o(p)$ and $B^o(p)$ based on the measurement of input and output data. Let T_s denotes the sampling time, and $NT_s = T$.

3.3.2 ILI Algorithm

Choose a reference signal *r(t)*, that is at least *max(m,n)* times continuously differentiable. Here, we consider the case when the system is not stable, and is stabilized by a feedback controller *K(p).* At the *j*-th iteration, inject the reference signal $r(t)$ into the closed loop architecture shown in Fig.3.2. Collect the error signal $e^j(t)$ when the estimates of $a_0{}^j,\ldots,a_{n-1}{}^j$ and $b_0{}^j,\ldots,b_{m-1}{}^j$ from the previous trial are given.

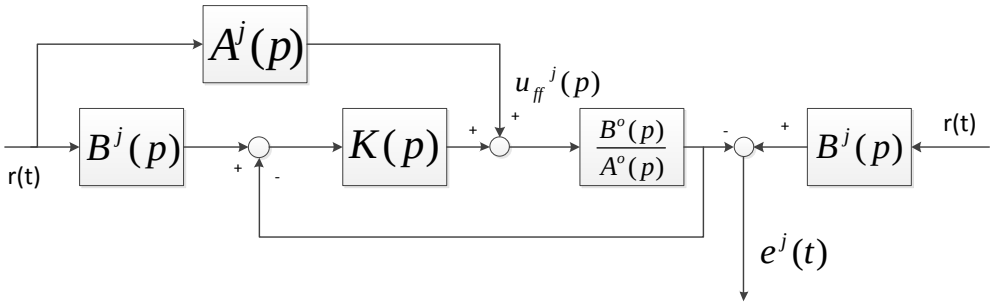

Figure 3.2 Closed Loop Architecture for ILI

Equations (3.38) and Eq.(3.39) define the estimates of the denominator and numerator at *j*-th trial.

$$A^j(p) = {a_0}^j + {a_1}^j p + {a_2}^j p^2 + \cdots + {a_{n-1}}^j p^{n-1} + p^n \quad (3.38)$$

$$B^j(p) = {b_0}^j + {b_1}^j p + {b_2}^j p^2 + \cdots + {b_{m-1}}^j p^{m-1} \quad (3.39)$$

Now we compute the feed-forward signal ${u_{ff}}^j(t) = A^j(p)r(t)$, and inject ${u_{ff}}^j(t)$ into the physical system $\frac{B^o(p)}{A^o(p)}$. Subsequently we can obtain error signal $e^j(t)$ from the closed loop architecture in Fig. 3.2.

$$e^j(t) = S(p)B^j(p)r(t) - T(p)A^j(p)r(t) \quad (3.40)$$

where

$$T(p) = \frac{\frac{B^o(p)}{A^o(p)}}{1 + \frac{B^o(p)}{A^o(p)}K(p)} \quad (3.41)$$

and

$$S(p) = \frac{1}{1 + \frac{B^o(p)}{A^o(p)}K(p)} \quad (3.42)$$

Now, denote the estimated parameters at j-th trial to be:

$$\gamma^j = \left[{a_0}^j \quad ... \quad {a_{n-1}}^j \quad {b_0}^j \quad ... \quad {b_{m-1}}^j \right]^T \quad (3.43)$$

The iterative identification procedure can be described as follows:

- Step1: define an initial estimate γ^0, set j = 0;
- Step2: Generate e^j from γ^j according to the closed loop architecture in Fig. 3.2.
- Step3: Update parameter set for the *j+1*-th trial based on the parameter set for *j*-th trial using Eq. (3.44)

$$\gamma^{j+1} = L_\gamma \gamma^j + L_e e^j \quad (3.44)$$

Where L_γ and L_e are the learning gains for γ^j and e^j respectively.

3.3.3 ILI Update Law

3.3.3.1 Recursive type learning law

Similar to the tracking problem in ILC, where we want to write the tracking error in terms of ILC input $u^j(t)$, the estimation error in ILI also needs to be expressed in terms of parameter set γ^j. Rewriting Eq. (3.40) in terms of γ^j, we obtain

$$\begin{aligned} e^j(t) &= S(p)B^j(p)r(t) - T(p)A^j(p)r(t) \\ &= -T(p)r_A(t)\gamma^j + S(p)r_B\gamma^j - T(p)p^n r(t) \\ &= -M\gamma^j - T(p)p^n r(t) \end{aligned} \quad (3.45)$$

Where

$$r_A(t) = \begin{bmatrix} r(t) & r'(t) & \dots & r^{(n-1)} & 0 & \dots & 0 \end{bmatrix} \quad (3.46)$$

$$r_B(t) = \begin{bmatrix} 0 & \dots & 0 & r(t) & r'(t) & \dots & r^{(m-1)}(t) \end{bmatrix} \quad (3.47)$$

$$M = [-T(p)r_A(t) + S(p)r_B(t)] \quad (3.48)$$

There are N samples between time interval [0,T], $e^j \in R^{(N+1)\times 1}$ and $r_A(t) \in R^{1\times(m+n)}$, $r_B(t) \in R^{1\times(m+n)}$, $M \in R^{N\times(m+n)}$.

Matrix $M \in R^{N\times(m+n)}$, and is not invertible. If we want to update the estimated parameters based on the estimation error, the dimension of the estimation error and the estimated parameter set must be the same. In other words, a transformation matrix is needed to project the estimation error to have the same dimension as the parameter set.

Choose a base function V_{df} of dimension $V_{df} \in R^{(N+1)\times(m+n)}$. Let the QR decomposition of V_{df} be

$$V_{df} = QR, Q^T Q = I_{n+m} \quad (3.49)$$

Define $\delta^j \in R^{(m+n)\times 1}$, the projected error can then be written as:

$$\delta^j = R^{-1}Q^T\varepsilon^j \quad (3.50)$$

Also, define $H^j \in R^{(m+n)\times(m+n)}$

$$H = R^{-1}Q^T M \quad (3.51)$$

$$L_\gamma = I \quad (3.52)$$

$$L_e = kH^{-1} \quad (3.53)$$

Substitute into , the parameter update law can be rewritten as

$$\gamma^{j+1} = L_\gamma\gamma^j + L_e\delta^j \quad (3.54)$$

where $0 < k < 1$. Substitute Eq. (3.45),3.51 3.52 and (3.53) into (3.44)

$$\begin{aligned}\gamma^{j+1} &= \gamma^j + kH^{-1}(-H\gamma^j - R^{-1}Q^T T(p)p^n r(t)) \\ &= (1-k)\gamma^j - kH^{-1}R^{-1}Q^T T(p)p^n r(t)\end{aligned} \quad (3.55)$$

The stability for the update on the parameter set is guaranteed when $0 < k < 1$.

Chapter 4

Parameter Estimation Simulation Results

Three parameter estimation methods – Least Squares Estimation (LSE), Gradient Adaptive Method and Iterative Learning Identification (ILI) – were introduced in the previous chapter. Parameter estimation results from each estimation algorithm are presented in this chapter. The estimations are based on simulated data, and the robustness of each estimation algorithm with the presence of measurement noise is also evaluated.

The purpose of this chapter is to evaluate the identification algorithms in simulation before their application in experiments. The simulation setup is modeled after the experimental setup. Identification algorithms discussed in the previous chapter are applied to the tractor model structure. In this research, as detailed in the previous chapters, a vehicle model from steer command to lateral position of a look-ahead point in front of the vehicle is a simplified second order model:

$$G(s) = \frac{b_1 s + b_0}{s^2} \qquad (4.1)$$

The closed loop response of the tractor is recorded for the identification. The reference signal used is a step, which is equivalent to a crop row change in experiment. For analysis purposes, the steering command recorded from the actual closed loop experiment is used as the input signal in the identification. By injecting the input signal to a model of the form in Eq. (4.1) with known parameters, the simulated output is recorded as the output signal used in identification.

4.1 Identification Results from classical methods

4.1.1 Least Squares Estimation (LSE)

In this study, the input signal is the recorded steering command from a closed loop experiment where the tractor is given a series of step reference signals. This input signal sequence is given in Fig. 4.1

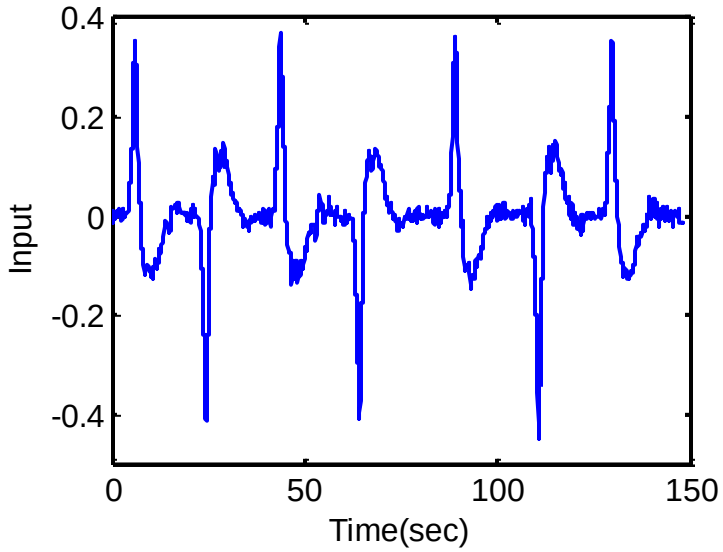

Figure 4.1 Identification Input Signal

The plant model used in simulation is:

$$G(s) = \frac{0.7s + 1.56}{s^2} \qquad (4.2)$$

Comparing Eq.4.2 with Eq. 4.1, the parameter values of b_1 and b_0 are: 0.7 and 1.56 respectively. Injecting the input signal shown in Fig. 4.1 into the plant model given in Eq. 4.2, the simulated output is shown in Fig. 4.2 .

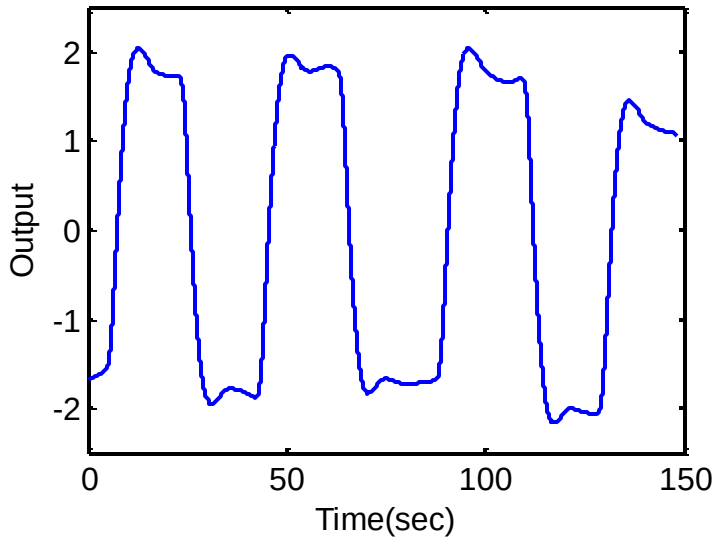

Figure 4.2 Identification Output Signal

Using the input and output data to estimate the parameters b_1 and b_0 based on the model structure of Eq. 4.1 , the estimated parameters are presented in Table 4.1.

Table 4.1 Estimated parameter values using LSE

		Parameter' b_1 '	Parameter' b_0 '
True parameter values		0.7	1.56
Estimated parameter values	Noise variance		
	0	0.7	1.56
	0.0001	2.0207	1.3456
	0.001	4.87	0.8821
	0.006	10.9303	-0.1006

Here, we inject a noise signal on the output of the plant. The noise is assumed Gaussian and white with different levels of variance. The estimation results with respect to different noise variance levels are also presented in Table 4.1. It can be observed from the table that noise level will significantly affect the estimation results. With a low noise level, the estimated parameter values are close to the true values. When the noise level is increased, the estimation accuracy is degraded. The estimated plant is actually non-minimum phase

when the noise variance is 0.006. Experimental estimation results using LSE also indicated a non-minimum phase system, and one of the explanations is the effect of noise as indicated in the simulation. The noise given here was assumed white and Gaussian; we anticipate that colored noise would have a similar negative effect, possibly even more severe.

We then construct the vehicle dynamics model using Eq. (4.1) by substituting the estimated parameter values in Table 4.1. Injecting the measured input into our estimated plant, the estimated plant output is obtained. Fig. 4.3 compares the estimated output with the different noise levels shown in Table 4.1. As evidenced, the estimated output matches the measured output from simulation when there is no measurement noise. Estimation results degrade with the increasing of noise level. Figure 4.3 (d) indicated a non-minimum phase estimate.

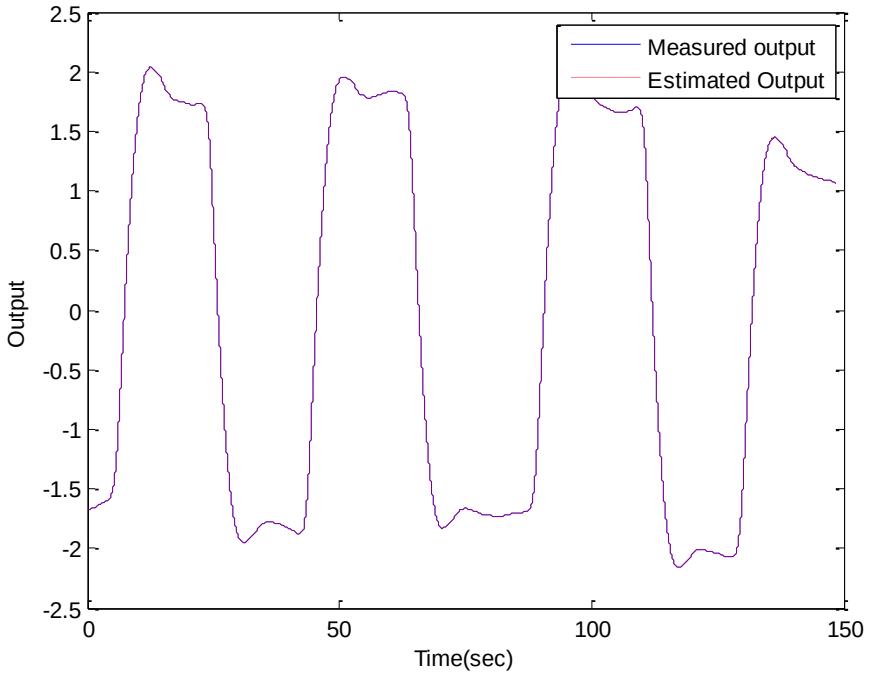

(a)

Figure 4.3 Comparison between estimated and measured output using LSE

(cont. on next page)

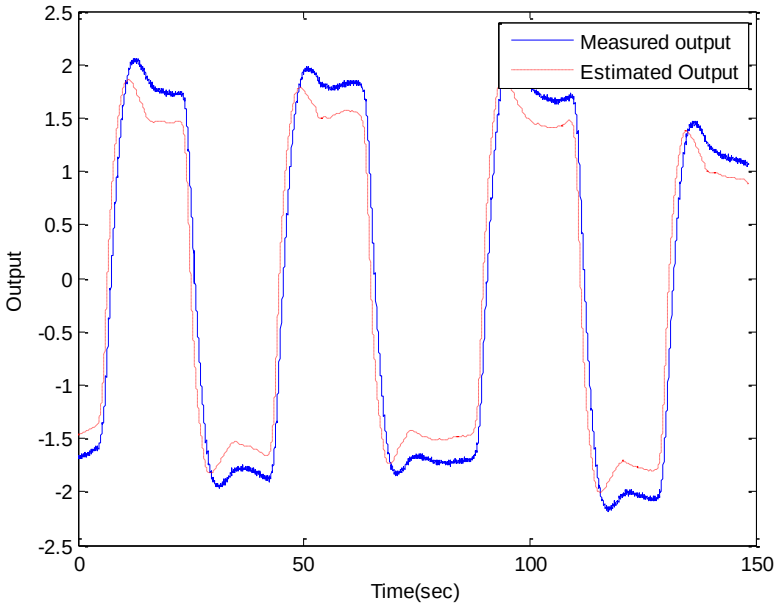

(b)

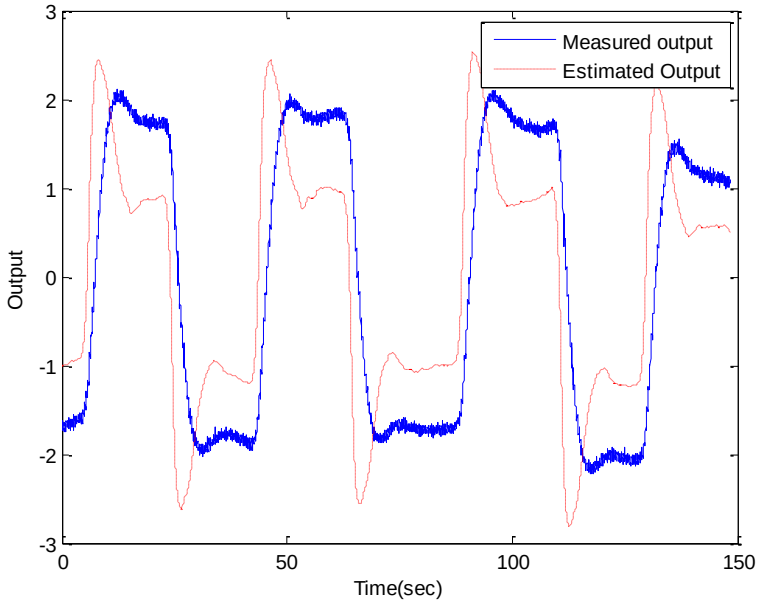

(c)

Figure 4.3 Comparison between estimated and measured output using LSE

(cont. on next page)

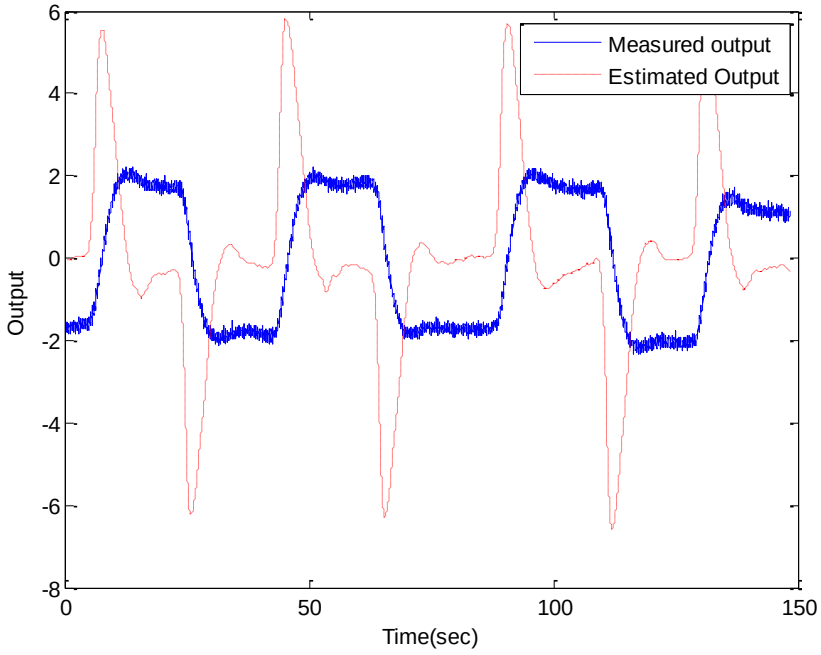

(d)

Figure 4.3 Comparison between estimated and measured output using LSE (a) Noise variance = 0 (b) Noise variance = 0.0001 (c) Noise variance = 0.001 (d) Noise variance = 0.006

4.2 Gradient based Adaptive Estimation Results

Use the same input and output signal as shown in Fig. 4.1 and Fig. 4.2, we performed gradient based adaptive estimation as detailed in chapter 3. The estimation results with respect to different noise levels are shown in Table 4.2. The estimated parameter values are calculated as an average of the last 30 data points where we made the assumption that the estimation has converged for the last 30 data points. The estimated parameter values are quite consistent with different noise levels. Comparing the estimated parameter values in Table 4.2 with the values in Table 4.1, we can see that gradient based adaptive estimation is more robust to noise compared with LSE when estimating this particular input signal and model structure.

Table 4.2 Estimated parameter values using gradient based adaptive estimation

		parameter' b_1 '	parameter' b_0 '
True parameter values		0.7	1.56
Estimated parameter values	Noise variance		
	0	0.6705	1.5614
	0.0001	0.6734	1.5666
	0.001	0.6797	1.5777
	0.006	0.6931	1.6013

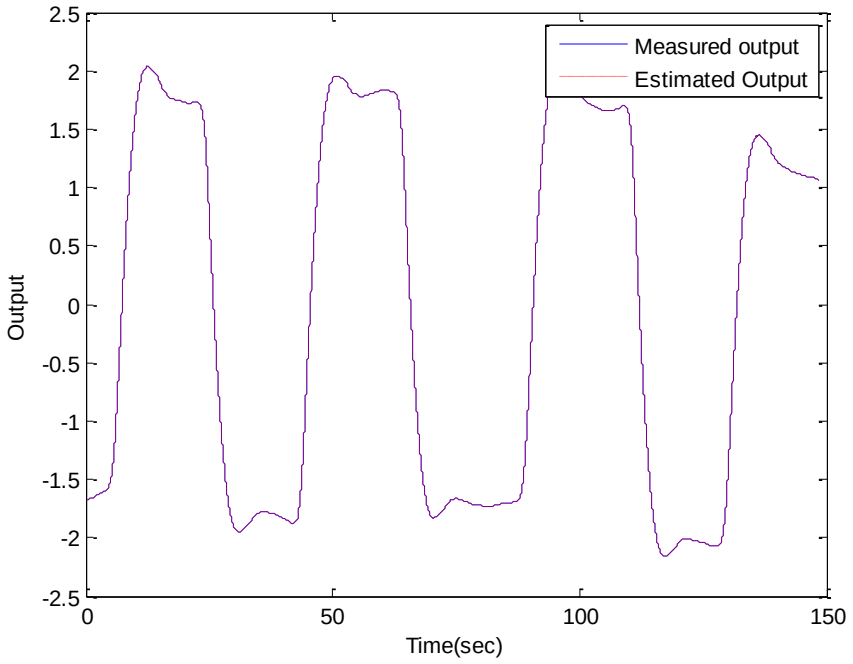

(a)

Figure 4.4 Comparison between estimated and measured output using gradient adaptive estimation

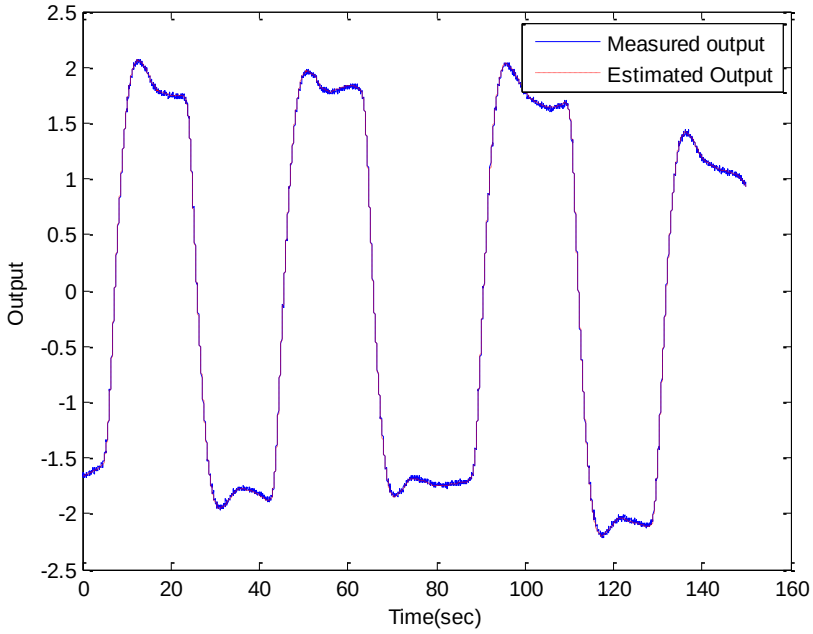

(b)

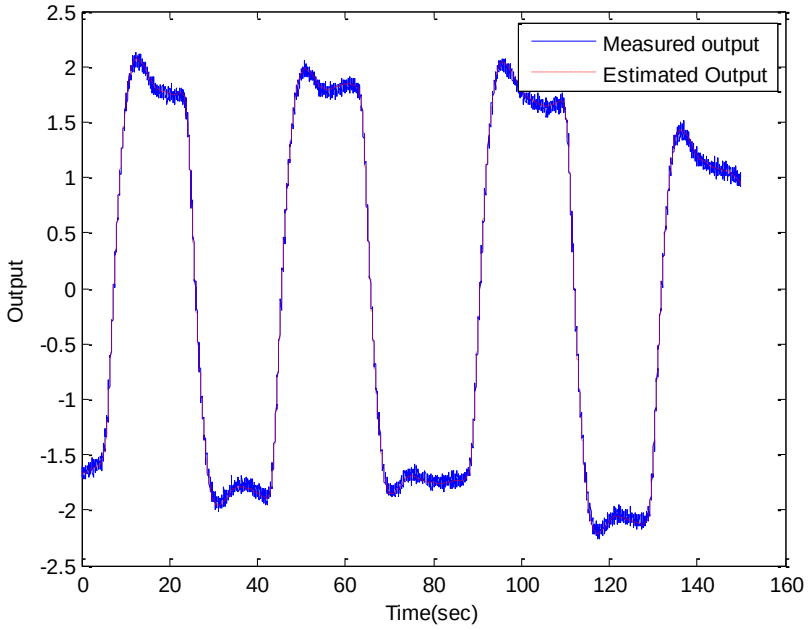

(c)

Figure 4.4 Comparison between estimated and measured output using gradient adaptive estimation

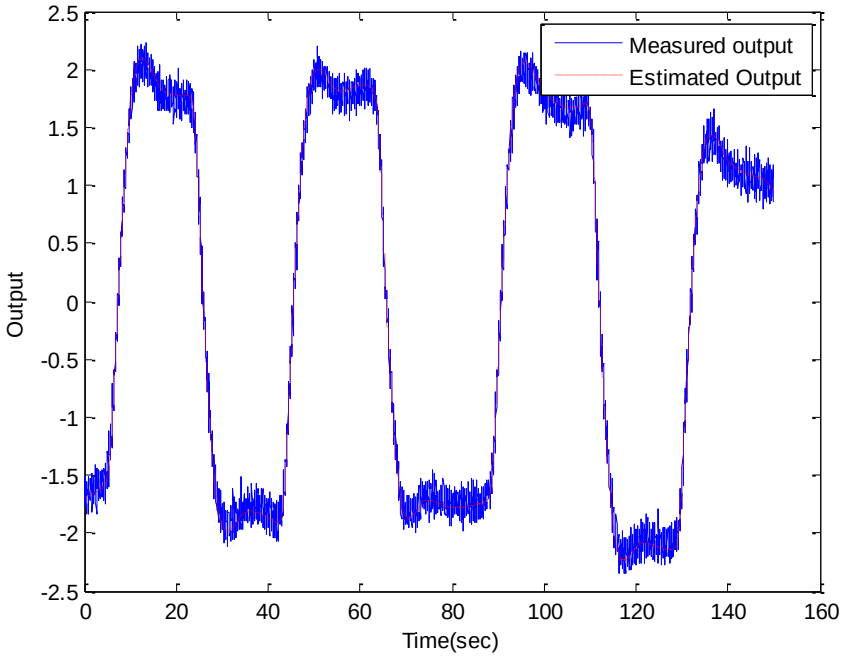

(d)

Figure 4.4 Comparison between estimated and measured output using gradient adaptive estimation (a) Noise variance = 0 (b) Noise variance = 0.0001 (c) Noise variance = 0.001 (d) Noise variance = 0.006

Fig. 4.4 (a)-(d) compares the estimated output with different noise levels shown in Table 4.2. As evidenced in Fig. 4.4, the transient behavior is captured quite well even with high noise levels. Comparing Fig. 4.4 with Fig. 4.3, the adaptive estimation approach appears to be more robust to noise than the LSE method using this particular type of input and model structure.

To evaluate the time that is necessary for the parameters to converge, we compare the estimation results when the reference signal consists of one, two, and seven series of steps. The case when the output is contaminated with a noise variance of 0.001 is considered. The parameter convergence results correspond to different lengths of reference signal are shown in Fig 4.6. The corresponding output trajectories are shown in Fig 4.5.

In Fig. 4.6 (a), the parameter values are consistent after the step change has occurred at about 10 sec which can be seen from the measured output trajectory in Fig 4.5 (a). In Fig.

4.6 (b), without the consideration of noise, the estimated parameter values are quite consistent after the second step change which occurred at about 30secs as indicated in Fig 4.5 (b). In Fig. 4.6 (c), the time it takes for the parameters to converge is the same as in Fig 4.5 (b). It indicates that after 2 steps, the estimated parameter values are quite constant. Therefore, we conclude that the time it takes for the parameters to converge is at least 40 sec, which includes two step changes.

The estimated parameter values for b_1 and b_0 are taken as the average of the last 30 data points in Fig. 4.6 (a) – (c) respectively. The vehicle dynamics model is constructed based on the estimated parameters. The estimated outputs are calculated by injecting the measured input into the estimated plant model, and are shown in Fig 4.5 (a) –(c). In Fig. 4.5 (a), the error between the estimated and measured output are quite large with the estimated parameters error for b_1 and b_0 being 2% and 14% respectively. Both Fig. 4.5 (b) and (c) have a good match between the estimated and measured output. This is consistent with the parameter convergence result shown in Fig. 4.6 (a) – (c) and the analysis above. The results from both Figure 4.5 and 4.6 indicate that the estimated parameter values will converge after two step changes.

One of the key limitations of using an adaptive estimation is that the parameter estimation results are also affected by noise and disturbances. As shown in Fig. 4.6 (c), although parameter convergence is achieved after approximately 40 sec, there are still a lot of variation in the estimated parameters at the data points when the tractor is changing lanes – e.g. estimation results at around 90sec. Therefore, the absolute converged values of the estimated parameters are hard to claim with the presence of noise.

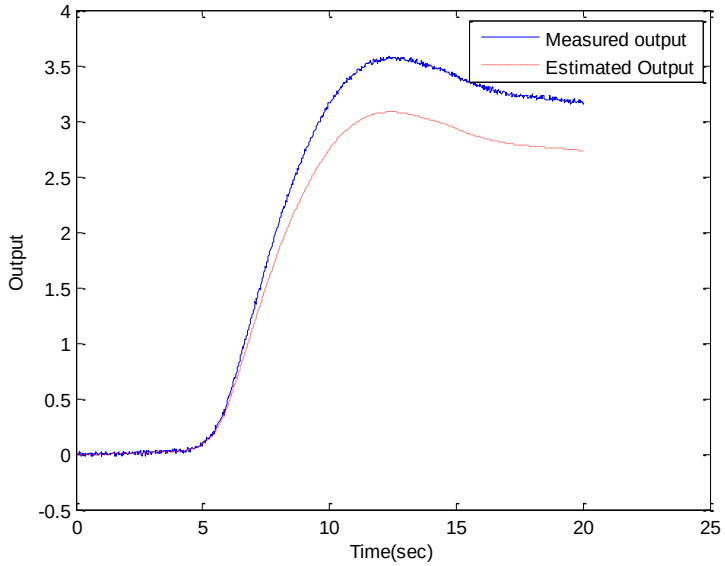

(a)

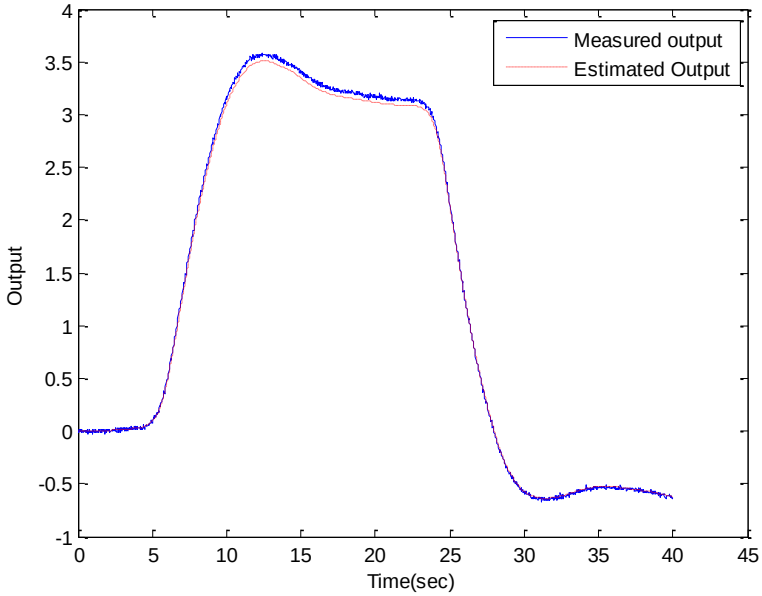

(b)

Figure 4.5 Comparison between estimated and measured output using gradient adaptive estimation (cont. on next page)

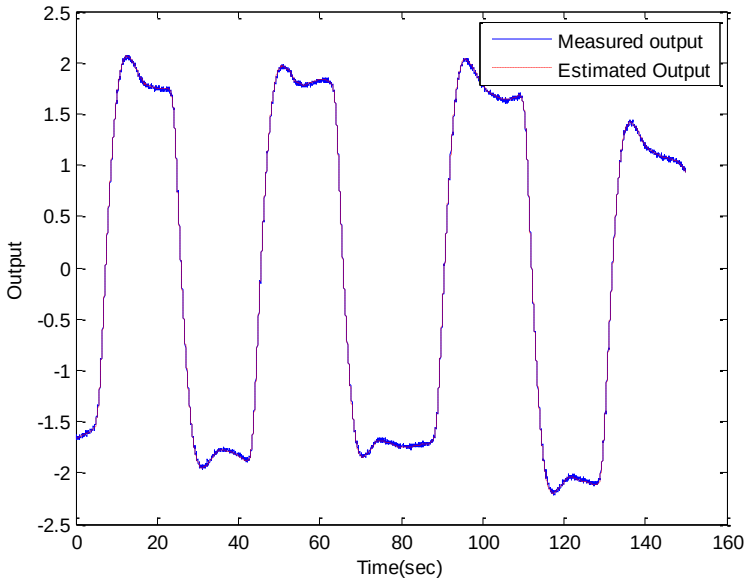

(c)

Figure 4.5 Comparison between estimated and measured output using gradient adaptive estimation (a) single step change -- 20 sec of data (b) two step changes -- 40 sec of data (c) a series of step changes --155 sec of data

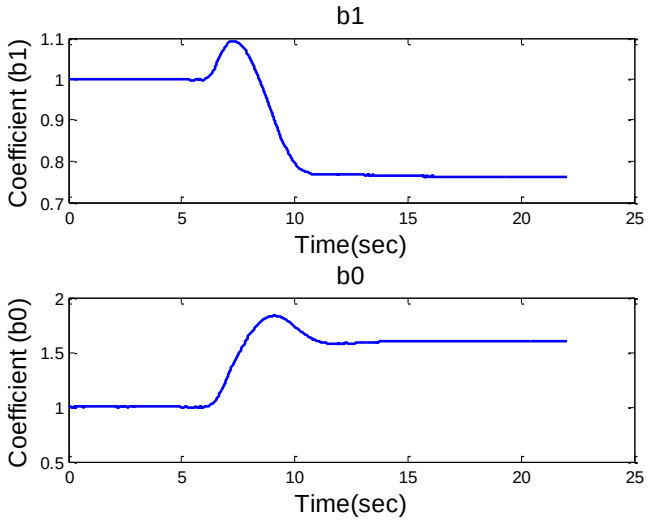

(a)

Figure 4.6 Parameter convergence results (cont. on next page)

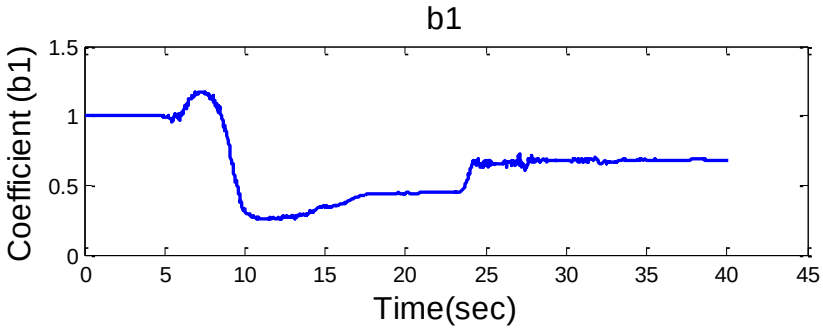

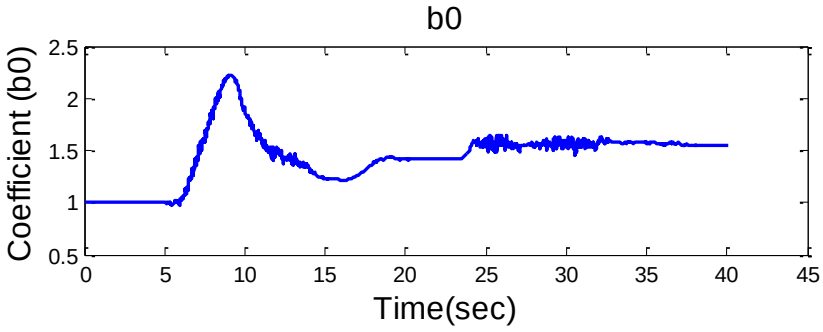

(b)

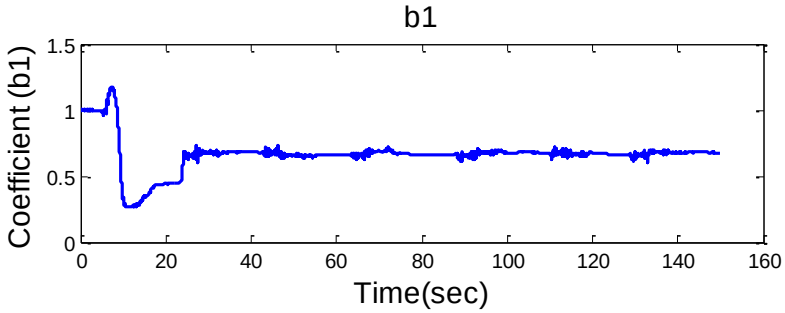

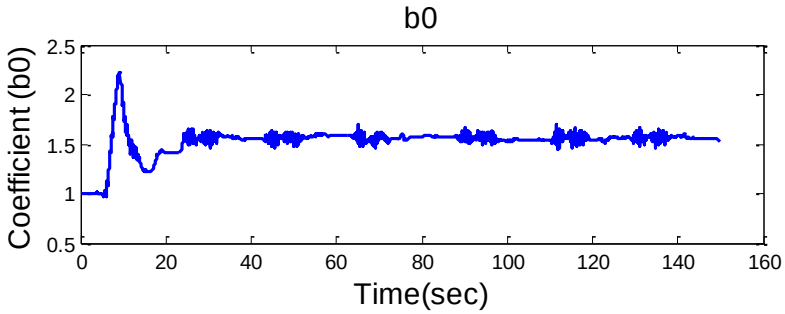

(c)

Figure 4.6 Parameter convergence results (a) single step change -- 20 sec of data (b) two step changes -- 40 sec of data (c) a series of step changes --155 sec of data

4.3 Iterative Learning Identification Results

4.3.1 Simulation Setup

The description of ILI is detailed in chapter 3. In this section, we will make it specific to our particular class of system. The closed loop architecture for a general ILI problem is shown in Figure 3.2. It requires the user to specify both a reference signal $r(t)$ and a feed-forward control input signal $u_{ff}(t)$, where the feed-forward control input signal $u_{ff}(t)$ will be changing from trial to trial. However, in our particular experimental system, only the reference signal can be specified. To accommodate our specific class of system, the scheme in Figure 3.2 is modified to the scheme in Fig. 4.7 and made specific to the plant given in Eq. (4.1).

We define the denominator and numerator of the system at the j-th trial as:

$$A(p) = p^2 \qquad (4.3)$$

$$\hat{B}^j(p) = \hat{b}_0^{\,j} + \hat{b}_1^{\,j} p \qquad (4.4)$$

where 'p' is defined as a differential operator. The reason this differential operator is used instead of Laplace operator is because that we are working in time domain in this study, and Laplace operator is defined in frequency domain.

Here we exploit process knowledge to identify only the numerator. The system denominator is known, and is therefore fixed for all trials. Parameters of the system numerator, on the other hand, will be updated at each trial. We define the unknown parameter set at the j-th trial to be.

$$\gamma^j = \begin{bmatrix} \hat{b}_0^{\,j} & \hat{b}_1^{\,j} \end{bmatrix}^T \qquad (4.5)$$

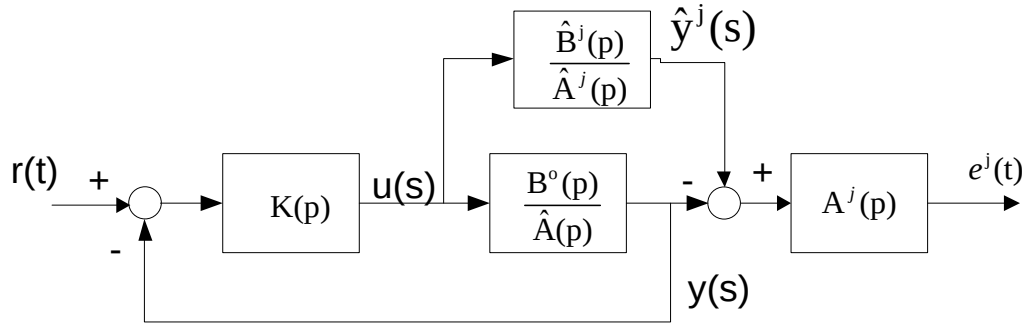

Figure 4.7 Closed loop identification architecture

With the new closed loop configuration as shown in Fig. 4.7, the estimation error can now be written as,

$$\begin{aligned} e^j(t) &= S(p)B^j(p)r(t) - T(p)A^j(p)r(t) \\ &= S(p)\begin{bmatrix} r(t) & r'(t) \end{bmatrix}\gamma^j - T(p)p^2 r(t) \end{aligned} \quad (4.6)$$

Where

$$T(p) = \frac{\frac{B^o(p)}{A^o(p)}}{1 + \frac{B^o(p)}{A^o(p)}K(p)} \quad (4.7)$$

$$S(p) = \frac{1}{1 + \frac{B^o(p)}{A^o(p)}K(p)} \quad (4.8)$$

Define

$$M = S(p)\begin{bmatrix} r(t) & r'(t) \end{bmatrix} \quad (4.9)$$

the estimation error can be further simplified to

$$e^j(t) = M\gamma^j - T(p)p^2 r(t) \quad (4.10)$$

Observing Eq. 4.9, we see that each entry in the matrix can be obtained experimentally.

If we inject reference signal $r(t)$ into the closed architecture shown in Fig. 4.8, and collect the error signal $err(t)$, the error signal is equal to the sensitivity function times the

reference signal. The error signal can therefore be expressed as in Eq 4.11. The second entry in the M matrix of Eq. 4.9 is the derivative of the error signal $err(t)$.

$$err(t) = S(p)r(t) \tag{4.11}$$

Therefore, the matrix M can be estimated from system closed loop test, and can be simplified to:

$$M = \begin{bmatrix} err(t) & err'(t) \end{bmatrix} \tag{4.12}$$

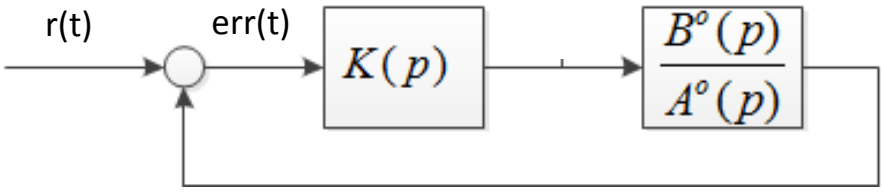

Figure 4.8 Closed loop architecture for estimating matrix M

Assume the time interval [0,T] is sampled at a frequency of $1/T_s$ and $NT_s = T$. The base function V_{df} can be defined as

$$V_{df} = \begin{bmatrix} r(0) & r'(0) \\ r(T_s) & r'(T_s) \\ \vdots & \vdots \\ r(NT_s) & r'(NT_s) \end{bmatrix} \tag{4.13}$$

Let the QR decomposition of V_{df} be:

$$V_{df} = QR, Q^T Q = I_{n+m} \tag{4.14}$$

The learning law is defined as:

$$\gamma^{j+1} = L_\gamma \gamma^j + L_e R^{-1} Q e^j \tag{4.15}$$

Where

$$L_\gamma = I \tag{4.16}$$

$$L_e = kH^{-1} \quad (4.17)$$

$$H = R^{-1}Q^T M \quad (4.18)$$

Where $0 < k < 1$ In this particular example, k is chosen to be 0.8. Stability is guaranteed with this choice of learning gains, and is discussed in more detail in Chapter3.

4.3.2 Simulation Results

Ten iteration trials were performed with a time window of 16 sec, which corresponds to a single step change as in Fig 4.5 (a). The feedback controller K(p) is a proportional-integral-derivative (PID) controller. The parameter updating results in Fig.4.9 start from two different initial conditions. With no noise in the simulation system, estimates of both b_1 and b_0 converge to their true values. At iteration 6, the estimation percentage errors for both parameters are 0.69% and 1.5% respectively when the initial estimates are both 1. Fig.4.9 also shows that the estimated parameters are almost the same as the true parameters after six iterations for the given reference trajectory. Comparing the convergence results from different initial conditions in Fig.4.9, the converged values of b_1 and b_0 are apparently insensitive to the choice of initial values.

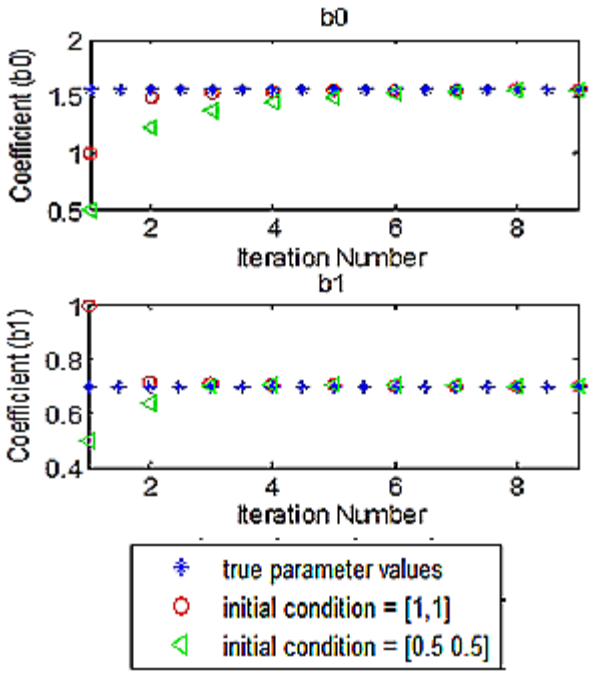

Figure 4.9 Convergence of parameters with initial estimates [1,1] and [0.5, 0.5]

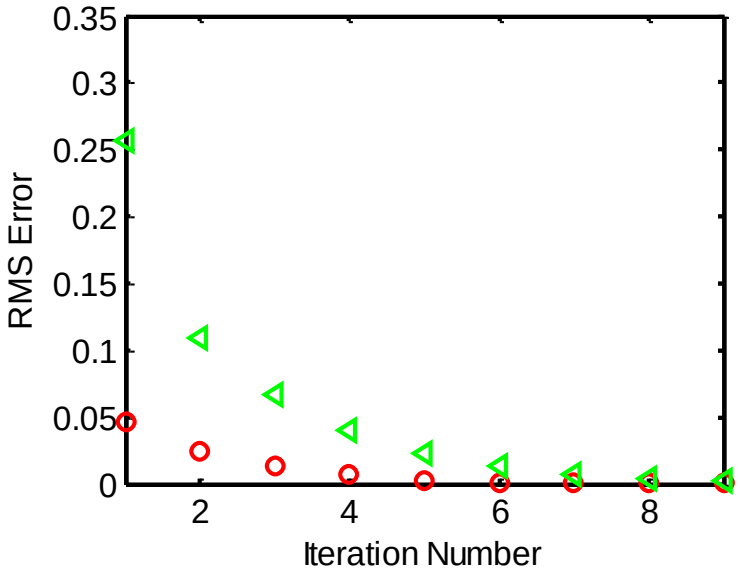

Figure 4.10 RMS Error

The RMS error in Fig.4.10 are calculated as the RMS error between the estimated output at each trial versus the measured output at each trial. The RMS errors indicated in Fig.4.10 show a clear trend of reduction, which is in accordance with the parameter

convergence results shown in Fig.4.9. After approximately 6 trials, the RMS error is very close to zero. The RMS error is reduced to zero when there is no noise in the estimation.

Table 4.3 also summarizes the parameter estimation results when noise is present in the system. It is evidenced from the table that the ILI estimation result is very robust to the measurement noise levels introduced here.

Table 4.3 Estimated parameter values using ILI

		Parameter 'b_1'	Parameter 'b_0'
True parameter values		0.7	1.56
Estimated parameter values	Noise variance		
	0	0.7	1.56
	0.0001	0.7004	1.5559
	0.001	0.6996	1.5528
	0.006	0.6979	1.5462

4.4 Practical Benefits of ILI

From the analysis above, LSE is not able to give a faithful estimation of the plant parameters when noise is present in the system. Both gradient based adaptive estimation and ILI are capable of giving faithful estimation for the plant parameters when the same level of noise is present in the system. Fig 4.5 (a) indicated that a single step maneuver is not sufficient for the parameters to converge using gradient based adaptive estimation. However, using the same reference and output signal, ILI can achieve parameter convergence. While there are other approaches available for parameter identification, there were significant key benefits in this application which made ILI particularly attractive. As mentioned, the field available for identification is limited. Contrary to a gradient based adaptive approach, which is suitable for on-line parameter identification, the ILI can be carried out on a small field section. In addition, the parameter convergence result can be noisy and easily affected by output noise disturbances in the case of adaptive estimation. ILI, on the other hand is capable

of retaining converged values in the presence of output noise with minimal parameter fluctuations.

Chapter 5

Parameter Identification Experimental Results

In the previous chapter, parameter estimation results from simulated data are discussed. In this chapter, we will introduce the experimental system, and the parameter identification results from experimental data.

The chapter will start by introducing the experimental tractor, followed by presenting the sensors used in the experimental system. Similar to the previous chapter, three different identification algorithms are discussed for parameter estimation. Experimental identification results from different identification algorithms showed different level of accuracy, and iterative learning identification shows the practical benefit that it can be performed in a relatively small section of field and therefore can be done prior to actual usage or engagement with crops.

5.1 Experimental Tractor

The identification approaches were tested on a full scale John Deere 8330 tractor equipped with StarFire^{TM} RTK receiver and an integrated AutoTrac^{TM} steering system. Fig.5.1 shows the system on which experimental data was obtained.

The automatic tractor is capable of following some designated trajectories: arcs, straight lines, and lane shifts. It is also capable of following user-defined arcs, which need to be programed before experiments. However, for a trajectory with high frequency reference content, the integrated AutoTrac^{TM} steering system will have a protection program to stop the tractor from following those trajectories. For the purpose of evaluating the identification algorithms, the chosen reference signal is a step trajectory, which corresponds to a lane shift,

and is easily available from the current integrated AutoTrac™ steering system. Since the step reference signal will contain significant high frequency content, the corresponding plant input signal — steered wheel angle — is sufficient excitation for the identification.

Figure 5.1 John Deere 8330 tractor equipped with StarFire™ RTK receiver and an integrated AutoTrac™ steering system

5.2 Sensors and Measurements

In this research, as detailed in the previous chapters, a vehicle model from steer wheel angle to lateral position of a look-ahead point in front of the vehicle is a simplified second order model:

$$G(s) = \frac{y(s)}{\delta(s)} = \frac{b_1 s + b_0}{s^2} \qquad (5.1)$$

where the input is steered wheel angle, and output is the lateral position. In this section, the measurement methods for input and output signal are introduced. Direct measurements are not possible due to the unavailability of sensors. However, based on mathematical / physical relationships between the signals, those measurements can be calculated from available data. The introduction is divided into two parts, output signal measurement and input signal measurement.

5.2.1 Output Signal Measurement

The model output signal is the lateral position of a look-ahead point in front of the vehicle. A StarFire™ RTK receiver that is used to measures the lateral position of the tractor is mounted on the top of the vehicle, which is not a look-ahead point. In the first half of the section, we will introduce the measurement of lateral position from this StarFire™ RTK receiver. In the next half, the method of calculating the lateral position from a look-ahead point is introduced.

5.2.1.1 Lateral position measurement from StarFire™ RTK receiver

Tractor position is measured from a StarFire™ RTK receiver that is mounted on the top of the vehicle (see Fig.5.1). Inaccuracy in the GPS is primarily due to distortion from 'billows' in the ionosphere, which introduce propagation delays that makes the satellite appear farther away than it really is. dGPS corrects for these errors by comparing the position measured using GPS with a known highly-accurate ground reference and then calculating the difference and broadcasting it to users. StarFire instead uses an advanced receiver to correct for ionospheric effects internally. To do this, it captures the military only P(Y) signal that is broadcast on two frequencies, L1 and L2, and compares the effects of the ionosphere on the propagation time of the two. Using this information, the ionospheric effects can be calculated to a very high degree of accuracy, meaning StarFire dGPS can compensate for variations in propagation delay.

The latitude and longitude position of the tractor obtained from the StarFire™ RTK receiver is in earth-fixed coordinates, and is converted to Cartesian coordinates for calculation purpose. A typical tractor trajectory of a lane shift experiment is shown in Fig. 5.2 (a).

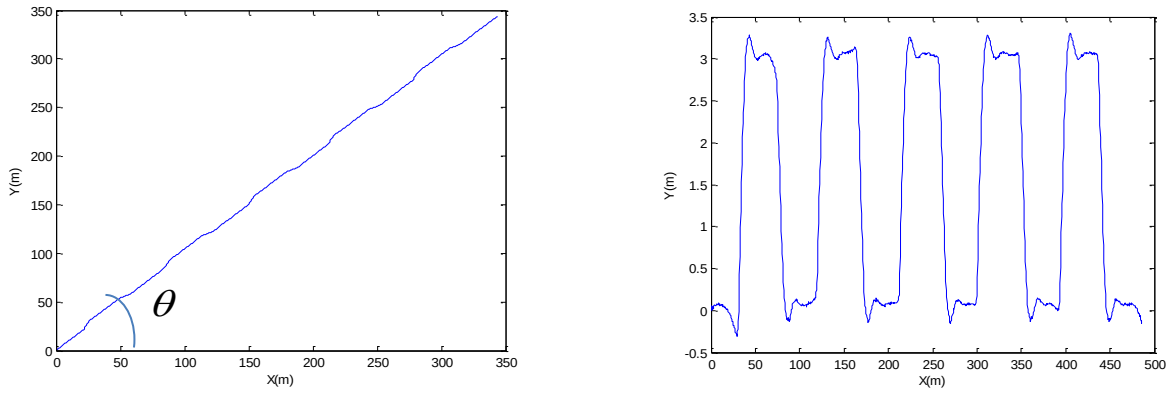

(a) (b)

Figure 5.2(a) tractor trajectory in Cartesian coordinate

(b) tractor trajectory in tractor coordinate

Examining Eq. 4.1, we are only interested in the lateral movement of the tractor. Therefore, the x-y coordinates in Cartesian coordinates should be transferred to the tractor coordinates to evaluate lateral position of the tractor. Eq. 5.2 shows the transformation from Cartesian coordinates to tractor coordinates, where θ denotes the orientation of the tractor trajectory as shown in Fig. 5.2 (a). Fig. 5.2 (b) illustrates the tractor trajectory in tractor coordinates, where the y axis denotes the tractor lateral position.

$$\begin{bmatrix} Trac\_x \\ Trac\_y \end{bmatrix} = \begin{bmatrix} \cos(\theta) & \sin(\theta) \\ -\sin(\theta) & \cos(\theta) \end{bmatrix} \begin{bmatrix} Cartesian\_x \\ Cartesian\_y \end{bmatrix} \quad (5.2)$$

5.2.1.2 Lateral position measurement from a look ahead point

The benefit of using this algorithm can be explained by a simple driving example. We all have the experience that if we fix our eyes on a location near the front of the vehicle when driving a straight line, the trajectory the car makes will be quite oscillatory. However, if the eyes are fixed on a location several vehicle length ahead of the vehicle, the trajectory the car makes is more likely to be straight and smooth. For the current ATU system, the StarFireTM RTK receiver that acts as the vehicle 'eyes' is mounted on top of the tractor as shown in Fig. 5.3. If no look ahead algorithm is used, the driving result will be quite similar to the case when our eyes are fixed on a location near the vehicle front axle when driving a straight line.

As shown Fig. 5.4 (a), when the look ahead distance is very small, the tractor trajectory is not stable when tracking a straight line. With a bigger look ahead distance, as shown in Fig 5.4 (b), using the same feedback controller, the tractor is stable when tracking a straight line.

One of the possible solutions is to move the position of the StarFire^{TM} RTK receiver and install it in front of the tractor using some mounting mechanisms. However, even if we can build a mounting mechanism on this experimental tractor, it will be quite difficult to commercialize, and make it standard on every tractor machine. On the other hand, if an arm is mounted in front of the tractor to position the StarFire^{TM} RTK receiver, the vibration of the arm will be bigger than the vibration of the tractor body. This will cause another control problem, which is similar to the header-height problem in a harvester [34]. If no control is in action, then the obtained data from the StarFire^{TM} RTK receiver will be quite oscillatory.

One other possible solution is to approximate the lateral deviation measured from a look ahead point using the data measured from the StarFire^{TM} RTK receiver that is mounted on top of the tractor. The scheme is shown in Fig. 5.3. In chapter2, the model output defined in Eq. 2.4 y_s is the measurement of lateral deviation from a sensor located a distance d_s ahead of the vehicle center of gravity, and can be expressed as:

$$y_s = y_r + d_s(\varepsilon - \varepsilon_d) \qquad (5.3)$$

where y_r is defined as the lateral distance between the vehicle c.g. and the center line of the road, and d_s is the look ahead distance. An assumption is made in this equation that the error between the measured heading angle ε and desired heading angle ε_d is small, and small angle approximation can be used. This equation enables us to calculate the lateral deviation even if the sensor is not located at a distance d_s ahead of the vehicle center of gravity. In our case, the sensor is located close to the center of gravity, and we assume that the sensor is located d_1 ahead of the center of the gravity. The measurement of lateral deviation from the StarFire^{TM} RTK receiver can be expressed in Eq. 5.4

$$y_1 = y_r + d_1(\varepsilon - \varepsilon_d) \qquad (5.4)$$

Now, assume we want to place the sensor at a distance d_1 ahead of the current location of the sensor, the measurement of lateral deviation at this look ahead point can be expressed in Eq. 5.5

$$y_s = y_1 + d_2(\varepsilon - \varepsilon_d) \qquad (5.5)$$

where the choice of the look ahead distance d_2 can be determined experimentally.

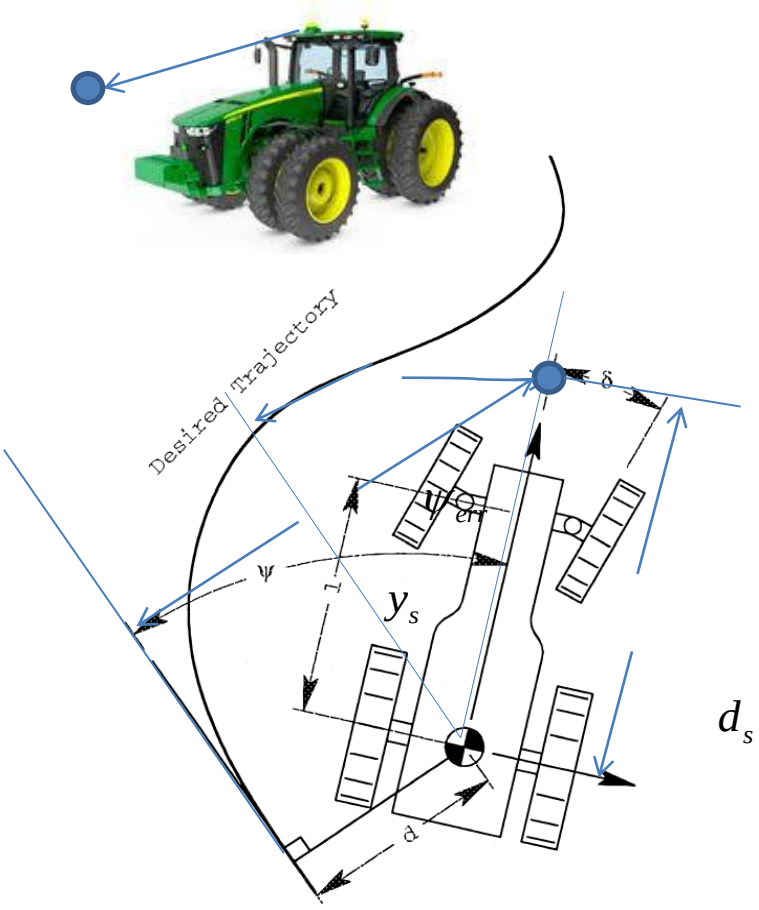

Figure 5.3 Look ahead algorithm

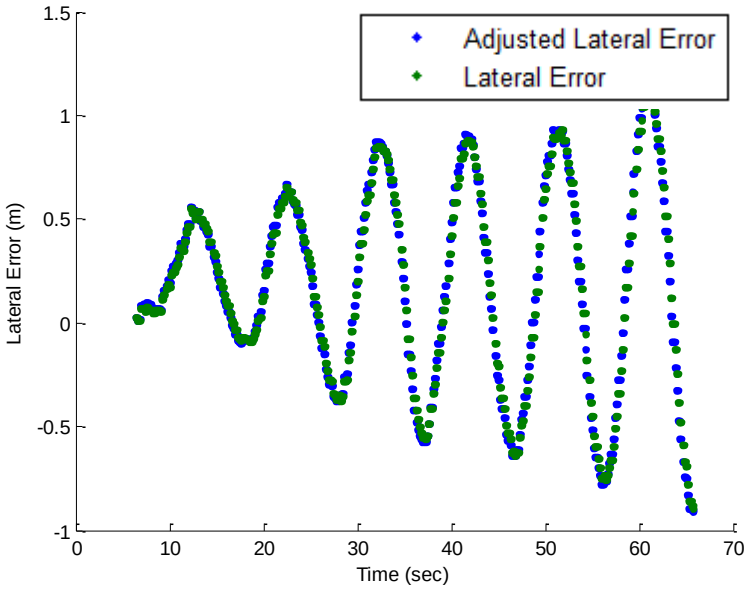

(a)

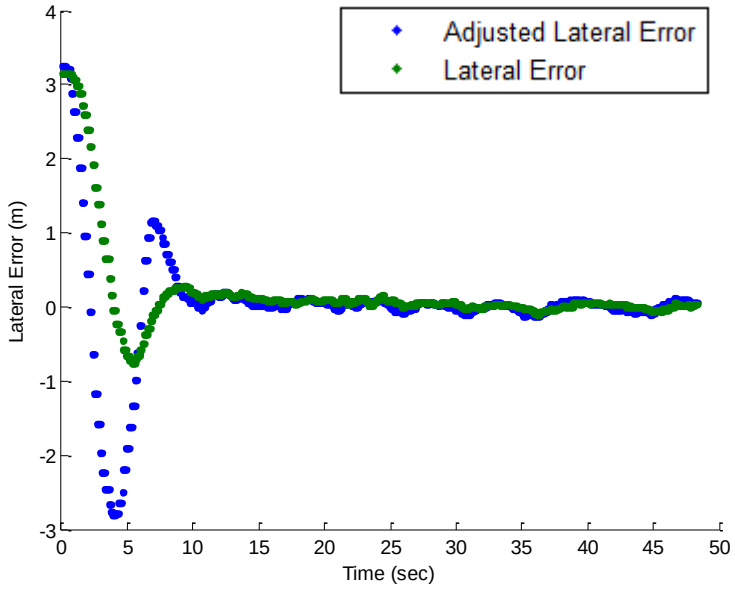

(b)

Figure 5.4 Effect of look ahead distance (a) look ahead distance is 0.3m (b) look ahead distance is 5m

5.2.2 Input Signal Measurement

In this section, we will introduce an alternative way to estimate the tractor steered wheel angle. Vehicle yaw rate can be measured from the StarFire™ RTK receiver, and is available for tractors with both integrated AutoTrac™ steering system and AutoTrac™ universal steering system. Therefore, if we can approximate steered wheel angle with yaw rate, then no additional sensor is needed for the tractors with an AutoTrac™ universal steering system. Yaw rate is defined as the rate of rotation of vehicle heading angle; the relationship between yaw rate and steered wheel angle can be expressed in Eq. 5.6 [35].

$$\frac{\dot{\psi}}{\delta} = \frac{U/L}{1+\frac{KU^2}{gL}} \qquad (5.6)$$

Definition of nomenclatures in Eq. 5.6 can be found in Table. 5.1

Table 5.1 Nomenclatures in Eq. 5.6

$\dot{\psi}$: yaw rate	δ : steered wheel angle	U : velocity
L: wheel base	K: understeer gradient	g: earth gravity

Note from Eq. 5.6 , for a certain vehicle in a certain operation condition, K, L and g are fixed. Therefore, the ratio between yaw rate and steered wheel angle is only velocity dependent. In the beginning of the study, we have already made the assumption that the longitudinal velocity of a vehicle is constant during operation. Since the lateral velocity in the tractor is small comparing to its longitudinal velocity in straight line/lane shift tracking, we further relax the assumption to that vehicle velocity is constant during operation. Therefore, the ratio between yaw rate and steered wheel angle is a constant:

$$k = \frac{\dot{\psi}}{\delta} \qquad (5.7)$$

To evaluate the relationship between velocity and the ratio between yaw rate and steered wheel angle, three different velocities were used in an experiment. Experimental tractors were equipped with an integrated AutoTrac™ steering system where the

measurement of steered wheel angle is available. For each velocity, yaw rate and steered wheel angle are recorded to calculate the ratio.

Fig.5.5 shows the experimental relationship between longitudinal velocity U and ratio k.

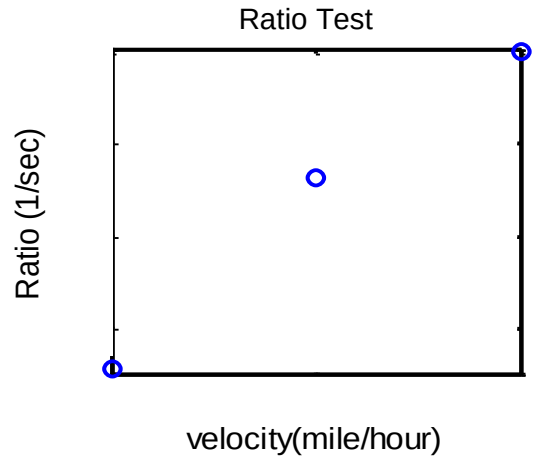

Figure 5.5 Relationship between velocity U and ratio k

To evaluate the relationship between operation conditions and the ratio between yaw rate and steered wheel angle, experiments were conducted on two different ground conditions and three different turning radii. The two different ground conditions are: (a) farm land on test site A, and (b) pavement grounds on test site B. The relationships are shown in Fig. 5.6.

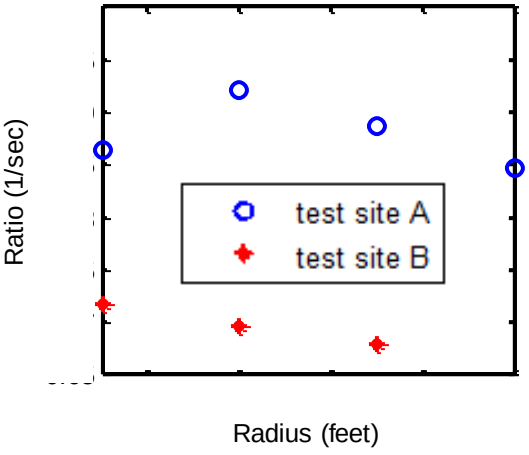

Figure 5.6 Relationship between operating conditions and ratio k

From Fig. 5.6 , we can see that the effect of turning radius on the ratio is not significant compared to the ground conditions. It is in accordance with the assumption we made at the beginning of the study that the ratio between yaw rate and steered wheel angle is only velocity dependent for a certain vehicle in a certain operation condition.

Steered wheel angle can be approximated by substituting the estimated ratio into Eq. 5.6.

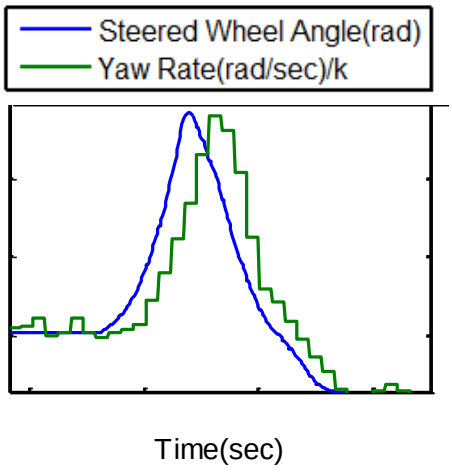

Figure 5.7 Yaw rate estimated and rate gyro measured steered wheel angle

Fig.5.7 compares the yaw rate estimated and rate gyro measured steered wheel angle. There is a pure delay between the yaw rate estimated and rate gyro measured steered wheel angle. This is caused by an inherent filter in the yaw rate sensor. From experimental data, the average pure delay can be approximated.

By rewriting Eq. 5.6 and taking the delay in the sensor into consideration, we can get Eq. 5.8

$$\delta = \frac{\dot{\psi}}{k} e^{-Ts} \qquad (5.8)$$

Eq.5.9 can be obtained by substituting Eq. 5.8 into Eq. 4.1,.

$$G(s) = \frac{y(s)}{\dot{\psi}(s)e^{-Ts}/k} = \frac{b_1 s + b_0}{s^2} \qquad (5.9)$$

Here, k is a constant and can be determined experimentally, e^{-Ts} is a pure delay in the system. Comparing Eq. 4.1 with Eq. 5.9, the dynamics of the system are not changed. Since the measurement of yaw rate is easily available from the StarFire^{TM} RTK receiver, in the

following research, we will evaluate the system transfer function using Eq. 5.9 instead of Eq. 4.1. Additionally, when referring to 'measured input signal' or 'steered wheel angle' this value will be result of measuring yaw rate and using Eq. 5.8 to determine the steering input.

5.3 Experimental Identification Results from classical ID methods

5.3.1 Least Square Estimation Results

In this section, we will evaluate the parameter estimation result from LSE using experimental data. The chosen reference is a series of step lateral signals with an amplitude of 3 meters, equivalent to a series of crop row changes. The controller is a well-tuned integrated AutoTrac^{TM} steering system. During the tests, the longitudinal speed is fixed at 5mph.

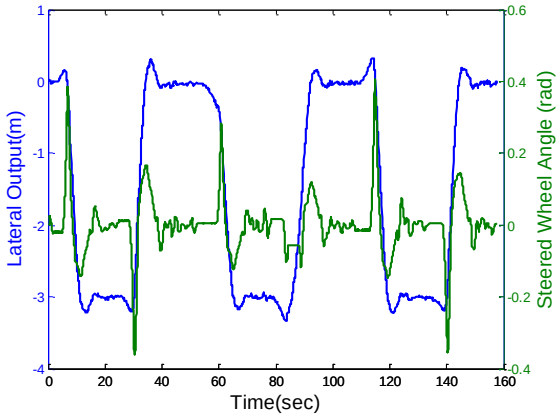

Figure 5.8 Experimental Input and Output Signal

The input (steered wheel angle) and output (lateral output) signals are recorded as discussed in Section 5.1, and are shown in Fig. 5.8. Using the LSE method discussed in Section 3.1, the estimation results of parameters b_1 and b_1 are shown in Table. 5.2. We can construct the vehicle lateral dynamics model using Eq. 5.9 by substituting the estimated parameter values. Injecting the measured input to our estimated plant, we obtained the estimated plant output. Fig. 5.9 compares the estimated output and the measured output for series of step maneuvers. The estimated model from LSE is a non-minimum phase system, which is clearly not true for the tractor model. One of the main reasons for the insufficiency

of LSE is that the input signal does not contain enough information, which is in accordance with the simulation result when we have a small SNR. The reasons of the failure of LSE algorithm is expected and discussed in detail with simulation results in Section 4.1.

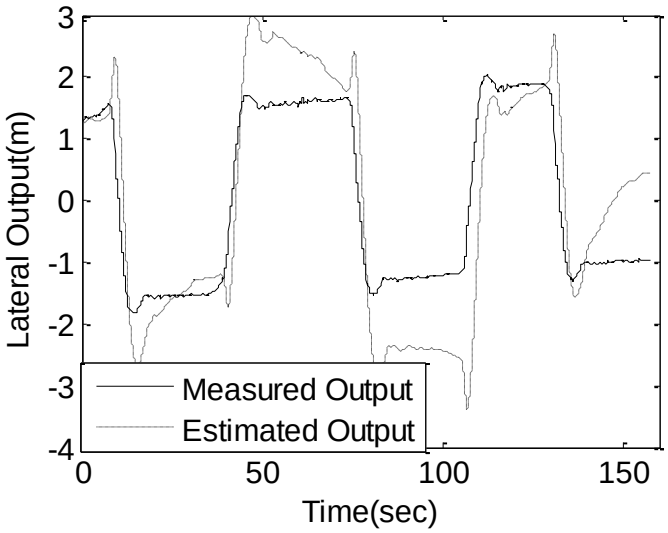

Figure 5.9 Comparison between the estimated output and measured output using the model from LSE

5.3.2 Adaptive Estimation Identification Results

The same input and output signals from Fig. 5.8 are used for the identification. Using the gradient based adaptive estimation method as discussed in Section 3.1, the estimation results of parameters b_1 and b_0 are also shown in Table, 5.2. Fig. 5.10 compares the estimated output and the measured output for a series of step maneuvers. As can be seen in the figure, the transient response is captured quite well.

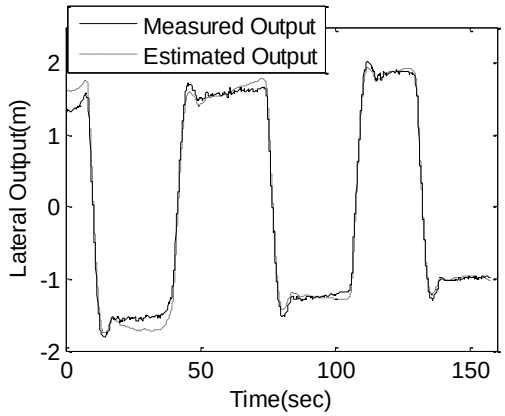

Figure 5.10 Comparison between the estimated output and measured output suing the model from gradient based adaptive estimation

5.4 Experimental Identification Results from ILI

The chosen reference for this identification approach is a single step maneuver with an amplitude of 3 meters. For consistency, the experiment is repeated for ten times with a time window of 16sec. Fig. 5.11 shows the measured input signal (steered wheel angle) and output signal (lateral output measured from the GPS sensor) for 10 iterations, and each input and output pair corresponds to one iteration.

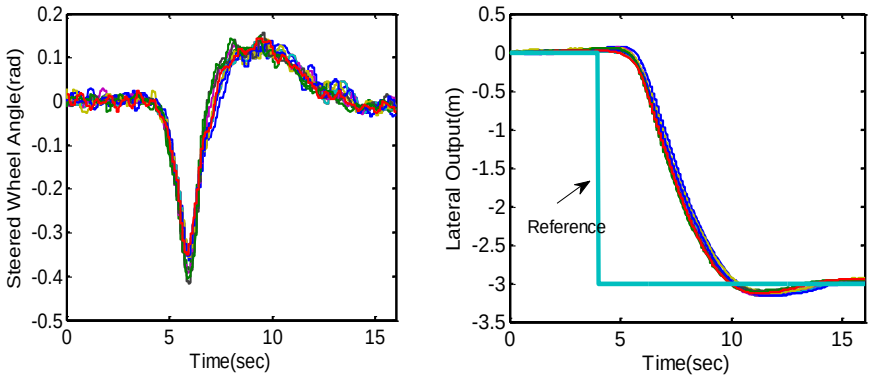

(a) (b)

Figure 5.11 (a) Experimental Inputs (b) Experimental Outputs

The experimental parameter update results are shown in Fig.5.12. The estimated parameter values are quite consistent after 6 iterations as the simulation results indicated in Section 4.3. Fig. 5.12 also compares the parameter convergence results by starting at

different initial values. As expected, the convergence result is not affected by the choice of initial values. Note from Fig. 5.12 that the convergence of parameters is not monotonic, and monotonic convergence is not guaranteed from the ILI algorithm we discussed here. It can be seen that some further work can be done to guarantee the monotonic convergence of the parameters.

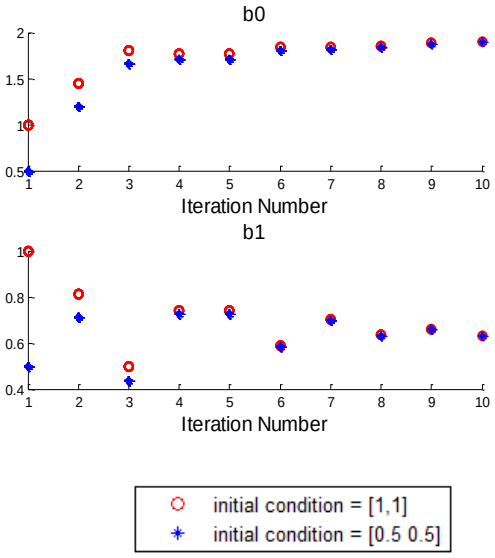

Figure 5.12 Convergence of parameters in experiment with initial estimates [1,1] and initial estimates [0.5, 0.5] respectively

The estimation results of parameters are taken as the average of the parameter values when convergence is observed. In this case, at iteration 8,9 and 10. The estimated parameter values b_1 and b_0 are 0.6398 and 1.8733 respectively. These values are compared with the estimated parameter values from the other identification algorithms in Table 5.2. The estimated output and the measured output are compared in Fig. 5.13. As evidenced, the transient behavior is captured quite well; this is sufficient information to supply a model-based controller design scheme.

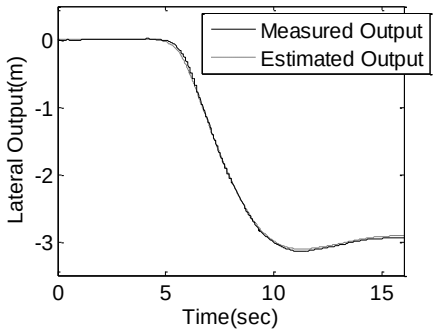

Figure 5.13 Comparison between the estimated output and the measured output using the model from ILI

Table 5.2 Estimated Parameters using three different identification algorithms

Identification Algorithm	System gain and zero		Model Parameters	
	‘ k ’	‘ a ’	‘ b_0 ’	‘ b_1 ’
LSE	-3.510	0.6150	2.1585	-3.510
Gradient	0.5941	-2.9830	1.7722	0.5941
ILI	0.6592	-3.0052	1.981	0.6592

From Table 5.2, the estimated system gain and zero from the ILI and gradient methods are very close. This indicated that the estimated vehicle models are quite consistent. The estimated system gain and zero from LSE is less reliable than the other two methods, as is indicated in the analysis in Section 5.2.

From the results given above, ILI was demonstrated to be successful in identifying model parameters for an agricultural tractor vehicle. While there are other approaches available for parameter identification, there were significant key benefits in this application which made ILI particularly attractive. The field area available for identification was limited. Contrary to a gradient based adaptive approach, which is suitable for on-line parameter identification, the ILI can be carried out on a small field section. In addition, the ILI is capable of identifying system parameters with a step signal which is easily available from the

current AutoTrac^{TM} system. As a result, it provides better estimation results than a batch least squares type of off-line approach.

5.5 Estimated Model Uncertainties

The estimated models from the LSE were non-minimum phase, which are clearly inaccurate for tractor models. Both gradient based adaptive estimation and ILI approaches provide faithful estimates of the tractor models. In this section, we will repeat the identification experiments, and find the estimated model uncertainties.

Adaptive estimation was repeated 5 times, and the corresponding estimation results were compared with the ILI approach. The estimated system gains and zeros are compared in Table 5.3.

Table 5.3 Estimated parameters from different tests

Algorithms	Tests	Estimated Gains	Estimated Zeros
Gradient based adaptive estimation	1	0.7112	-2.4741
	2	0.6911	-2.3230
	3	0.6793	-2.4060
	4	0.6830	-2.4671
	5	0.6213	-2.5205
ILI	10 tests	0.7742	-2.4764

The Bode and Root locus plot for each estimated model is plotted and compared in Fig. 5.14.

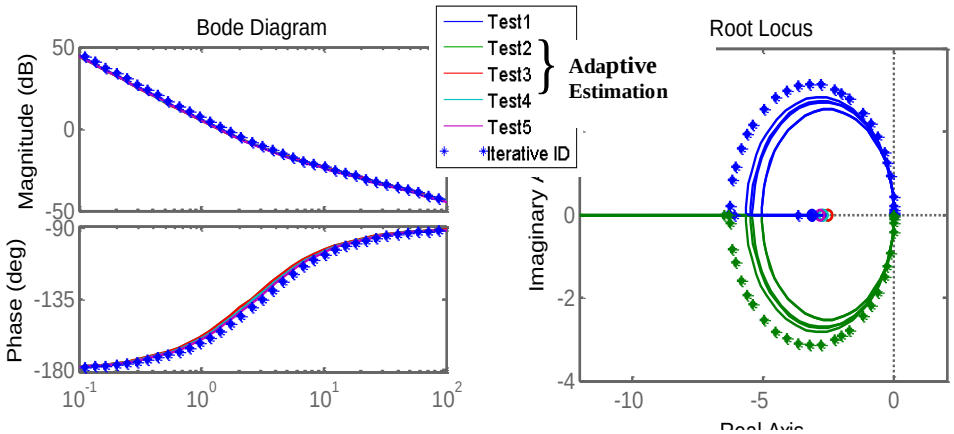

Figure 5.14 Estimated models from different tests

From the figure, the Bode and Root locus plots for the estimated models from different tests are very similar. It indicates that the estimated models are quite consistent. To analyze the model uncertainties at different frequencies, we first found a 'nominal' model by taking the average magnitude and phase values from different tests for each frequency. Then, we can calculate the maximum percentage magnitude and phase difference between the estimated models and the 'nominal' model for each frequency using formula Eq. 5.10.

$$|\Delta G| = \left| \frac{G(w) - G_n(w)}{G_n(w)} \right| * 100\% \qquad (5.10)$$

The bode plot of the maximum percentage difference between the estimated model and the 'nominal' model is shown in Fig.5.15.

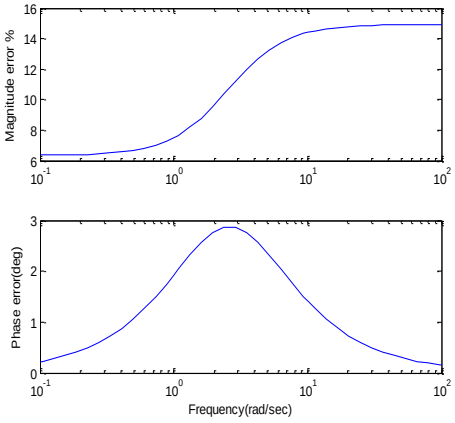

Figure 5.15 Model Uncertainties

From Fig.5.15 , the phase difference between the estimated model and the 'nominal' model is quite small for all frequencies. Since the sampling rate of the sensor in the tractor system is quite low, the tractor controller is operating in low frequency ranges. The magnitude difference in low frequencies is relatively small as shown in Fig. 5.15. This indicates that the model uncertainty is small in the range of tractor operating frequencies. This low uncertainty will be beneficial for any controller design.

5.6 Steering actuator model identification

In the closed loop configuration shown in Fig. 1.3, the controller output is the hand wheel angle command. Therefore, for the purpose of controller design, we need to know the model from the hand wheel angle to the vehicle lateral position. The relationship between the hand wheel angle and lateral position is shown in Eq. 5.11

$$\frac{\text{lateral position}}{\text{hand wheel angle}} = \frac{\text{steered wheel angle}}{\text{hand wheel angle}} \frac{\text{yaw rate}}{\text{steered wheel angle}} \frac{\text{lateral position}}{\text{yaw rate}} \qquad (5.11)$$

In the previous sections, we identified the vehicle model from yaw rate to lateral position. In this section, we will focus on the dynamic model from hand wheel angle to the yaw rate. The steering actuator model is from the hand wheel angle to the steering wheel angle, and the relationship between steering wheel angle and yaw rate is linear in a fixed operating condition, and is discussed with more detail in section 5.2.2. Therefore, the main challenge in identifying the model from hand wheel angle to the yaw rate now lies in the identification of the actuator model.

As mentioned in section 5.2.2, the measurement of steered wheel angle is not available in the current AutoTrac Universal kit. When tractor is static, the steered wheel angle can be measured manually using a protractor. An experiment is designed to evaluate the static relationship from the hand wheel angle to the steered wheel angle. The hand wheel angle is manipulated manually and is recorded from the vehicle Control Area Network (CAN). Its corresponding steered wheel angle is measured using a protractor when the tractor is parked. The measurement of steered wheel angle is shown in Fig. 5.16. The relationship between the hand wheel angle and the steered wheel angle is plotted in Fig. 5.17 , where each dot in the figure represents an experiment point. There is a maximum encoder counts that the

'actual hand wheel angle' can reach, this is also the maximum data point we can measure as shown in Fig. 5.17. From Fig. 5.17 we can see that the static relationship between the hand wheel angle and the steered wheel angle is linear.

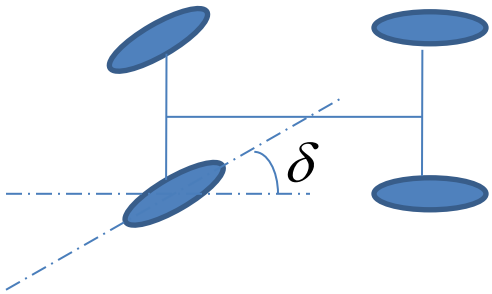

Figure 5.16 Static measurement of steered wheel angle

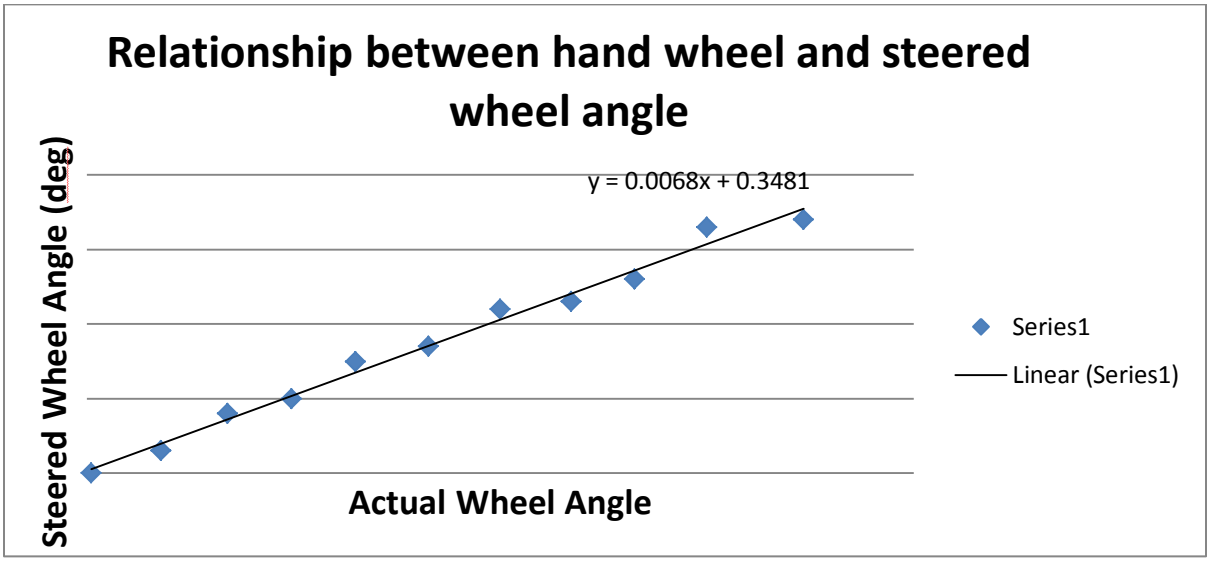

Figure 5.17 Relationship between hand wheel and steered wheel angle

Examining Eq. 5.11, the first term in the right hand side of the equation represents the actuator model, and is linear in static. The second term is the relationship between steered wheel angle and yaw rate, which is also linear in a fixed operating condition. The third term represents the vehicle dynamics model, and is discussed in section 5.1-5.4. Let us now lump the first and second term together, and assume that the dynamic model from hand wheel angle to yaw rate is linear. A chirp signal with the low frequency range is injected to the hand

wheel angle to identify the model from the hand wheel angle to yaw rate. The identified model is linear with a pure delay and a d.c. shift, and can be written in Eq. 5.12

$$\psi = 0.0041\delta e^{-0.2s} + 0.02 \qquad (5.12)$$

The comparison between the estimated yaw rate from Eq. 5.12 and the measured yaw rate is shown in Fig. 5.18. It is shown from the figure that the identified model is capable of capturing the dynamics of the system.

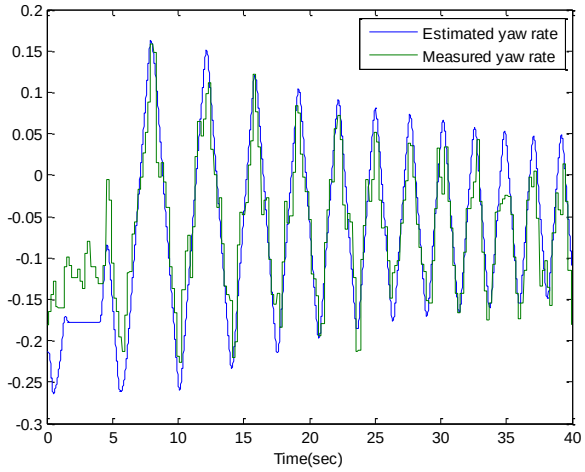

(a)

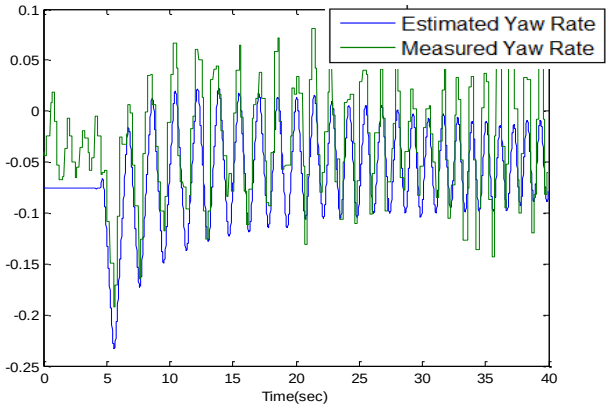

(b)

Figure 5.18 Comparison between estimated and measured yaw rate (cont. on next page)

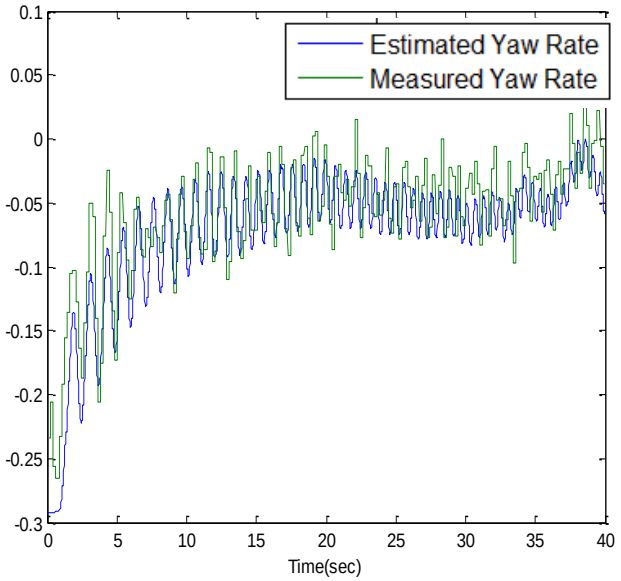

(c)

Figure 5.18 Comparison between estimated and measured yaw rate (a) Chirp input: low frequency range (b) Chirp input: mid frequency range, (c) chirp input: high frequency range

To sum up, the relationship between the hand wheel angle and yaw rate is linear. The model from yaw rate to vehicle lateral position is described in Eq. 5.9. The study for the identification of those two models is complete. Therefore, if the actual hand wheel angle can follow exactly what it is commanded to be, then a controller can be readily designed to achieve desired performance using a pole placement method. However, it is observed in the study that rate limit and saturation exists in the steering actuator, and the relationship between the desired/ commanded hand wheel angle and the actual hand wheel angle is shown in Fig. 5.19. In Fig. 5.19, the red line represents the desired/commanded wheel angle, and the magenta line is the actual wheel angle. In the simulation, two nonlinearity blocks are used to represent the nonlinear dynamics of the actuator – a saturation block and a rate limit block. The values of those two nonlinearities are determined experimentally. The blue line in Fig. 5.19 represents the simulated hand wheel angle. It can be observed from Fig. 5.19 that rate limit and saturation are the main nonlinearity that can be observed for the actuator.

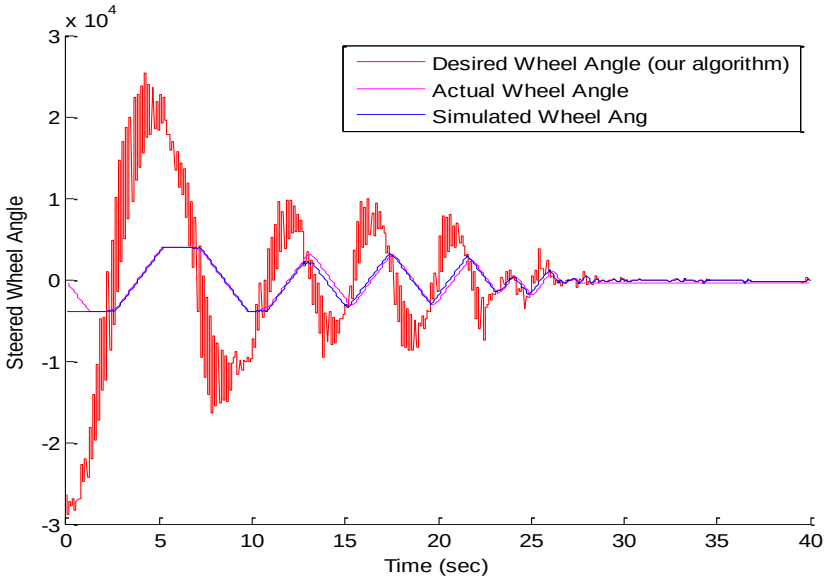

Figure 5.19 Rate limit and nonlinearity in steering actuator

Chapter 6
Automatic Controller Design and Experimental Results

In the previous chapters, we have introduced a method of determining the tractor lateral dynamics model from experimental data. However, verification of the identification should be seen in the light of the intended purpose of the model [28]. As is detailed in the first chapter, the purpose of system identification is to enable us to design an automatic controller for an agriculture vehicle. In this chapter, we will show the design of a feedback controller based on the identified model, and the system closed loop performance with the designed controller in the loop. We will also introduce the setup of a hardware-in the loop test system, a controller design method, and the experimental test results with the prototype controller in the loop.

An overview of the hardware-in the loop test system is shown in Fig. 6.1. The reference signal is user defined. In this study, dSPACE is used as rapid control prototyping tool, and it will be introduced with more details in the following sections. The output from the prototyping controller is hand wheel angle command. The inner closed loop for the hand wheel angle is not considered in the study, and it is integrated in ATU system. The output from the steering actuator is the actual steered wheel angle of the tractor. The tractor dynamics model measures from the steered wheel angle (input) to the lateral position (output). The position of the tractor is measured by a StarFire^{TM} RTK receiver. Experimental system identification is detailed in Chapter5 which takes into account both the dynamics of the steering actuator and the dynamics of the vehicle. The controller is designed based on the

identified system model. This controller is prototyped on the dSPACE system, and the loop can be completed.

This chapter is organized as follows; Section 1 will introduce the rapid control prototyping system used in the study. Section2 will be focusing on the controller design with Section3 presenting the experimental result with the prototyping controller used as a feedback controller.

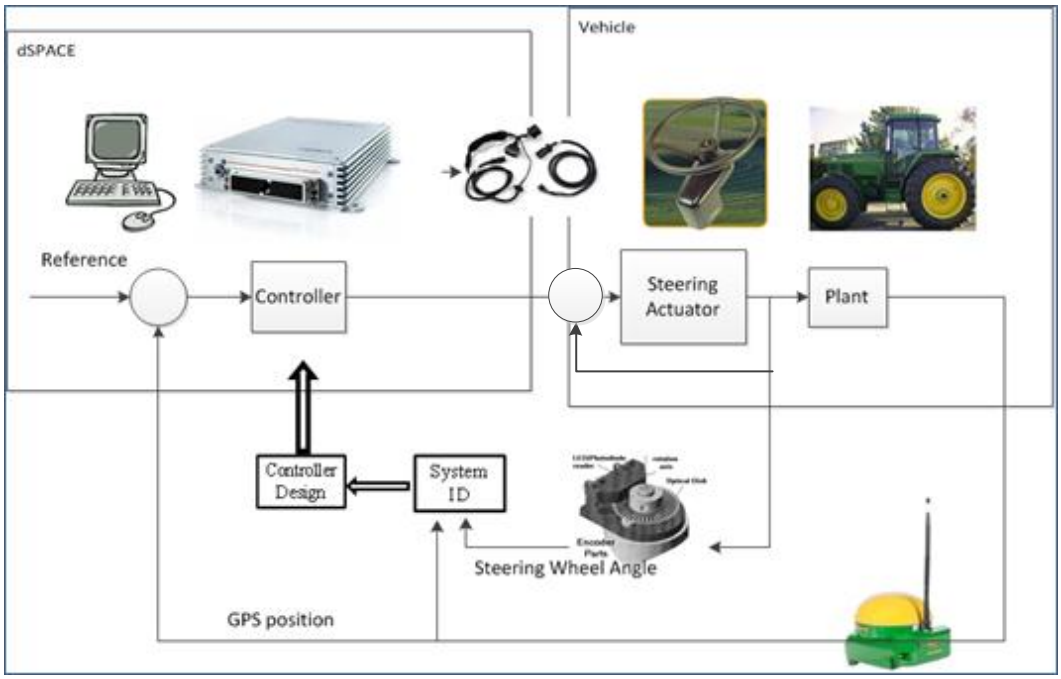

Figure 6.1 Hardware-in the loop test system configuration

6.1 Introduction of the rapid prototyping controller: dSPACE

dSPACE is a rapid prototyping system that was mainly designed for automotive research. No C-code programming is needed to design the controller. Block diagrams and state diagrams in Simulink are the starting points for the function prototyping. To perform a prototyping, the Simulink block diagrams are implemented on a dSPACE prototyping system. dSPACE prototyping systems therefore act as a real prototype control unit. To analyze a prototyping experiment, dSPCE prototyping systems record all the data in real time, and any desired control parameters can be optimized online.

There are different types of dSPACE hardware systems available in the market for different research purposes. The product used in this research is called MicroAutoBox (see Figure 6.2), which has comprehensive automotive I/O channels, and can be easily installed for tests on different vehicles. The MicroAutoBox also offers interfaces for the vehicle Controller Area Network (CAN), which is a vehicle bus standard designed to allow devices to communicate with each other without a host computer.

Figure 6.2 MicroAutoBox

In our experimental system, all the devices communicate via the vehicle CAN, and the command for the hand wheel angle can also be transmitted using a CAN message to the steered wheel actuator. There are two main files that need to be built to enable the MicroAutoBox to talk to the vehicle CAN; One is the Simulink file, which specifies the prototyping controller; the other is an experimental file that is built within the window of the dSPACE control desk, which will plot and save the messages available from the CAN.

As shown in Fig. 6.1, a dSPACE MicroAutoBox is a feedback controller in the hardware in the loop test. Therefore, the input to the prototype system is sensor information, and the output from the prototype system is the controller output. Correspondingly, there are two types of CAN message blocks used in the Simulink file: one is the receiver, and the other is the transmitter. On top of that, a 'CAN controller setup' block is also used to specify the attributes of the CAN messages. For each CAN message received/transmitted from the

Simulink block, its message identifier, message length and message composition need to be specified.

After specifying all the input and output CAN messages in the Simulink file, a designed controller can be implemented using the Simulink block diagrams the same way as building a regular Simulink file. Once the design is completed, this Simulink file can be built, and all the signals generated from this Simulink file are available in the dSPACE control desk.

Building the experiment file for the dSPACE Control Desk is quite straight forward. The signals that are generated from the Simulink file can be logged/ viewed by directly dragging them to a scope block. Fig. is a screen shot for the dSPACE experiment file, which contains a scope block. After connecting the actual hardware with the MicroAutobox, the hardware will be shown in the platform of the dSPACE control desk. The experiment is ready to go when green light is shown in the platform window.

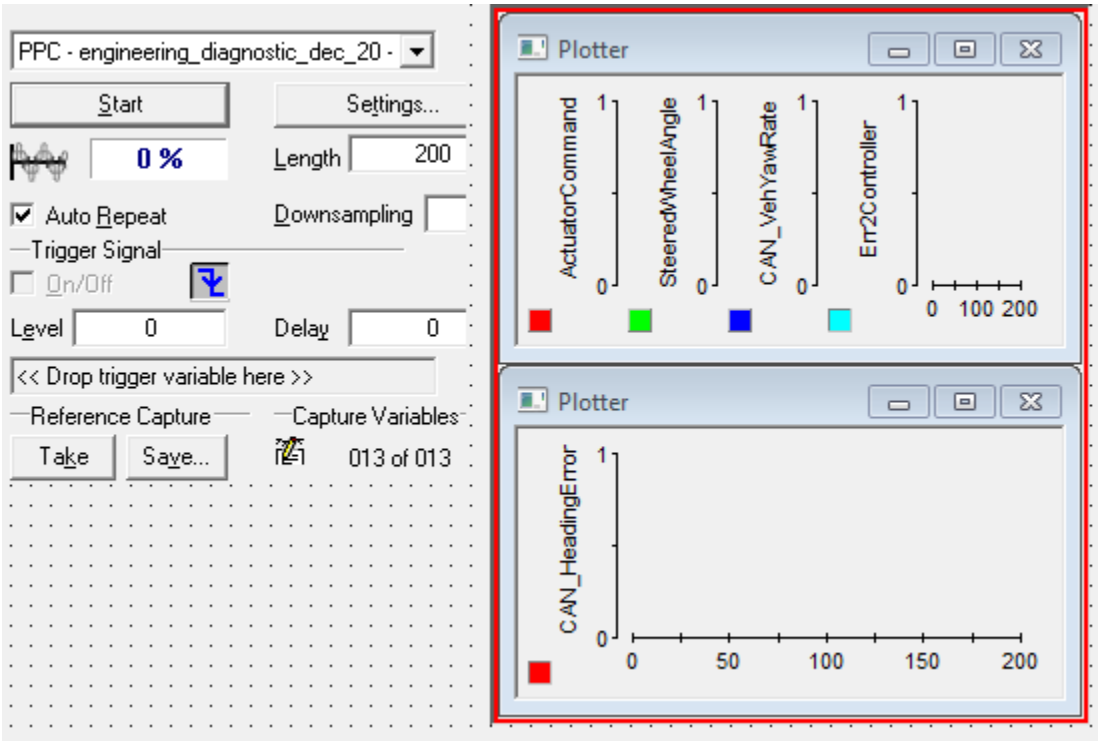

Figure 6.3 dSPACE experimental file

6.2 Feedback Controller Design

In this section, feedback controller design techniques are introduced. The first subsection introduces the determination of desired closed loop pole location from control's perspective with the second subsection introducing pole placement methods.

6.2.1 Determining desired closed loop poles

Control systems are designed to perform specific tasks. The requirements imposed on the control system are usually spelled out as performance specifications. The specifications may be given in terms of transient response requirements and steady state requirements. The specifications must be given before the design process begins. In this study, transient response specifications such as settling time and maximum overshoot are given. The locations of desired closed loop poles are therefore calculated based on the specifications.

There are certain limitations that exist in the current tractor system, such as: system delay, slow sampling rate, saturation and rate limit in the actuator. Those limitations will limit the closed loop performance. A possible set of transient response specifications is to have a settling time t_s of 10sec, and a maximum percentage of overshoot M_p of 10%. Eq. 6.1 and Eq. 6.2 illustrate the relationship between the transient specification and the damping ratio and natural frequency of the desired closed loop poles.

$$t_s = \frac{4}{\zeta w_n} \text{ (2\% criteria)} \qquad (6.1)$$

$$M_p = e^{-(\zeta/\sqrt{1-\zeta^2})\pi} \qquad (6.2)$$

The locations of desired closed loop poles can thus be determined from the specifications. The vehicle dynamics model is second order, and if we assume the controller is 1st order, the minimum number of closed loop poles is going to be 3. Therefore, other than these two dominant closed loop poles, there is one non-dominant pole that we need to specify. If the non-dominant pole is not specified, the location of this non-dominant pole can actually have an effect on the overall system performance. In this study, we are placing the

non-dominant pole at a position that is 5 times faster than the dominant closed loop poles. Based on the specifications, the dominant closed loop poles should be placed at

$$s_{1,2} = -0.4 \pm 0.5458i \quad (6.3)$$

The non-dominant closed loop poles should be placed at

$$s_3 = -2 \quad (6.4)$$

The relationship between the location of pole in s-plane and z-plane is illustrated in Eq. 6.5, where *s* denotes the pole location in s-plane, and T_s denotes the sampling rate.

$$z = e^{sT_s} \quad (6.5)$$

Thus, the desired closed loop pole locations in z-plane are can be calculated using Eq. 6.5

6.2.2 Pole placement

There are different techniques to place the closed loop poles at the desired locations. Those we have covered in this study are: root locus design, state space method, and direct solution of the characteristic equations. The designs in s-plane and z-plane are very similar, and the designs between each domain can be easily mapped using Eq. 6.5. Transfer functions between each domain are transformed using Zero Order Hold (ZOH), which assumes the control inputs are piecewise constant over the sampling period T.

Root locus design is one way of placing the closed loop poles. From the location of the desired dominant closed loop poles, angle deficiency can be calculated. A lead/lag controller can then be designed to compensate the angle deficiency. Root locus design is very efficient in placing the dominant closed loop poles. However, one of the problems is that if we want to specify the location of the non-dominant pole, root locus design can become very hard to use. The characteristic of the root-locus design is its being based on the assumption that the closed-loop system has a pair of dominant closed loop poles [36]. In our control system, the locations of all three closed loop poles need to be specified to ensure the performance. In addition, root locus is very nice to use when the plant model is fixed. However, since the system model can be arbitrary, and the controller design is to be made automatic, root locus design is not the best choice.

One other way to place the closed loop poles is by using state space method. There are two steps in the design. The first step is to place the dominant closed loop poles at the desired locations using state space feedback controller design assuming all states are observable. The next step is to design a reduced order observer to place the observer pole at the non-dominant location. An important assumption is made here that the system is both controllable and observable. Although from the experiments, the identified system is both controllable and observable, there is no guarantee that this assumption is valid.

Another way to place the closed loop poles is to directly solve the characteristic equations. Assume a lead/lag compensator can be denoted by the following equation,

$$\frac{k_1 z - k_2}{z - k_3} \qquad (6.6)$$

There are three unknown parameters in the compensator, k_1, k_2, k_3. The identified vehicle system model from previous chapters in continuous form can be written as:

$$G(s) = \frac{b_1 s + b_0}{s^2} \qquad (6.7)$$

ZOH is used to transform the design from Laplace domain to Z-domain, and Eq. 6.8 shows the transformation:

$$G(z) = (1 - z^{-1}) Z\left\{\frac{G(s)}{s}\right\} \qquad (6.8)$$

where $Z\left\{\frac{G(s)}{s}\right\}$ is the shorthand for $Z\left\{L^{-1}\left\{\frac{G(s)}{s}\right\}\right\}$ and $Z\{\cdot\}$, $L\{\cdot\}$ denote the z and Laplace transforms respectively. By applying the transform shown in Eq. 6.8 to Eq. 6.7, the discretized vehicle system model can be written as:

$$G(z) = \frac{b_{z1} z - b_{z0}}{z^2 - 2z + 1} \qquad (6.9)$$

Thus, From Eq. 6.6 and Eq. 6.9, the closed loop characteristic equation can be calculated as:

$$(z^2 - 2z + 1)(z - k_3) + (b_{z1} z - b_{z0})(k_1 z - k_2) = 0 \qquad (6.10)$$

The desired characteristic equation calculated based on the locations of desired closed loop poles can be written as:

$$(z - z_1)(z - z_2)(z - z_3) = 0 \qquad (6.11)$$

To place the closed loop poles at the desired locations, Eq. 6.10 should be set equal to Eq. 6.11 . To set the equivalence, there are going to be three equations. There are also three unknown variables, k_1, k_2, k_3, and the solution should be unique. This type of solution requires the least computational cost.

6.3 Controller Performance Analysis

In this section, we will present the tractor closed loop performance with the prototype controller in the loop. This prototype controller is designed with the following time domain requirement: dominant closed loop poles are placed to satisfy the following transient specifications: settling time is 10 sec, and maximum overshoot is 10%. The non-dominant pole is to be placed 5 times faster than the dominant poles. The overall closed loop system configuration is shown in Fig.6.. The steering actuator and vehicle model are identified experimentally using the methods detailed in Chapter 5. The linear models of the steering actuator and vehicle model are lumped together as an overall plant model, and this model is used for the controller design. The steering controller is designed by solving the characteristic equations as illustrated in Section 6.2. Figure 6. compares the simulated and measured lateral position from a look ahead point that is ds ahead of vehicle c.g. From the figure, we can see that the simulated output is capable of capturing the transient behavior of the system. First of all, this is an indication that the controller designed can meet the expectation set at the beginning of the study. In addition, it has also demonstrated that the model identified from chapter 5 is accurate enough for the purpose of controller design.

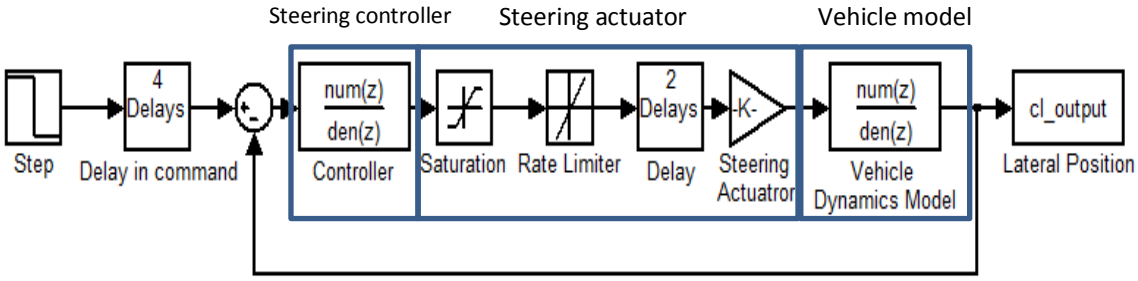

Figure 6.4 Closed loop configuration

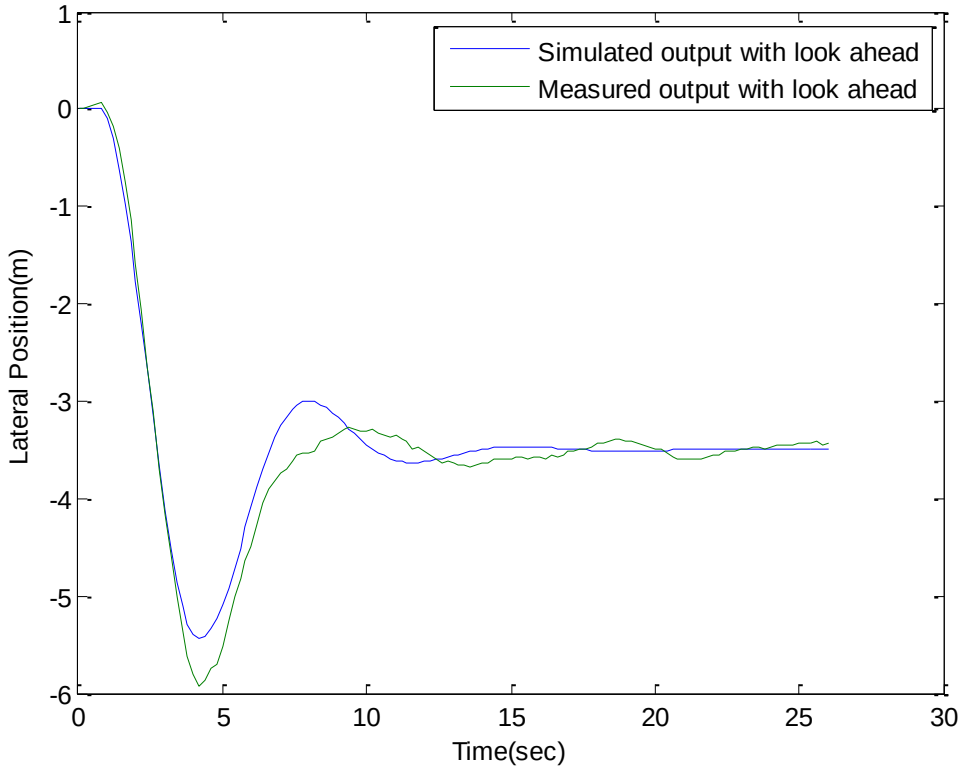

Figure 6.5 Simulated and measured lateral position from a look ahead point

Figure 6. shows the tractor lateral position that is measured from the Star Fire receiver which is mounted on top of the vehicle. This will represent the actual tractor lateral movement in the field. As expected, the behavior that is measured from the tractor itself is

going to be better than measured from a look ahead point. The figure shows the tractor changing from one crop lane to the other, and the transition is rather smooth.

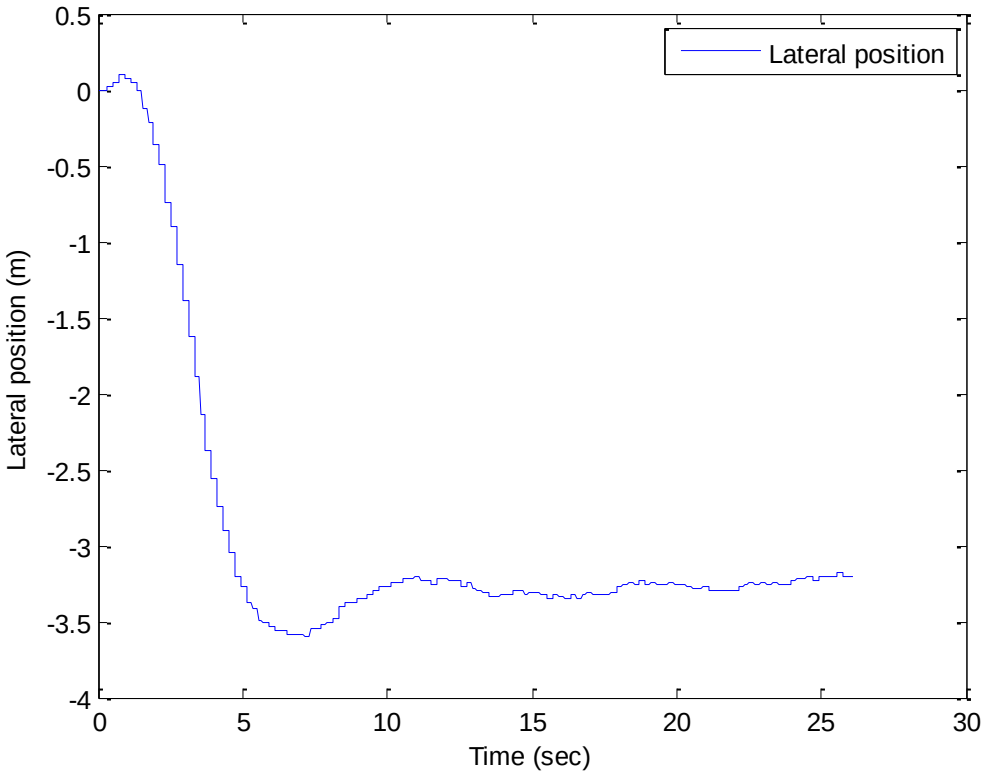

Figure 6.6 Measured lateral position from Star Fire receiver

Chapter 7
Field Test Results

In this chapter, extensive field test results for both the prototype controller and an well-tuned ATU controller are presented for comparison purpose. Two different types of trajectories have been used, a straight line trajectory, and a curve trajectory. The tests were conducted in two different speeds, 5mph and 10mph. Except for line acquiring; a planter is mounted and kept down in the field for all of the tests performed at 5mph.

This chapter is organized as follows; section1 will introduce the test setups. Section2 will present the field test result for steady state tracking, which includes results for a straight line tracking and curve tracking with section3 presenting the line acquiring result

7.1 Test Setup

All tests shown in this chapter were conducted on a John Deere 8410 tractor with AutoTrac^{TM} Univeresal system installed. Hardware setup for this test follows the same hardware setup as discussed in Chapter 6. Tests were performed in a John Deere experimental farmland, where the slope of the test farm is representative for a typical farm land.

Controller design follows the steps discussed in Chapter 6. An adaptive estimation is performed to find a model for the tractor. A controller is then designed based on the identified model and the desired closed loop pole locations. This designed controller is used as the prototype controller for all tests shown in this chapter. The ATU controller has been tuned before the experiment by an expert.

7.2 Steady State Tracking

7.2.1 Straight line following

Straight line following has been tested on both ATU and the prototype controller. Two different speeds are used in the experiment, 5mph and 10 mph. For a 5mph test, a planter was attached. The planter was lifted up for 10mph test to protect the equipment from damage.

Assume that the data is normally distributed, at a 95% confidence level, the lateral error and heading error are shown in Table 7.1.

Table 7.1 Straight line following

	Speed	Lateral Error (m)	Heading Error (deg)
ATU	5mph	0.0460	0.6105
Prototype	5mph	0.0453	0.7014
ATU	10mph	0.1026	1.1023
Prototype	10mph	0.0955	1.1149

From the table, we can see that the prototype controller achieves similar performance as the ATU controller in straight line following.

7.2.2 Curve following

Curve following has also been tested on both ATU and the prototype controller. Two different speeds are used in the experiment, 5mph and 10 mph. For a 5mph test, a planter was attached. The planter was lifted up for 10mph test to protect the equipment from damage.

The trajectory of a prototyping controller following the curve is shown in Fig. 7.1. Assume that the data is normally distributed, at a 95% confidence level, the lateral error and heading error are shown in Table 7.2.

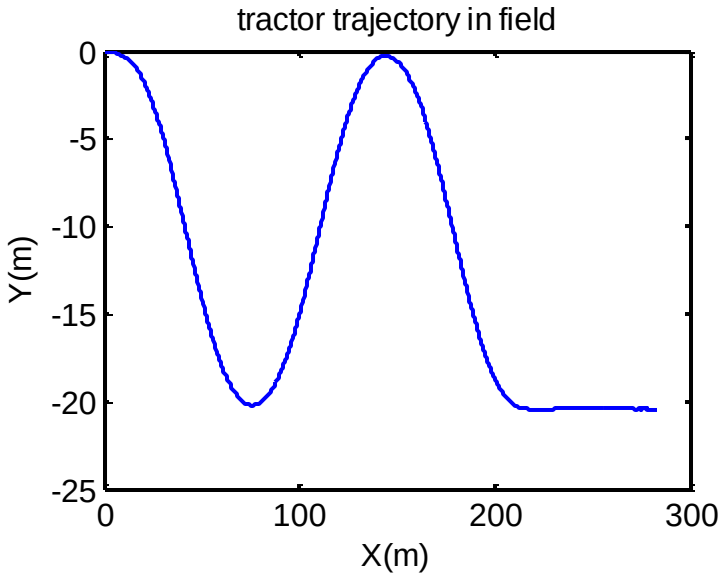

Figure 7.1 Curve following

Table 7.2 Curve following

	Speed	Lateral Error (m)	Heading Error (deg)
ATU	5mph	0.096	1.6815
Prototype	5mph	0.1056	1.9407
ATU	10mph	0.6871	2.3724
Prototype	10mph	0.8384	4.0178

Comparing Table 7.2 with Table 7.1, lateral error and heading error for curve following are bigger than straight line following as expected. From Table 7.2, the prototype controller is having a bigger level of error compared to the ATU controller especially for the case of fast speed curve following.

In current design, the curvature of a desired path is seen as a disturbance to the control system. In other words, the control system is not modified for a curve tracking from a straight line following. One of the possible ways to improve the curve following accuracy is to add the curvature information as a feedforward signal in the control loop. In this way, the controller will react to the curvature information before the lateral error is showing up, and performance improvement can be expected.

7.3 Line acquiring

In this part of the experiment, the tractor is starting from a parallel line 1.54 m away from the desired trajectory. Only 5mph tests are performed, and the planter is lifted up throughout the test.

For the ATU controller, during 20 tests, 0% overshoot is achieved. Using 5% criteria, the average settling time of system step response is 8.3 sec. A typical line acquiring plot for ATU controller is shown in Fig.7.2

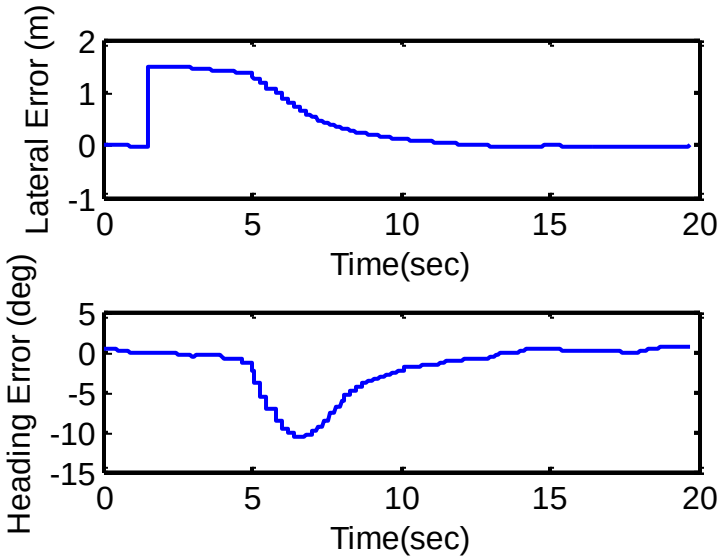

Figure 7.2 ATU Line Acquiring

For the prototype controller, during 20 tests, 15 line acquiring trajectories don't include an overshoot. For the rest 5 tests, an average of 1.92% overshoot is observed. Using 5% criteria, the average settling time is 7.07 sec. A typical line acquiring plot with and without overshoot are shown in Figure 7.3 (a) and (b) respectively. It can be observed from the plots that the prototype controller is capable of achieving similar level of performance as an expert-tuned ATU controller in line acquiring.

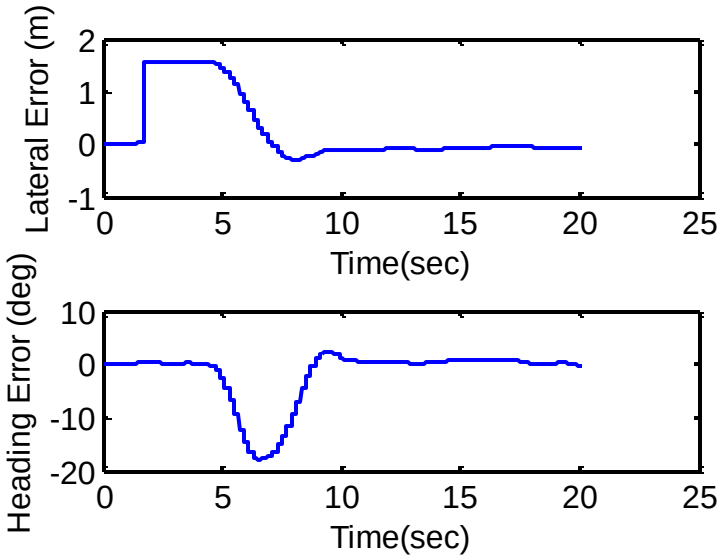

(a)

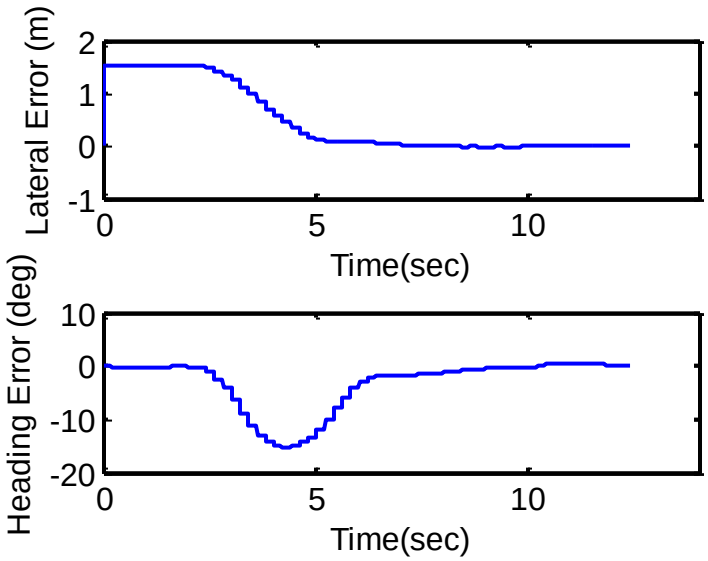

(b)

Figure 7.3 Prototype line acquiring (a) with overshoot (b) no overshoot

Chapter 8
Conclusion and Future Work

The main objective of this study was to develop an automated agricultural vehicle guidance system that can be easily transplanted from vehicle to vehicle. One of the possible solutions to this problem is to perform system identification, and then design a feedback controller based on the identified system model. A method to perform practical tractor dynamics identification with constraints is the main contribution of this paper. The identification can be broke down into two major parts: determining a tractor model structure and identifying unknown parameters in the tractor model. A summary of each of these components and possible extensions of the research will be given in this chapter.

8.1 Determine Tractor Model Structure

The first step in performing tractor model identification is to determine a model structure based on the tractor's dynamic analysis. Instead of using a well-known 4^{th} order bicycle model, a simplified 2^{nd} order model is developed to represent the tractor dynamics. From the simulation results presented in this study, a 2^{nd} order model can be representative for tractor dynamics in low frequency operations that are typical of most field operations. This 2^{nd} order model structure was also tested using experimental data, and it is shown in this study that a 2^{nd} order model is suitable for the intended closed loop application. In this 2^{nd} order model, there are two unknown parameters to be estimated, and the results for determining the unknown parameters are presented in section 7.2.

8.2 Parameter Estimation Methods

The purpose of parameter estimation is to identify the unknown parameters in a pre-determined tractor model structure for the purpose of controller design. The current work has further challenged associated with constraints in identification field area and limitations in the selection of reference trajectories. This work has compared two classic parameter estimation approaches (LSE and adaptive estimation) with a new parameter estimation approach (ILI). LSE is one of the most popular methods for parameter identification. However, for this particular type of tractor model structure with the consideration of constraints on sensor Signal Noise Ratio (SNR) and selection of reference trajectories, the model estimated from LSE is not faithful in its convergence to appropriate plant parameters. Gradient based adaptive estimation is capable of giving a faithful estimation for the tractor model. However, the area needed for identification is quite large. For the system under study here, the area constraints are exceeded for the gradient based approaches. In addition, although gradient based adaptive estimation is quite robust to noise, the estimation result is easily affected by ground disturbances such as a big bump that occurred towards the end of the test.

This work presented the framework for Iterative Learning Identification (ILI) and, to the knowledge of the author, presented one of the first implementations of ILI on an experimental system. The ILI was demonstrated to be successful in identifying model parameters for an agricultural tractor vehicle. While there are other approaches available for parameter identification, there were significant key benefits in this application which made ILI particularly attractive. As discussed in Chapter 5, the field available for identification is limited. Contrary to a gradient based adaptive approach, which is suitable for on-line parameter identification, the ILI can be carried out on a small field section. Additionally, the ILI is capable of identifying system parameters with a step signal which is easily available from the current AutoTrac^{TM} system. As a result, it provides better estimation results than a batch type of least square type identification.

A feedback controller is designed based on the identified model using the ILI approach. This controller was prototyped and tested on a John Deere 7700 tractor. The tractor closed loop performance is capable of satisfying the desired performance. A closed loop

simulation is capable of representing the tractor transient behaviors. It has demonstrated that the model identified is accurate enough for the controller design.

8.3 Future Work

While ILI has shown to be a very viable technique in this work, there is room for improvement. As shown in the simulation and experimental results for ILI, the parameter convergence is not monotonic. Using techniques from available ILC results [33], alternative update designs for ILI will be developed. This may include a norm-optimal design for the parameter update law.

In addition, the current ILI framework is in Laplace domain indicative of continuous time system representation. As indicated in Chapter 4, implementing this algorithm requires taking derivatives for the reference signal and the error signal. The number of derivatives depends on the model order. For example, for a first order model, we need to take a 1^{st} order derivative for the reference and error signal. For a 4^{th} order model, we need to take 4^{th} order derivative for the reference and error signal. This can be implemented for a low order model. However, the implementation of this algorithm for a high order model will be limited. In addition, to implement the design in experiment, all data needs to be sampled. Therefore, it will be very beneficial for both the design procedure and the actual implementation procedure to translate the design from Laplace domain to z-domain indicative of a discrete time system representation.

List of References

[1] Gan-Mor,S., and Clark,R.L. , "DGPS-Based Automatic Guidance-Implementation and Economical Analysis," in *ASAE Annual Interanational Meeting*, Sacramento, CA, USA, 2001, p. Paper No. 011192.

[2] M., Deboer, J.L. Watson, "Who will benefit from GPS Auto Guidance in the Corn Belt?," Purdue University, West Lafayette, 2002.

[3] F.L. Willrodt, "Steering attachment for tractors," 1506706, 1924.

[4] F.W. Andrew, "Automatic tractor control," 2259193, 1941.

[5] Reid, J.F., Zhang, Q., Noguchi, N., and Dickson, M., "Agricultural automatic guidance research in North American," *Computers and electronics in agriculture*, vol. 25, no. 1-2, p. 155, 2000.

[6] R., H.Seufer Keicher, "Automatic guidance for agricultural vehicles in Europe," *Computers and electronics in agriculture*, vol. 25, no. 1/2, pp. 169-194, 2000.

[7] T. Torii, "Research in autonomous agriculture vehicles in Japan," *Computers and electronics in agriculture*, vol. 25, no. 1/2, pp. 133-153, 2000.

[8] Li, M., Imou, K., Wakabayashi, K., and Yokoyama, S., "Review of researc on agricultural vehicle autonomous guidance," *International Journal of Agricultural and Biological Engineering*, vol. 2, no. 3, pp. 1-16, Sep 2009.

[9] Qiu, H.C., Zhang, Q., Reid, J.F., "Evaluation of Tri-R Robotic Driver for tractor guidance on corn fields," in *Agruicultural Equipment Technology Conference*, Louisville, Kentucky, 1999.

[10] Benson, E.R., Reid, J.F., and Zhang, Q., "Machine Vision-Based Guidance System for an Agricultural Small-Grain Harvester," *American Society of Agricultural Engineerings*, vol. 46, no. 4, pp. 1255-1264, Mar 2003.

[11] O'Connor, M., Elkaim G., Parkinson B., , "Kinematic GPS for closed-loop control of farm and construction vehicles," *Palm Springs*, pp. 12-15, Sept 1995.

[12] T. Bell, "Automatic tractor guidance using carrier-phase differential GPS," *Computers and electronics in agriculture*, pp. 53-66, 2000.

[13] Stombaugh, T.S., Bensen, E.R., Hummel,J.W., "Guidance Control of Agricultural Vehicles at High Field Speeds," *Transactions of the American Society of Agricultural Engineers*, vol. 42, no. 2, pp. 537-544, 1999.

[14] Karkee, M., and Steward, B.L., "Parameter estimation and validation of a tractor and single axle towed implement dynamic system model," *Computers and Electronics in Agriculture*, pp. 135-145, 2011.

[15] Sakai, F., and Sugie, T., "Continuous-time Systems Identification Based on Iterative Learning Control," in *Proceedings of the 16th IFAC World Congress*, Prague, 2005.

[16] Sakai,F., and Sugie, T., , "A Continuous-time Closed-loop Identification Method Based on Iterative Learning Control Concepts," in *Proceedings of the 46th IEEE Conference on Decision and Control*, New Orleans, 2007, pp. 12-14.

[17] Campi, M. C.,Sugie, T. , and Sakai, F., "An Iterative Identification Method for Linear Continuous-Time Systems," *IEEE Transactions on Automatic Control*, vol. 53, no. 7, pp. 1661-1669, Aug 2008.

[18] Bristow,D. A., Tharayil,M. , and Alleyne, A. G., "A Survey of Iterative Learning Control," *IEEE Contro System Magazine*, vol. 26, no. 3, pp. 96-114, June 2006.

[19] Rajesh Rajamani, "Chapter2 Lateral Vehicle Dynamics," in *Vehicle Dynamics and Control*, Federick F. Ling, Ed. NY: Springer Science+Business Media, Inc., 2006.

[20] M. O'Connor, G. Elkaim and B. Parkinson, "Cariier-phase DGPS for Closed Loop Control of Farm and Construction Vehicles," *Navigation Journal of the Institute of Navigaion*, vol. 43, no. 2, pp. 167-178, Summer 1996.

[21] Guldner, J., Tan, H.-S and Patwardhan, S., , "Analysis of automatic steering control for highway vehicle with look-down lateral reference systems," *Vehicle System Dynamics*, vol. 26, no. 4, pp. 243-269, 1996.

[22] S., Brennan, and A., Alleyne, "Using a Scale Testbed: Controller Design and Evaluation," *IEEE Control Systems Magazine*, vol. 21, no. 3, pp. p 15-26, Jun 2001.

[23] SI. Eom, EJ. Kim, TY. Shin, MJ. Lee, and F. Harashima, "The Robust Controller Design for

Lateral Control of Vehicles," in *2003 IEEE/ASME International Conference on Advanced Intellegent Mechatronics*, 2003, pp. 570-573.

[24] H. peng and M. Tomizuka, "Preview Control for Vehicle Lateral Guidance in Highway Automation," *Transactions of the ASME. Journal of Dynamic Systems, Measurement and Control*, vol. 115, no. 4, pp. 679-86, Dec 1993.

[25] M. Karkee, and BL. Steward, "Study of the Open and Closed Loop Characteristics of a Tractor and a Single Axle Towed Implement System," *Journal of Terramechanics*, vol. 47, no. 6, pp. 379-393, 2010.

[26] H. Peng and M.Tomizuka, "Preview Control for Vehicle Lateral Guidance in Highway Automation," in *Proceedings of American Control Conference*, Boston, 1991, pp. 3090-3095.

[27] T.S., Stombaugh, E.R., Bensen, J.W., Hummel, "Guidance Control of Agricultural Vehicles at High Field Speeds," *Transactions of the American Society of Agricultural Engineers*, vol. 42, no. 2, pp. 537-544, 1999.

[28] T. Soderstrom, and P. Stoica, *System Identification*. Englewood Cliffs: Prentice Hall, 1989.

[29] G. Tao, *Adaptive Control Design and Analysis*. New Jersey, American: John Wiley &Sons Inc, 2003.

[30] F. Sakai, and T. Sugie, "Continuous-time Systems Identification Based on Iterative Learning Control," in *Proceedings of the 16th IFAC World Congress*, Prague, 2005.

[31] F., Sakai, and T., Sugie, "A Continuous-time Closed-loop Identification Method Based on Iterative Learning Control Concepts," in *Proceedings of the 46th IEEE Conference on Decision and Control*, New Orleans, 2007, pp. 12-14.

[32] M. C. Campi, T. Sugie, and F. Sakai, "An Iterative Identification Method for Linear Continuous-Time Systems," *IEEE Transactions on Automatic Control*, vol. 53, no. 7, pp. 1661-1669, Aug 2008.

[33] D. A. Bristow, M. Tharayil, and A. G. Alleyne, "A Survey of Iterative Learning Control," *IEEE Contro System Magazine*, vol. 26, no. 3, pp. 96-114, June 2006.

[34] Y., Alleyne, A.G., Xie, ""Foundamental Limits in Combine Harvester Header Height Control"," in *American Control Conference*, San Francisco, 2011.

[35] J.Y., Wong, *Theory of Ground Vehicles*. Canada, pp.350, : John Wiley& Sons, Inc., 2001.

[36] K. Ogata, *Modern Control Engineering*, 4th ed. New Jersey: Prentice Hall, 2002.